Inaugural dissertation

for

obtaining the doctoral degree

of the

Combined Faculty of Mathematics, Engineering and Natural Sciences

of the

Ruprecht-Karls-University

Heidelberg

Presented by:

M.Sc. Foteini Fotopoulou

born in: Cholargos, Greece

Oral examination: 23.07.2024

Exploring the stochastic nature of ageing: Insights from the hematopoietic system as a model

Referees:

Prof. Dr. Benedikt Brors

Dr. Michael Milsom

From someone not particularly fond of even numbers

"Even numbers run contrary to my heart;
I want nothing to do with them.
Their lives are too comfortably arranged,
they stand on their feet too solidly
and have not the slightest desire to
change location.
They are satisfied, conservative, without
anxieties:
they have solved every problem,
translated every desire into reality
and grown calm.
It is the odd number which conforms to
the rhythm of my heart.
The life of the odd number is not at all
comfortably arranged.
The odd number does not like the world
the way it finds it,
but wishes to change it,
add to it,
push it further.
It stands on one foot,
holds the other ready in the air, and
wants to depart.
Where to?
To the following even number, in order
to halt for an instant,
catch its breath,
And work up fresh momentum."

N. Kazantzakis, *Report to Greco*

Summary

Ageing is traditionally viewed as the deterministic functional decline of organisms. However, from an evolutionary perspective, aged organisms have surpassed their reproductive phase and are therefore less subjected to selective pressures, leading to the accumulation of random errors across various biological tiers of their being. These stochastic errors are crucial in understanding why ageing manifests differently across individuals.

This thesis generally aimed to explore the stochastic aspects of ageing, using the hematopoietic system as a model. In the first part, I focused on examining the endogenous mechanisms facilitating the gradual acquisition of random somatic mutations in hematopoietic stem cells (HSC) during normal ageing, as these cells are responsible for the lifelong system regeneration. Somatic mutagenesis is universal and constant over time; however, the mutational rates vary among different cell types. Here, I used whole genome sequencing (WGS) and mouse models to inspect single HSC genomes in depth and quantify their mutational burdens, by interrogating their clonal progeny. Assuming that this acquisition takes place in a linear fashion, as previously suggested, I estimated that murine HSCs accumulate 44 single nucleotide variants (SNV) per genome per year, a rate almost three times faster than that observed in human counterparts. Moreover, the SNV landscapes formed in murine HSCs appeared analogous to those in humans, shaped by processes reflecting self-renewal activity, metabolic dependencies and cellular state. However, no further alterations were detected regarding other mutational types.

Apoptosis has been regarded as the guardian of the HSC genome under stress, providing tumor-suppressive function against cells harboring driver mutations. To understand its impact during normal ageing, I blocked the intrinsic apoptotic pathway in HSCs using a conditional Bak $^{-/-}$ Bax$^{\delta/\delta}$ mouse model. Strikingly, the perturbation did not alter the mutational burdens in HSCs, challenging the established views about this mechanism. Shifting the focus of analysis on the states of HSCs, I examined dormant and actively cycling cells, using a label-retention mouse model that allows the easy separation of these two fractions by flow cytometry. Despite originating from the same donors, dormant HSCs exhibited significantly fewer mutations than their active counterparts. Moreover, mutational signature analysis attributed this difference mainly to the decreased divisional activity of dormant cells; otherwise, their mutational landscapes appeared similar. This observation highlighted that dormancy, rather than apoptosis, is the primary mechanism maintaining genomic integrity within the HSC pool during physiological ageing, while HSC activation allows SNV accumulation over time.

In the second part of my thesis, I aimed to explore the intrinsic origins of the inter-individual heterogeneity observed in hematological ageing. To address this, I first compiled a comprehensive murine dataset characterizing extensively the hematological profiles of young,

middle-aged and old individuals using flow cytometry, multi-omics and bone histology. With this dataset in hand, I first explored potential associations among classical indicators of hematological ageing, such as HSC expansion, myeloid cell production, and HSC functionality, as assessed through competitive transplantation assays. Interestingly, in young mice, some of the metrics were interconnected, suggesting a finely regulated system under homeostasis. However, in old mice, a unique variability of phenotypes emerged, alongside a lack of correlations among the different metrics.

Transplantations using bone marrow from donors of the three different age groups into young myeloablated recipients revealed some degree of overlap in hematologic phenotypes regardless of donor age. This observation pinpointed that the aged phenotype is also regulated by the niche. Analysis of single-cell RNA-sequencing data from both hematopoietic and niche cells revealed a remarkable bone marrow remodeling in old mice, including the emergence of a novel and heterogeneous mesenchymal stromal progenitor population -Adipo-CAR3-, observed in this study for the first time. This population served as the epicenter of an inflammatory network involving neutrophils and HSCs. However, the niche phenotype did not correlate with other hematopoietic metrics in a manner that could explain the overall system behavior, suggesting that the lack of regulation that characterizes old age may expose each organism to stochastic events able to determine its phenotype.

In conclusion, this thesis highlighted the often overlooked role of stochasticity as a fundamental aspect of ageing. The results from the first part challenged conventional beliefs about how HSCs manage DNA damage and mutagenesis under physiological conditions. Unlike studies relying on strong stressors to explore genotoxic responses, my findings shed light on sources of endogenous routine damage that accumulates steadily over time. Furthermore, through a murine epidemiological study included in the second part of this work, I observed that as the hematopoietic system ages, it gradually loses its ability to regulate its phenotype. Ultimately, it is likely that this leads to a transition towards a highly stochastic state, where random errors can alter its characteristics causing phenotypic variability.

Zusammenfassung

Das Altern wird traditionell als deterministischer Funktionsrückgang von Organismen betrachtet. Aus evolutionärer Sicht haben ältere Organismen ihre Reproduktionsphase hinter sich gelassen und sind daher einem geringeren Selektionsdruck ausgesetzt, was zur Anhäufung von Zufallsfehlern auf den verschiedenen biologischen Ebenen ihres Lebens führt. Diese stochastischen Fehler sind von entscheidender Bedeutung, um zu verstehen, warum sich die Alterung bei den einzelnen Individuen unterschiedlich äußert.

Ziel dieser Arbeit war es, die stochastischen Aspekte des Alterns am Beispiel des hämatopoetischen Systems zu untersuchen. Im ersten Teil habe ich mich auf die Untersuchung der endogenen Mechanismen konzentriert, die den allmählichen Erwerb zufälliger somatischer Mutationen in hämatopoetischen Stammzellen (HSZ) während des normalen Alterns ermöglichen, da diese Zellen für die lebenslange Regeneration des Systems verantwortlich sind. Die somatische Mutagenese ist universell und im Laufe der Zeit konstant; die Mutationsraten variieren jedoch zwischen den verschiedenen Zelltypen. Hier habe ich mit Hilfe der Ganzgenomsequenzierung (whole genome sequencing; WGS) und Mausmodellen einzelne HSZ-Genome eingehend untersucht und ihre Mutationslast quantifiziert, indem ich ihre klonale Nachkommenschaft untersucht habe. Unter der Annahme, dass dieser Erwerb linear verläuft, wie zuvor angenommen, schätzte ich, dass HSZ der Maus 44 Einzelnukleotidvarianten (single nucleotide variants; SNV) pro Genom und Jahr akkumulieren, eine Rate, die fast dreimal so hoch ist wie die der menschlichen Zellen. Darüber hinaus schienen die SNV-Landschaften, die sich in den HSZ der Maus bildeten, denen des Menschen zu entsprechen, da sie durch Prozesse geformt wurden, die die Selbsterneuerungsaktivität, metabolische Abhängigkeiten und den Zellzustand widerspiegeln. Bei anderen Mutationstypen wurden jedoch keine weiteren Veränderungen festgestellt.

Die Apoptose gilt als Wächter des HSZ-Genoms unter Stress und hat eine tumorunterdrückende Funktion gegenüber Zellen, die Treibermutationen aufweisen. Um die Auswirkungen der Apoptose während des normalen Alterns zu verstehen, habe ich den intrinsischen apoptotischen Weg in HSZ mithilfe eines konditionalen $Bak^{-/-}$ $Bax^{\delta/\delta}$ Mausmodells blockiert. Bemerkenswerterweise änderte sich die Mutationslast in den HSZ durch die Störung nicht, was die gängigen Ansichten über diesen Mechanismus in Frage stellt. Um den Schwerpunkt der Analyse auf den Zustand der HSZ zu verlagern, untersuchte ich ruhende und aktiv proliferierende Zellen unter Verwendung eines Mausmodells mit Markierungsretention, das eine einfache Trennung dieser beiden Fraktionen durch Durchflusszytometrie ermöglicht. Obwohl sie von denselben Spendern stammten, wiesen ruhende HSZ deutlich weniger Mutationen auf als ihre aktiven Gegenstücke. Die Analyse der Mutationssignatur führte diesen Unterschied hauptsächlich auf die verringerte Teilungsaktivität der ruhenden Zellen zurück;

ansonsten war die Mutationslandschaft der Zellen ähnlich. Diese Beobachtung unterstreicht, dass die Ruhephase und nicht die Apoptose der primäre Mechanismus zur Aufrechterhaltung der genomischen Integrität innerhalb des HSZ-Pools während der physiologischen Alterung ist, während die HSZ-Aktivierung eine SNV-Akkumulation im Laufe der Zeit ermöglicht.

Im zweiten Teil meiner Dissertation wollte ich die Ursachen für die bei der hämatologischen Alterung beobachtete interindividuelle Heterogenität untersuchen. Zu diesem Zweck habe ich zunächst einen umfassenden Datensatz von Mäusen zusammengestellt, der die hämatologischen Profile von Individuen jungem, mittlerem und hohem Alters mithilfe von Durchflusszytometrie, Multi-omics und Knochenhistologie umfassend charakterisiert. Anhand dieses Datensatzes untersuchte ich zunächst potenzielle Zusammenhänge zwischen klassischen Indikatoren der hämatologischen Alterung, wie der HSZ-Expansion, der Produktion myeloischer Zellen und der HSZ-Funktionalität, wie sie in kompetitiven Transplantationstests ermittelt wurden. Interessanterweise waren bei jungen Mäusen einige der Messgrößen miteinander verbunden, was auf ein fein reguliertes System in der Homöostase hindeutet. Bei alten Mäusen hingegen zeigte sich eine einzigartige Variabilität der Phänotypen und ein Mangel an Korrelationen zwischen den verschiedenen Messgrößen.

Bei der Transplantation von Knochenmark von Spendern der drei verschiedenen Altersgruppen in junge, myeloablierte Empfänger zeigte sich eine gewisse Überschneidung der hämatologischen Phänotypen unabhängig vom Alter des Spenders. Diese Beobachtung deutet darauf hin, dass der Altersphänotyp auch durch die Knochenmark-Nische reguliert wird. Die Analyse von Einzelzell-RNA-Sequenzierungsdaten sowohl von hämatopoetischen als auch von Nischenzellen ergab einen bemerkenswerten Knochenmarkumbau bei alten Mäusen, einschließlich der Entstehung einer neuen mesenchymalen stromalen Vorläuferpopulation – Adipo-CAR3 -, die in dieser Studie zum ersten Mal beobachtet wurde. Diese Population diente als Epizentrum eines entzündlichen Netzwerks, an dem Neutrophile und HSZ beteiligt waren. Der Nischenphänotyp korrelierte jedoch nicht mit anderen hämatopoetischen Metriken in einer Weise, die das Verhalten des Gesamtsystems erklären könnte, was darauf hindeutet, dass die fehlende Regulierung, die das Alter kennzeichnet, jeden Organismus stochastischen Ereignissen aussetzt, die seinen Phänotyp bestimmen können.

Zusammenfassend lässt sich sagen, dass diese Arbeit die oft übersehene Rolle der Stochastik als grundlegender Aspekt des Alterns hervorhebt. Die Ergebnisse des ersten Teils stellten herkömmliche Annahmen darüber in Frage, wie HSZ unter physiologischen Bedingungen mit DNA-Schäden und Mutagenese umgehen. Im Gegensatz zu Studien, die sich auf starke Stressfaktoren stützen, um genotoxische Reaktionen zu erforschen, werfen meine Ergebnisse ein Licht auf die Quellen endogener Routineschäden, die sich im Laufe der Zeit stetig anhäufen. Darüber hinaus habe ich in einer epidemiologischen Studie an Mäusen, die Teil des zweiten Teils dieser Arbeit ist, beobachtet, dass das hämatopoetische System mit zunehmendem Alter allmählich seine Fähigkeit verliert, seinen Phänotyp zu regulieren. Letztendlich führt dies

wahrscheinlich zu einem Übergang in einen hochgradig stochastischen Zustand, in dem zufällige Fehler seine Eigenschaften verändern können, was zu phänotypischer Variabilität führt.

Acknowledgments

This four-year PhD journey has been a remarkable chapter in my life, made possible by the contributions of many individuals. I owe a significant debt of gratitude to each of them and would like to acknowledge their support in the following pages.

First of all, I am very grateful to my supervisor, **Dr. Mick Milsom,** for letting me embark on this journey in his lab and pursue exciting research projects under his guidance. Your scientific enthusiasm has been very inspiring from the very first day. I deeply appreciate the time and efforts you invested in me, leading me closer to the scientist I aspire to be. Importantly, thank you for striving to be a real mentor and not just another scientific supervisor. If I had to do it all again, I would still choose your lab.

Next, I want to thank the members of my thesis advisory committee, **Prof. Dr. Benedikt Brors, Dr. Inigo Martincorena**, **Dr. Jan Korbel**, and **Prof. Dr. med. Carsten Müller-Tidow,** for the valuable scientific input and interesting discussions. I really enjoyed every TAC meeting. Additionally, I sincerely thank **Prof. Dr. Nina Papavasiliou** and **Dr. Judith Zaugg** for taking the time to join my PhD defense committee.

Moving to the HSC-mutagenesis crew, I owe a very big thanks to **Dr. Megan Druce,** whose PhD work has set a solid basis for mine. Thanks for the time you devoted to me in my early stages; you really taught me a lot. Working with you was always fun and I would have definitely loved to have you around for longer. Thanks also to **Viktoria Flore** for spending her MSc thesis time tirelessly working on the project. I missed late-night Slack messages after you left. Finally, thanks to **Dr. Alex Cagan** for his general contribution to this work and all the time he has taken to answer all my questions.

Thank you to the person who gets excited with uncorrelated metrics, **Dr. Charles Dussiau.** I am thrilled that you decided to join the stochasticity project and that I have gotten to work with you. Thanks for your infectious scientific enthusiasm and for always keeping cool when things don't work. I truly cherish everything you taught me, and it is a lot. You are a great scientist, and I hope to work with you again in the future.

A huge thank you to **Melanie Ball**, who, apart from supporting me in every possible aspect of lab reality also became my first friend in Heidelberg. Thanks for taking special care of my training with mouse-shaped marshmallows and later for assisting in every experiment of mine when I transitioned to real mice. This experimental support that you unconditionally provided to everybody truly reflects your personality. Therefore, I want to extend my appreciation for all

the times that you supported me outside of the lab, too, and I hope I have been at least half as good a friend to you as you have been to me.

Very big thanks to my PhD-sibling, **Esther Rodriguez Correa**, with whom I had the pleasure of sharing this journey. Additionally, sharing the office with you made the days brighter, even the tough ones. Thanks for being the lab's rock and always willing to help. But even more, thanks for all the fun times outside of it, especially the most dangerous ones. I hope we will continue making nice memories together in places far, far away.

Thanks, of course, to "my bro", **Ian Ghezzi.** It has been even more enjoyable since you joined the lab. Thanks for all those long experiments you signed up for, especially during your first weeks, and your eagerness to learn everything quickly. Also, thanks for ensuring we always have good coffee in the office and for all the deep conversations we've shared.

The early post-Covid era was perhaps the happiest, marked by much teamwork and re-acquaintance with a more social lifestyle. Thanks to **Theo Aurich** for all the great energy he brought inside and outside the lab and for hosting great culinary events in his place. **Robin Berner** and **Dhyani Shah**, it was great having you around as well, even for a little while.

Nevertheless, the Milsom lab has always been unique in spirits. Thanks to all the additional members with whom our times overlapped, even partially: **Dr. Susanne Lux, Dr. Ana-Matea Mikecin, Dr. Ruzhica Bogeska, Dr. Jeyan Jayarajan, Dr. Marleen Büchler-Schäff, Julia Knoch, Helene Foissner, Selin Erdogru, Lena Bognar, Sena Alptekin, Sercan Öz** and **Lina Merg**. Thanks for your help and support, and I am happy I learned something different while working with each one of you. I would have never imagined that early morning wake-ups would be so much fun if it wasn't for all of you.

Special thanks also to the lab bench neighbor and world traveller, **Tasneem Cheytan**. I am deeply grateful that I got to know you and become your friend. Chats with you are always soothing. Thanks for all the fun breaks in the lab and for tolerating all the distractions I was causing while you were in the middle of some reaction because "that was my last experiment". Importantly, thanks for all the beautiful moments away from the lab, and I hope we will collect even more of them in the next months.

Thanks, of course, to the bigger **HI-STEM** lab family. It has been amazing working around all of these talented people. Credits to **Prof. Dr. Andreas Trumpp** for creating such an environment. In addition, big thanks to **Dagmar Wolf** and **Erika Krückel** for dealing with everybody's scary bureaucratic procedures.

I cannot leave aside all the DKFZ core facilities that made my work much more manageable. Special thanks to the **Flow Cytometry** team, **Dr. Steffen Schmitt, Dr. Marcus Eich, Florian Blum, Tobias Rubner** and **Klaus Hexel,** for their assistance with the sorter setups and all of

their advice. Additionally, big thanks to the **NGS,** and **Omics IT and Data Management core facilities** for all their insights and support. Finally, a shoutout to the **Barriere D animal caretakers**, who take daily care of a large number of mice for the sake of our science.

In this last part, I want to devote some special appreciation space to those who built my supporting mechanism outside the lab. First of all, thanks to **Eren**. Even though you were among the first people I met during our PhD selection round, I would have never imagined that we would also become flatmates. I am grateful for all the laughs, the wine-and-therapy sessions and all the different ways you can cook your potatoes. Credits also to the 4G team: **Anna, Elena** and **Danai** for all the «τσάι και συμπάθεια» (tea and sympathy) sessions to manage stress levels.

I will always be immensely thankful to my family. **Μαμά και μπαμπά**, η λέξη «ευχαριστώ» είναι πολύ λίγη για να αποτυπώσει την ευγνωμοσύνη που νιώθω για όσα έχετε κάνει για μένα. Ευχαριστώ που με μάθατε να μην παραιτούμαι και που υποστηρίζετε διαρκώς κάθε απόφασή μου, ακόμα κι αν αυτό στο παρελθόν σήμανε να ζήσω μακριά σας. Επίσης, ευχαριστώ τον αδερφό μου, **Σωτήρη**, για όλα τα χρόνια που με ανέχτηκε και που συνεχώς με στηρίζει με το δικό του τρόπο. Είστε όλοι σας υπέροχοι και μου λείπετε κάθε μερα.

Last but never least, the biggest thank you of all goes to my partner, **Guido,** for keeping me sane and making me laugh every single day. Thanks for making me a better person, Gui. I am really looking forward to our next chapter, whatever this may bring. It can only be awesome.

Table of Contents

SUMMARY I

ZUSAMMENFASSUNG III

ACKNOWLEDGMENTS VII

TABLE OF CONTENTS XI

1 INTRODUCTION 1

1.1 The fundamentals of ageing 1

1.1.1 The general biological aspects of ageing 1

1.2 The hematopoietic system as a model to study ageing 3

1.2.1 Adult hematopoiesis 3

1.2.2 Ageing hematopoiesis 4

1.3 HSC genomic integrity during ageing 6

1.3.1 Sources of genomic damage in old HSCs 7

1.3.2 Repair mechanisms in HSCs 8

1.3.3 Apoptosis 9

1.4 Somatic mutagenesis 11

1.4.1 Methods to study mutagenesis in normal tissues 12

1.4.2 Age-associated mutagenesis in human HSPCs 13

1.4.3 Clock-like mutational signatures 13

1.4.4 Clonal hematopoiesis and leukemic transformation 14

1.5 The bone marrow niche 16

1.5.1 Non-hematopoietic cellular components and molecular signals 16

1.5.2 Age-driven niche remodeling 17

2 AIMS (PROJECT 1) 19

3 RESULTS (PROJECT 1) 20

3.1 Deciphering mutagenesis in single murine HSC genomes by interrogating their clonal progeny 20

3.2 Detailed characterization of the age-associated mutagenesis in murine HSCs. 22

3.2.1 Aged murine HSCs display increased SNV burdens 23

3.2.2 No mutational hotspots are evoked during ageing 24

3.2.3 The endogenous mutagenic processes between murine and human HSCs are analogous 25

1.1 Examining the role of intrinsic apoptosis as genotoxic guardian of HSCs during physiological ageing 29

1.1.1 Selective blocking of intrinsic apoptosis in HSCs *in vivo* 29

3.2.4 Lack of apoptotic ability does not increase mutagenesis in HSCs 32

3.2.5 Apoptosis-deficient HSCs are governed by the same mutagenic processes as their WT counterparts 33
3.3 The impact of dormancy on the genomic integrity of HSCs 36
3.3.1 Dormancy as a barrier against somatic mutation acquisition 36
3.3.2 Mutational profiling suggests that mitotic latency protects the genome of dormant HSCs during ageing 39
3.4 Acceleration of cell division through HSC inflammatory response 42
3.4.1 Induce HSC activation with pI:pC 42
3.4.2 Exploring the actual genomic burden under inflammation in nano-scale 43
4 DISCUSSION (PROJECT 1) 46
4.1 Exploring the endogenous age-related mutagenesis in murine HSCs 46
4.2 The complex mutational landscape of aged HSCs informs about divisional history, cellular state and metabolic dependencies 47
4.3 HSCs do not trust their genomic integrity on apoptosis over time 49
4.4 Genomic stability is another advantage of dormant HSCs 50
4.5 Inflammation-driven HSC attrition is potentially not exerted through increased mutational burdens 51
4.6 Conclusions 52
5 AIMS (PROJECT 2) 54
6 RESULTS (PROJECT 2) 55
6.1 Heterogeneity in hematological ageing is largely unexplored 55
6.1.1 Generation of a comprehensive dataset to explore the intricacies of the ageing process 55
6.1.2 Phenotypic variance increases with age 57
6.1.3 Ageing heterogeneity expands in all major tissues of native hematopoiesis 61
6.2 Age-associated niche remodeling as potential influence of the overall phenotype 64
6.2.1 Emergence of a new heterogeneous adipocyte-progenitor population in the aged niche 64
6.2.2 Adipo-CAR3 cells display a distinct inflammatory transcriptomic profile 67
6.2.3 Formation of a Neutrophil-Adipo-HSC network in the aged bone marrow 69
6.2.4 The old-specific inflammatory network does not explain the distinct aged phenotypes 72
6.3 Lifelong inhibition of critical inflammatory pathways does not prevent hematological ageing 75
6.3.1 Inhibition of TNF and IL-1 is not beneficial for the hematopoietic system 75
7 DISCUSSION (PROJECT 2) 79
7.1 Minimal regulation during ageing exposes the hematopoietic system to randomness ... 79
7.2 Bone marrow reacts to stress by generating transcriptionally unique stromal populations mediating complex niche networks 80
7.3 Revisiting the role of IL-1 and TNFα: Inhibition of two critical ageing-related pathways fails to decelerate its emergence 82

7.4 Future perspectives 83
8 MATERIALS & METHODS 85
8.1 Mouse models 85
8.2 Animal treatment protocols and procedures 85
8.2.1 Label-retention assay 85
8.2.2 Tamoxifen treatment 86
8.2.3 Chronic polyinosinic : polycytidylic acid (pI:pC) treatment 86
8.2.4 Competitive transplantation assay 86
8.3 Sample collection 86
8.3.1 Blood collection 86
8.3.2 Bone marrow collection 87
8.3.3 Spleen collection and digestion 87
8.3.4 Tail collection 87
8.4 Clonal expansion of single LT-HSCs 87
8.4.1 Depletion of mature cell lineages 87
8.4.2 Single-LT-HSC sorting 88
8.4.3 *In vitro* clonal expansion of single LT-HSCs 90
8.4.4 Colony size and viability assessment 91
8.5 WGS library preparation 91
8.5.1 DNA extraction 91
8.5.2 DNA shearing with sonication 92
8.5.3 WGS library preparation and sequencing 92
8.6 WGS analysis 93
8.6.1 Read alignment 93
8.6.2 SNV calling 93
8.6.3 Indel calling 94
8.6.4 SV calling 94
8.6.5 Callable genome estimation and variant normalization 95
8.6.6 Variant annotation 95
8.6.7 Mutational profile and signatures analysis 95
8.7 Flow cytometry analysis 96
8.7.1 Analysis of peripheral blood 96
8.7.2 Bone marrow analysis 97
8.7.3 Analysis of splenic populations 98
8.7.4 Flow cytometry data analysis 99
8.8 Single-cell RNA sequencing and gene expression analysis 101
8.8.1 Serial sorting of hematopoietic populations 101
8.8.2 Bone digestion and purification of niche populations 102
8.8.3 Single-cell gene expression library construction 102
8.8.4 Gene expression analysis 103
8.9 Statistics and further data analysis 104

8.10 Code and file availability 105
CONTRIBUTIONS 106
BIBLIOGRAPHY 108
SUPPLEMENTARY 126
LIST OF ABBREVIATIONS 138
SELECTED PRESENTATIONS & PUBLICATIONS 142
Poster Presentations 142
Oral Presentations 142
Publications 142

1 Introduction

1.1 The fundamentals of ageing

Currently, world's population is consistently shifting towards higher age ranges. Estimates suggest that by the middle of this century, the fraction with individuals over 60 years of age will nearly double. This demographic shift is primarily driven by advancements in healthcare and technology, leading to increased life expectancy[1,2]. However, this longevity does not necessarily equate to an improvement in quality of life, since the healthspan -the period defining life in good health- does not increase proportionally[1,2]. As a result, elderly experience prolonged periods of poor health.

There are multiple challenges faced by the elderly. Morbidities detected with high prevalence in the old population include neurodegenerative disorders, diabetes, osteoarthritis, cardiovascular diseases and cancer -among others[2,3]. Furthermore, it is not uncommon for individuals to suffer from multiple co-morbidities simultaneously, which complicates treatments and management strategies[4].

Ageing is a highly individualised process, varying significantly from one person to another. This variation can be attributed to a combination of factors, such as genetic predispositions to disease, socio-economic status, lifestyle choices and lifelong experiences. Each of these elements plays a crucial role in determining the quality of life and health outcomes in the elderly years[2,3].

Studying ageing is crucial for several reasons. Understanding the fundamental mechanisms of this process and the factors contributing to its diversity can help in developing targeted interventions aimed at improving healthspan and overall well-being in the elderly. Furthermore, an ageing population has significant economic implications, influencing workforce dynamics, pension systems and healthcare costs[1]. By delving into the biological roots of ageing, researchers can uncover underlying causes of decline and disease, which is essential for designing effective treatments and preventive measures that can significantly enhance the quality of life.

1.1.1 The general biological aspects of ageing

Advancements in ageing research have identified twelve hallmarks that provide a comprehensive framework for understanding the complex biology underlying this process[5]. They are categorized in three groups: primary, antagonistic and integrative. The first category describes errors occurring at the molecular and cellular level and includes genomic instability, telomere

attrition, epigenetic alterations, loss of proteostasis and impaired autophagy[5]. The antagonistic hallmarks align with the concept of antagonistic pleiotropy, offering benefits in youth but proving detrimental in old age; and include cellular senescence, mitochondrial dysfunction and deregulated nutrient-sensing[5]. Finally, the integrative hallmarks reflect damage accumulated from the previous categories that can no longer be compensated, covering stem cell exhaustion, altered intercellular communication, inflammageing and microbiota dysbiosis[5] (Fig.**1.1**).

Genomic instability is a hallmark quite relevant to this thesis, that is the outcome of genomic errors due to exogenous or endogenous sources of damage. Moreover, repair mechanisms lose their efficiency with age, resulting in the accumulation of somatic mutations: single-base substitutions, structural variants and larger chromosomal rearrangements[5,6]. In parallel, the gradual shortening of telomeres after each cell division can trigger DNA damage response that can halt the cell cycle and induce cellular senescence[5,7,8]. Additionally, during ageing, epigenetic alterations such as altered DNA methylation patterns or erroneous post-translational modifications of histones can lead to aberrant chromatin configuration, able to influence gene expression and myriad downstream processes[5,9].

Another relevant hallmark to the topic of this thesis is cellular senescence which is triggered by extensive damage inside the nucleus. It is mainly manifested by cell cycle arrest, mediated by division regulators such as tumor protein 53 (TP53), cyclin-dependent kinase inhibitors 16 and 21 (p16 and p21) and retinoblastoma protein 1 (RB1); and by its senescence-associated secretory phenotype (SASP), permitting the release of inflammatory molecules that exert paracrine functions in the neighboring cells[5,8,10]. Additionally, the integrative hallmarks are of particular importance for this thesis. First and foremost, vertebrate ageing goes hand in hand with a low-grade systemic inflammation, simply termed "inflammageing", which is a general indication of frailty. This inflammation not only results from other hallmarks but also triggers them[5,11]. Furthermore, old tissues are characterized by poor regeneration capacity due to the exhaustion of their stem cells, which primarily reflects impaired differentiation and, in some cases, reduced numbers[5,12]. Finally, age-associated alterations in intercellular communications, which will also be discussed later in this thesis, further complicate functional networks by introducing noise and erroneous signaling[5,13].

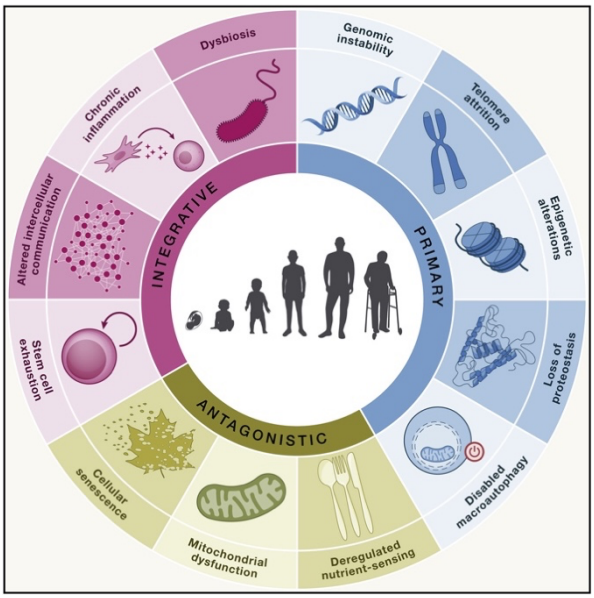

Figure 1.1. The hallmarks of ageing. Reprinted from López-Otín et a., Cell (2023); with permission from Elsevier.

1.2 The hematopoietic system as a model to study ageing

The hematopoietic system serves as an excellent proxy for ageing research. As the most extensively studied tissue in the body, it provides a rich repository of scientific data and insights that can be leveraged for more in-depth understanding. Furthermore, it is a hierarchical system, that owes its lifelong regeneration to a rare population of hematopoietic stem cells (HSCs). These cells possess a remarkable differentiation capability that permits the production of all the effector cell types found in the blood. This capacity to generate a wide array of cells from a single origin not only highlights the dynamic nature of the system but also its adaptability[14–16]. Importantly, thorough research has facilitated the development of high-purity isolation strategies for both stem and effector cells, making it an exemplary system for studying the broader phenomena of ageing[17].

1.2.1 Adult hematopoiesis

Adult hematopoiesis, the process describing the generation of new blood cells, starts around the time of birth as HSCs have established their permanent residence inside the bone marrow[18]. HSCs exert two unique critical functions: they self-renew to sustain the stem-cell reservoir throughout an individual's lifespan, and they engage in complex differentiation processes that produce the mature cells comprising blood's cellular compartment. These capabilities mark HSCs as the sole long-lived cells with multipotent properties within the hematopoietic system. As one descends, the hematopoietic pyramid that simplifies the system and the stem cells engage in lymphoid, myeloid or megakaryo-erythroid lineage programs, both self-renewal capacity and

multipotentiality decrease, illustrating a gradual specialization towards specific cellular functions[19,20].

In contrast to the highly proliferative nature of HSCs during development, adult HSCs predominantly reside in a quiescent state within the G_0 phase of the cell cycle[19,21]. This quiescent state, which is reversible, features reduced mitochondrial activity and a metabolic profile that is largely glycolytic[22,23]. Autophagy plays a crucial role in sustaining HSC survival during that period[24,25]. Importantly, quiescence is not a binary state; rather, multiple levels of quiescence likely exist. Moreover, quiescence and dormancy, which is a term for its prolongation, are critical for HSC function, since they preserve their self-renewal capacity and multipotentiality[19,21]. HSCs exit quiescence and engage in the cell cycle in response to homeostatic needs or external stimuli, such as infections[26,27]. This ability to switch from one state to another underscores their adaptive ability to the organisms' needs.

The HSC population is divided into long-term HSCs (LT-HSC) and short-term HSCs (ST-HSC). LT-HSCs exhibit the ultimate regenerative potential and remain highly quiescent, whereas ST-HSCs initiate the differentiation cascade as the primary multipotent progenitors. This hierarchical relationship is defined by LT-HSC giving rise to ST-HSCs. In murine systems, the distinction between them relies on the CD34 marker, which is not expressed by LT-HSCs. In contrast, all human HSPCs express CD34; therefore, isolation strategies differ across the two species. Murine HSCs, together with the downstream multipotent progenitors (MPPs), can be found in the LSK fraction of the bone marrow, marked by the absence of lineage-specific antigens and the expression of stemness surface markers such as Sca-1 and c-Kit. This expression pattern reverses as the differentiation progresses, with cells losing stemness markers and acquiring lineage-specific marker combinations[28].

1.2.2 Ageing hematopoiesis

The hematopoietic system deteriorates with age. Humans and most mouse strains display a remarkable increase in HSC numbers with age[29–31]. However, the expansion of these cells varies significantly among older individuals, as opposed to the regulated HSC levels observed in the young[31]. Furthermore, when HSC functionality is tested through transplantations, reduced regenerative ability and lack of multipotentiality are observed. More specifically, old HSCs favor myeloid and megakaryocytic production over lymphoid output[32,33].

HSCs constitute a diverse population, containing specific-lineage-primed stem cells. According to this dogma, ageing is characterized by an accumulation of myeloid-primed HSCs within the bone marrow, leading to a scarcity of lymphoid-primed HSCs[31–34]. It has also been suggested that the ability of HSCs to self-renew may align closely with myeloid-differentiation programs, explaining why extensive myeloid production and uncontrolled expansion of the stem cell reservoir overlap[35]. Alternatively, it has been proposed that while myeloid differentiation

proceeds by default, lymphopoiesis requires active suppression of myeloid-related genes to occur. Thus, ageing-related failures in gene regulation could further impair the lymphoid output by old HSCs[36].

The composition of the mature cell compartment also changes dramatically with age. As already mentioned, a notable decline in lymphoid differentiation from old HSCs eliminates B and T cell numbers. In addition, continuous thymic involution over time reduces even further the generation of new T cells, diminishing the elderly's capacity for adaptive immunity[35,37,38]. This reduction in adaptive immune response is linked to an increased susceptibility to infections in older individuals[38]. Simultaneously, there is an expansion in the fraction of the innate immune system, including granulocytes, monocytes and dendritic cells. This expansion often leads to a state of hyperactivation, resulting in the systemic release of pro-inflammatory cytokines, contributing to the phenomenon of inflammageing[11,39]. Chronic inflammation coupled with inherent myeloid bias increases the susceptibility of the aged population to hematologic malignancies, such as acute myeloid leukemia (AML)[40]. Furthermore, while red blood cell (RBC) numbers often remain stable, hemoglobin levels drop, hinting at problematic erythropoiesis. These observations coincide with the higher incidence of anemia observed among the elderly[41]. Finally, another age-related change is enhanced megakaryopoiesis, which leveraging from the systemic inflammatory status of the organism, can result in platelet hyperactivation, increasing the risk of clotting events[42] (Fig. **1.2**).

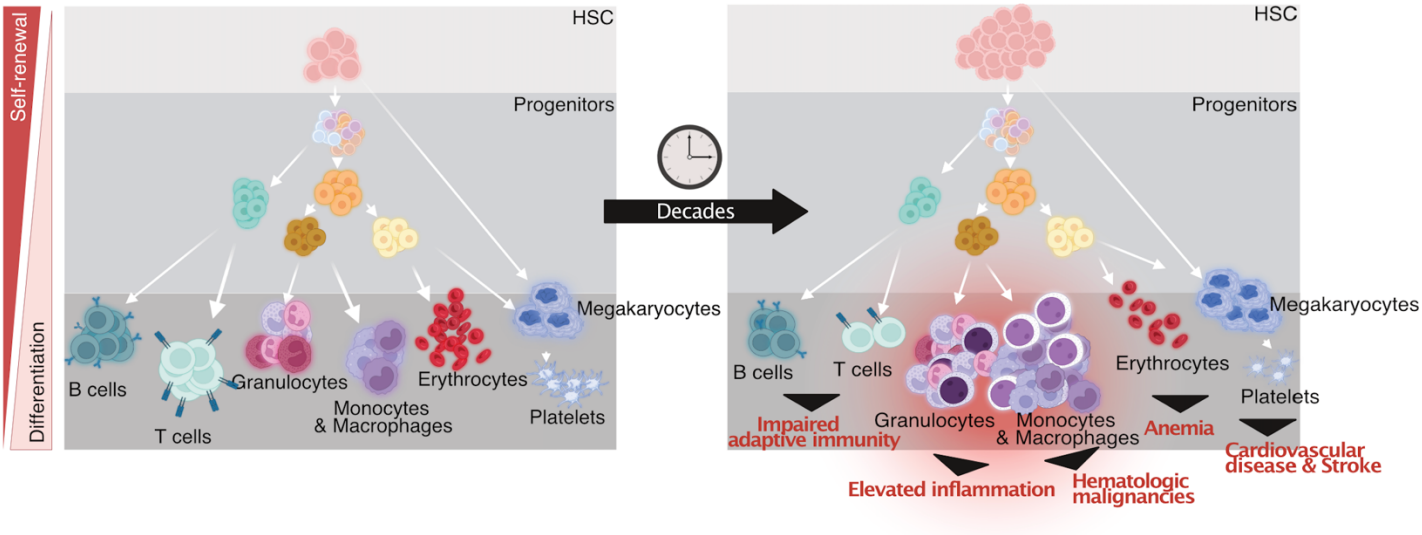

Figure 1.2. Simplified representation of normal adult and ageing hematopoiesis. Figure created with BioRender.com.

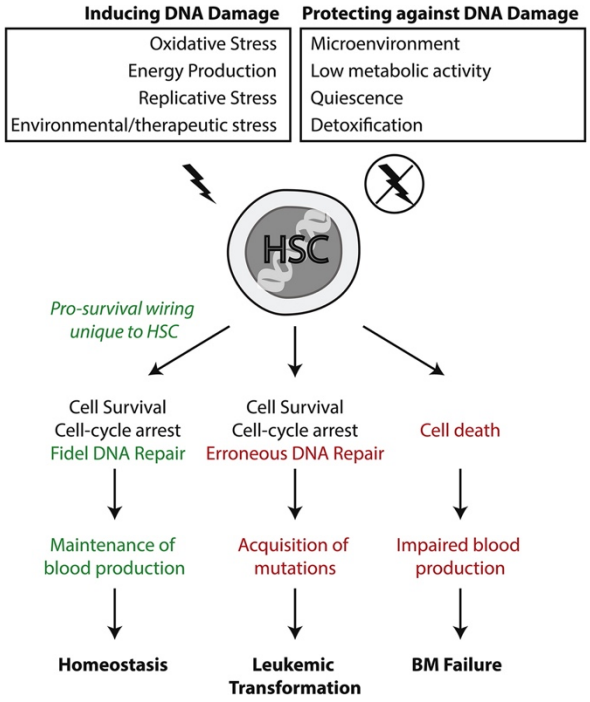

Figure 1.3. Potential outcomes of DNA damage occurring in HSCs. Reprinted from Bakker S.T & Passegué E., *Exp Hematol*, (2013); with permission from Elsevier.

1.3 HSC genomic integrity during ageing

The age-associated functional decline of HSCs is prominently marked by genomic alterations. DNA damage is the primary catalyst for genomic instability, which, if left unrepaired, can result in the accumulation of mutations, such as single nucleotide variants (SNVs), small insertions and deletions (indels), or larger structural variants (SVs)[6,12,17,43]. Maintaining the genomic integrity of HSCs is crucial because these long-lived cells are responsible for sustaining the hematopoietic system throughout life. Any compromise to their genomic stability can significantly impact their function and the system's overall health[12,17,43].

DNA damage events trigger the response of a complex machinery, referred to as DNA damage response (DDR). Depending on the severity of the damage, HSCs can either pause the cell cycle to facilitate repair or initiate the apoptotic pathway if the damage is irreparable. In the case that the damage meets the repair capacity of the cell, two scenarios are possible. The repair process may either proceed faithfully, preserving the genome's integrity or inadvertently introduce mutations[12,17,43]. Should these mutations prove detrimental to cell survival, apoptosis may be triggered retrospectively. DDR safeguard ensures that severely compromised cells do not persist and contribute to potential dysfunction or leukemic transformation within the hematopoietic system[12,17,43] (Fig. **1.3**).

1.3.1 Sources of genomic damage in old HSCs

Studies using mouse models with genetic deficiencies in key DNA repair components or telomerase genes have established the importance of genomic integrity for HSC function[17,44]. Consistent with their age-associated functional decline, old HSCs display elevated levels of DNA damage. This damage has been predominantly identified through the γH2AX marker and alkaline comet assays that reveal DNA strand breaks, and reflects the influence of both endogenous and exogenous genotoxic factors[45–47].

In addition to the telomere attrition discussed earlier, HSCs are exposed to numerous events of endogenous DNA damage daily due to routine cellular processes. A primary source of genomic instability is the generation of reactive oxygen species (ROS) within the cell. ROS are produced in metabolically active cells, as byproducts of oxidative phosphorylation (OxPhos). Interestingly, ROS formation has been linked with accelerated HSC ageing and functional exhaustion[48]. Another significant threat comes from endogenous metabolites like aldehydes, such as formaldehyde, that can induce chromosomal aberrations. Furthermore, studies with mice lacking genes for aldehyde detoxification and aldehyde-induced damage repair (*Aldh2, Adh5, Fancd2*) presented aged hematopoietic phenotypes with dysfunctional HSCs[49,50]. Moreover, replication stress, which represents the stalling of the replication fork due to factors such as repetitive DNA sequences, unrepaired lesions, or ribonucleotide misincorporation, also contributes to DNA damage in cycling cells[51]. In HSCs, this phenomenon is particularly consequential, since abrupt activation of dormant HSCs can significantly elevate DNA damage levels[27].

Although not everyone is exposed to strong exogenous damaging factors, they have attracted considerable research attention. Ionizing radiation (IR) is perhaps the most well-studied exogenous source. Patients undergoing bone marrow transplantation are often subjected to IR, due to the high sensitivity of the hematopoietic system to this treatment. IR causes extensive DNA damage in HSCs, triggering apoptotic cell death in an attempt to contain this damage. The primary mechanism of IR involves the production of ROS, leading to oxidative stress[52–54]. In addition to radiation, alkylating agents such as cisplatin and cyclophosphamide are frequently used as chemotherapeutic drugs that also have genotoxic effects. These agents function by adding alkyl groups to DNA, resulting in various DNA lesions, including cross-links, single-strand (SSB) and double-strand breaks (DSB)[53]. Moreover, the genotoxic nature of these drugs raises the risk of inducing secondary malignancies, such as leukemia[55].

In summary, DNA is constantly subjected to damaging events resulting from routine cellular processes and environmental stimuli. This damage, if left unresolved, can lead to a functional decline in HSCs, similar to that observed in advanced age, as well as disease emergence and malignant transformation. Understanding these dynamics is crucial for mitigating their impact and improving health outcomes.

1.3.2 Repair mechanisms in HSCs

Failure to accurately repair DNA damage in HSCs results in bone marrow failure and leukemogenesis. HSCs exhibit a unique response to damage compared to their progeny, characterised by slower repair and lower apoptotic thresholds. Moreover, the efficiency of the repair also depends on the cellular state of HSCs at the time of the damage[54].

The primary resolution for DSBs in highly quiescent cells like HSCs is the non-homologous end joining (NHEJ) pathway. This pathway initiates promptly after the damage, although it is error-prone and responsible for most structural aberrations in human cancers[43,54]. NHEJ begins when the Ku70 and Ku80 protein heterodimer attaches to the broken DNA ends. These proteins then recruit the DNA-dependent protein kinase, catalytic subunit (DNA-PKcs) and Artemis to process the break, which is eventually sealed by ligase IV[56]. NHEJ does not use a homologous template, making it operational throughout the entire cell cycle[54,56].

On the other hand, homologous recombination (HR) is a precise repair pathway that uses the homologous region from the sister chromatid to mend DSBs. Consequently, HR is limited to the S and G_2 phases of the cell cycle when sister chromatids are available[43,56]. The process starts when the DNA is carefully resected at the breakpoints to remove overhangs. The protein mediator Rad51 plays a pivotal role by forming a single-strand DNA filament, which then searches for and invades a homologous DNA sequence. With the aid of other proteins, such as the breast cancer susceptibility (BRCA) members, this invasion facilitates the alignment and exchange of genetic material between the damaged DNA and its undamaged homologous counterpart. Following the exchange, the DNA strands are extended and ligated, effectively repairing the break while maintaining the DNA's genetic integrity[56,57].

Other repair mechanisms address various types of lesions. Base excision repair (BER) targets and fixes small, non-helix-distorting base lesions caused by oxidation or methylation through a process involving glycosylases that recognise and remove damaged bases, followed by endonucleases, polymerases, and ligases that repair the gap[56]. Nucleotide excision repair (NER) addresses bulkier, helix-distorting lesions like those caused by UV radiation by excising a short single-stranded DNA segment containing the lesion and filling the gap with newly synthesized DNA[56]. Mismatch repair (MMR) corrects base-base mismatches and insertion-deletion loops occurring during DNA replication and recombination. MMR proteins detect and excise the errors, and the strand is subsequently repaired[56]. Lastly, translesion synthesis (TLS) allows DNA replication to bypass lesions that would otherwise stall the replication fork by using specialized TLS polymerases that can synthesise across damaged DNA, albeit with a higher risk of introducing mutations[56,58].

Taken together, DSB resolution distinguishes quiescent from active HSCs. Quiescent HSCs lack sister chromatids and rely primarily on NHEJ, which is imprecise. Additionally, it has been proposed that repair during quiescence faces further challenges due to low transcription levels,

which results in insufficient expression of necessary repair components[46]. In contrast, cycling HSCs can employ both NHEJ and HR to ensure faithful damage resolution[59].

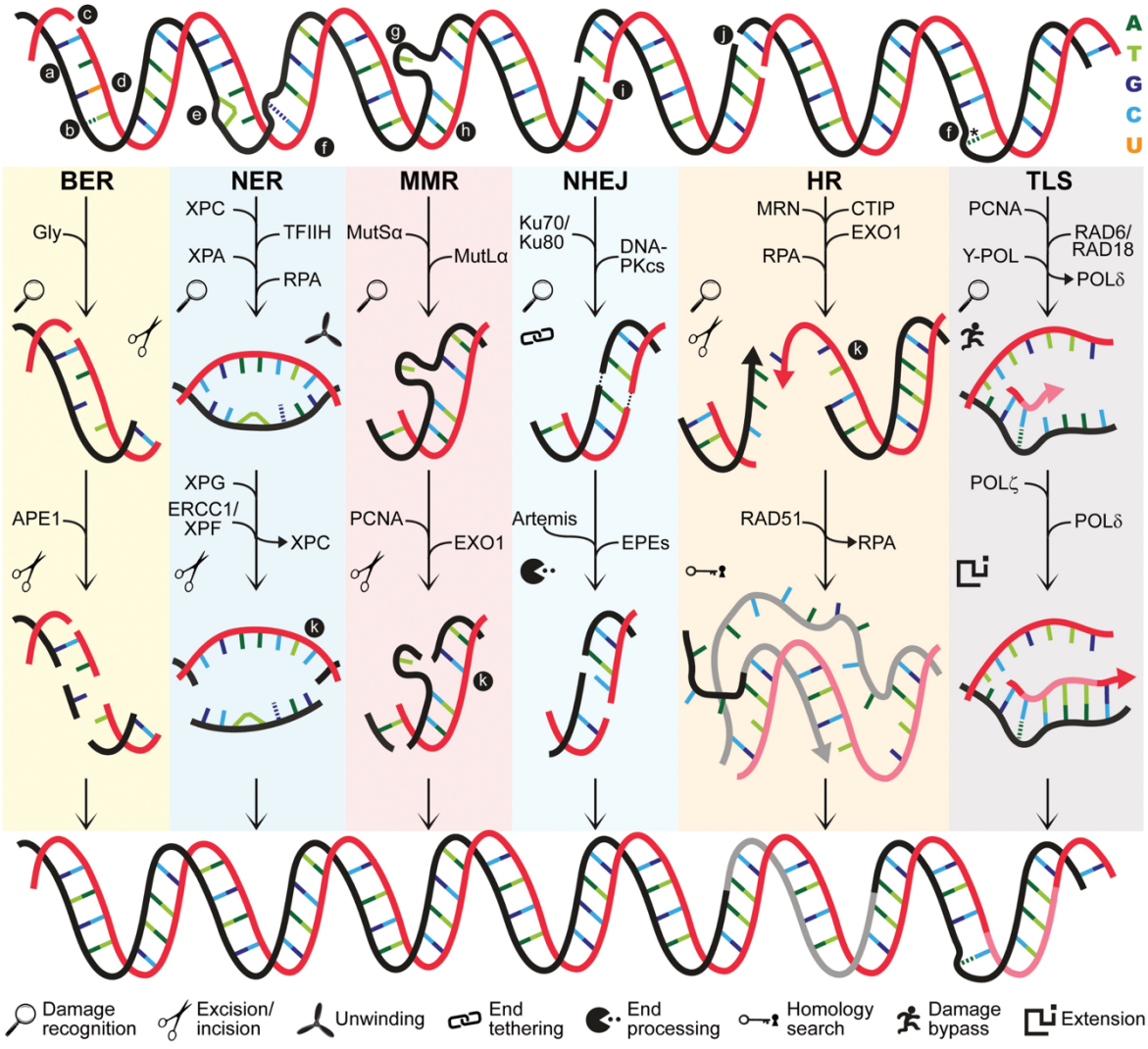

Figure 1.4. Main DNA repair pathways. Adapted from Vitale, I. et al., *Mol Cell* (2017)[56]. Reprinted with permission from Elsevier.

1.3.3 Apoptosis

Apoptosis is a type of programmed cell death that is genetically regulated and crucial for maintaining tissue homeostasis during development and adulthood[60]. It often serves as an anti-tumor mechanism, systematically eliminating cells that have sustained extensive damage or have the potential for malignant transformation[56,60,61]. By doing so, apoptosis ensures the removal of

cells that threaten tissue integrity[56,60]. Apoptosis acts through two main pathways: the intrinsic and the extrinsic.

Intracellular stressors, including genotoxicity, trigger the intrinsic apoptotic pathway, regulated by the B-cell lymphoma-2 (Bcl-2) family of proteins[60,62]. The initial death signal is transmitted by members of the BH3-domain-only subfamily, which includes BID, BAD, PUMA and NOXA[60,62]. These factors activate the pro-apoptotic proteins BAK and BAX, which then migrate to the mitochondrial membrane and initiate its permeabilisation. Mitochondrial permeabilisation releases cytochrome C into the cytosol, triggering apoptosome formation and subsequent activation of effector caspases, such as Caspase-3 (Cas3), which catalyse cell death[60,62]. The result is cell shrinkage, chromatin condensation, fragmentation and blebbing. The process concludes with the formation of apoptotic bodies containing cellular remnants that attract phagocytes[60].

Extrinsic apoptosis, on the other hand, responds to extracellular stress signals that bind to death receptors. These signals include tumor-necrosis factor α (TNFα) or the Fas-ligand (FasL), which bind to their respective receptors, TNF receptor I (TNFR1) and Fas (CD95). This pathway is mitochondria-independent. Upon receiving death signals, initiator caspases such as Cas8 and Cas10 are activated. These, in turn, are responsible for activating effector caspases -Cas3, Cas6 or Cas7- to mediate cell death[60].

A variety of signals can initiate apoptosis. In HSCs, intrinsic apoptosis is crucial for regulating the size of the stem cell reservoir. This was evidenced by an enlargement of the HSC population after overexpression of the Bcl-2, which blocks apoptosis[63]. Additionally, HSCs are considered particularly sensitive to genotoxic damage, an intracellular signal that prompts intrinsic apoptosis. This sensitivity ensures that HSCs preferentially undergo apoptosis rather than risk the genomic integrity of the entire system[52,64,65].

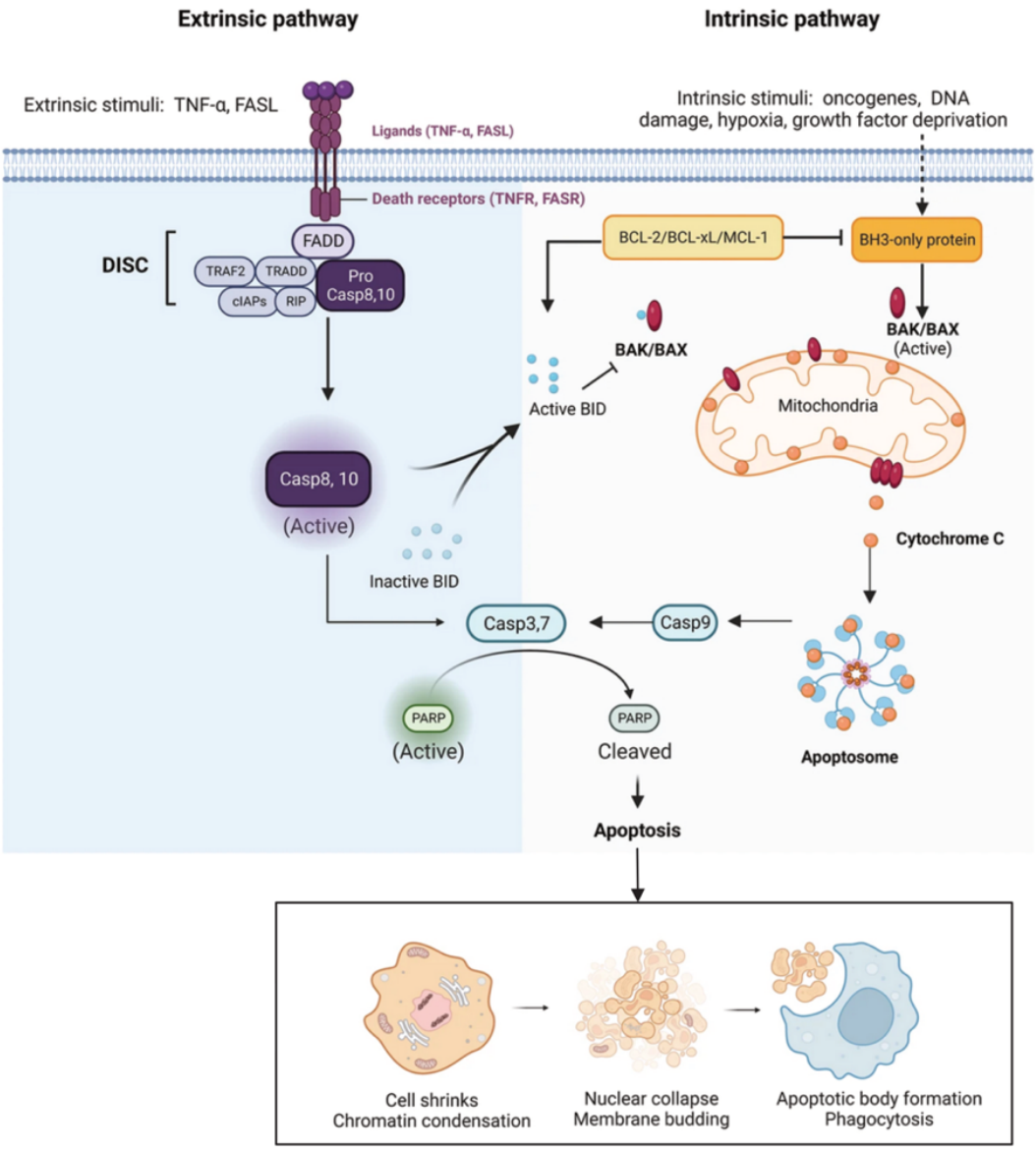

Figure 1.5. Extrinsic and intrinsic apoptosis. Adapted from Park, W. et al., *Exp Mol Med* (2023)[60]. Reprinted under a Creative Commons Attribution 4.0 International License: http://creativecommons.org/licenses/by/4.0/

1.4 Somatic mutagenesis

In multicellular organisms, random mutations occur in each postzygotic cell due to inefficient DNA repair or during replication. These mutations are acquired independently across different cells, leading to tissue mosaics[6]. Over time, repeated DNA damage encounters result in a buildup of somatic mutations. Although most of these mutations are neutral and do not affect cellular homeostasis, some can confer selective advantages to the carriers, leading to clonal expansions within the tissues. In contrast, others may contribute to dysfunctions and disease emergence[6].

Therefore, understanding the mutagenic impact of ageing is crucial for comprehending the progression of age-related changes and disease at the genomic level.

1.4.1 Methods to study mutagenesis in normal tissues

The majority of random somatic variants acquired in cells over time are usually unique to their carriers, or they may be shared among a few cells of the same tissue. Consequently, when a large population of cells is examined, each variant is represented by very low variant allele frequencies (VAF). In contrast, germline or somatic mutations that occur early during the development display higher VAFs. Similarly, driver mutations in malignant entities also present high VAFs due to the clonal nature of cancer. Based on this, addressing whole-genome mutagenesis in normal tissues has been quite challenging[61,66].

Bulk approaches such as whole genome sequencing (WGS) or whole exome sequencing (WES) detect variants with high VAFs, making them practical tools for the interrogation of malignant clones[66]. These methods have also been applied to stem cells cultured *in vitro* to generate single-cell derived clones for subsequent WGS or WES analysis[67,68–70]. In HSCs, single-cell transplantations further enable clonal production *in vivo*, allowing sufficient cellular output for genomic interrogation[49]. Additionally, the clonal progeny of intestinal stem cells can be studied thanks to the architecture of colonic crypts, each derived from a single stem cell. Laser-capture microscopy techniques are instrumental in isolating specific crypts from tissue slides[71,72]. A significant advantage of assessing mutational burdens of single cells by interrogating their clonal progeny is the deep sequencing readout offered, which can yield more robust results[73]. However, these approaches do not apply to postmitotic cells[74].

Alternatives like duplex-consensus DNA sequencing (DS) and whole genome amplification (WGA) are available for cells that lack proliferative capacity[75–77]. DS tags each DNA strand with a unique barcode or molecular identifier (UMI), allowing for the aggregation of molecules with the same tags to establish a consensus sequence. Only variants present in the consensus sequences of both strands are considered genuine mutations. This method offers meagre error rates and accepts low DNA inputs but does not provide single-cell resolution as it averages the mutational burden across many molecules[77]. Conversely, WGA attempts to address the division limitation and achieve single-cell resolution by amplifying a single genome using random primers and highly processing polymerases before standard library preparation. However, this strategy includes errors introduced by the polymerases during the primary amplification that are perceived as true mutations[75,76].

Significant technological advancements continue to enhance the methods used to study mutagenesis in normal tissues. Library platforms, sequencing strategies and computational tools are becoming increasingly sophisticated, enabling the examination of complex genetic questions with greater precision. However, currently, the most effective approach for in-depth study of

HSC genomes involves the interrogation of clonal progeny. This method has provided substantial insights into the age-associated mutagenesis in human HSCs, revealing how somatic mutations influence HSC clonal dynamics.

1.4.2 Age-associated mutagenesis in human HSPCs

Over time, mutagenesis occurs continually within somatic genomes, yet it exhibits tissue-specific patterns[6]. The interrogation of single HSCs from healthy human donors has confirmed that the accumulation of somatic mutations occurs steadily. The primary type of mutations detected is SNVs, with an accumulation rate of approximately 15 SNVs per genome per year. Indels also follow a similar trend, although their rate is significantly slower, with about 0.71 indels fixed per genome per year. More complex structural rearrangements are generally not observed during normal ageing[68,69].

Interestingly, despite the differences in DNA damage resolution methods, HSCs display mutational burdens comparable to those observed in their multipotent progenitor (MPP) progeny[68,69]. However, the mutational burdens exhibited by mature blood cell types can vary, depending on the role of each population. For example, granulocytes show similar SNV burdens to HSCs, suggesting that despite the multiple divisions they undergo during differentiation, they do not accumulate additional variants[74]. On the other hand, lymphocytes typically display higher mutational burdens than HSCs, a phenomenon attributed to somatic hypermutation (SHM) responsible for the diversity of their antigen receptors[78,79].

While it has been established that hematopoietic stem and progenitor cells (HSPCs) continue to acquire mutations over time -even without underlying pathologies and related treatments- the basal mechanisms driving this accumulation remain unclear. Further research is therefore necessary to elucidate why these changes occur naturally.

1.4.3 Clock-like mutational signatures

Mutational signatures are distinctive patterns of mutations that accumulate in a cell's DNA, providing insights into the underlying processes contributing to its mutational landscape. These signatures can arise from various sources, such as replication errors, environmental exposures, or engaging in specific DNA repair pathways[80–83]. Although signatures have been identified for all types of mutations[80,84,85], single-base substitution (SBS) signatures are more frequently used. These patterns are deciphered by analysing the trinucleotide context of substitutions – consisting of the point mutation and its adjacent nucleotides, across 96 possible combinations. Essentially, these signatures manifest as distinct distribution patterns across the 96 combinations[82]. The

Catalogue of Somatic Mutations in Cancer (COSMIC) is a central repository that collates detailed information on described somatic signatures in human cancer and normal tissues[86].

Mutational signatures often exhibit tissue-specific behaviours that reflect unique mutagenic influences to each cell type or tissue. For instance, specific signatures may be prevalent in skin cells due to exposure to ultraviolet light (UV), whereas others might be more common in lung tissue due to cigarette smoke[82]. These findings highlight the role of external and internal factors in shaping the mutational landscape of different cells. In normal human HSPCs, three main mutational signatures appear consistently active over time: SBS1, SBS5 and HSPC signature. These signatures are described as "clock-like", referring to their characteristic to accumulate mutations in a predictable, time-dependent manner[68].

SBS1 consists of C>T transitions at CpG islands of the genome, where cytosine is typically methylated. This signature reflects the spontaneous deamination of 5-methyl-cytosine (5-metC), substituted by a T after a round of cell division. Hence, SBS1 is considered a mitotic clock and can be used to track the divisional history of a cell[82,87]. In contrast, SBS5 is a ubiquitous signature, but its origin remains enigmatic. Its distribution presents a variety of substitutions without distinct peaks, justifying its term as a "flat" signature[82,87,88]. It has been suggested that SBS5 likely reflects endogenous routine cellular damage or biological noise[87]. Unlike SBS1 and SBS5, which are found in nearly all cell types, including the germline, the HSPC signature is exclusive to HSPC genomes and has not yet been catalogued in COSMIC. It was initially identified by Osorio et al. in adult HSPCs from healthy human donors, but its contribution in cord blood HSPCs appears minimal. The HSPC signature also displays a clock-like behaviour, likely mirroring the cumulative genomic alterations stemming from stem cells' proliferation and metabolic activities[68].

In conclusion, studying the mutational landscapes and extracting the unique signatures from HSPCs provides valuable insights into the balance of mutagenic processes occurring within these cells. Repair mechanisms, cell division, and metabolism are crucial in shaping this balance, especially since HSPCs are largely shielded from external environmental factors. Investigating these signatures helps illuminate how HSPCs maintain their integrity and functionality amidst cellular turnover and reveals the dynamic nature of their state transitions between activity and quiescence.

1.4.4 Clonal hematopoiesis and leukemic transformation

The continuous accumulation of somatic mutations in human HSPCs contributes to the emergence of age-related clonal hematopoiesis (ARCH) or clonal hematopoiesis of indeterminate potential (CHIP)[61,69]. In this process, one or few HSPCs gain a proliferative advantage attributed to a somatic mutation, becoming dominant in blood cell production[61,69,89]. ARCH is diagnosed

after blood sequencing when mutations occur with VAFs exceeding 2%[61,69,89–92]. As recently reported, while multiple expanded clones typically manifest universally after the age of 70, the original mutations that cause their expansion appear much earlier in life but require time to reach detectable levels, explaining their prevalence in older populations[69,89].

Although ARCH arises without the immediate presence of hematologic malignancies, it consists a significant risk factor for the development of blood neoplasms, solid tumors and cardiovascular disease[61,93]. Aligned with the two-hit theory of cancer development, ARCH is characterised by driver mutations in genes like *TET2*, *DNMT3A*, *IDH1*, and *ASXL1*, which are often implicated in leukemias. These mutations usually affect epigenetic regulator genes that influence the self-renewal capacity of HSPCs, acting as the first hit. Downstream mutations in tumor-suppressor genes can then lead to leukemic transformation[89–91,93,94]. However, the role of ARCH in the development of malignancies in other organs remains elusive, underscoring the complexity of its implications for human health[61].

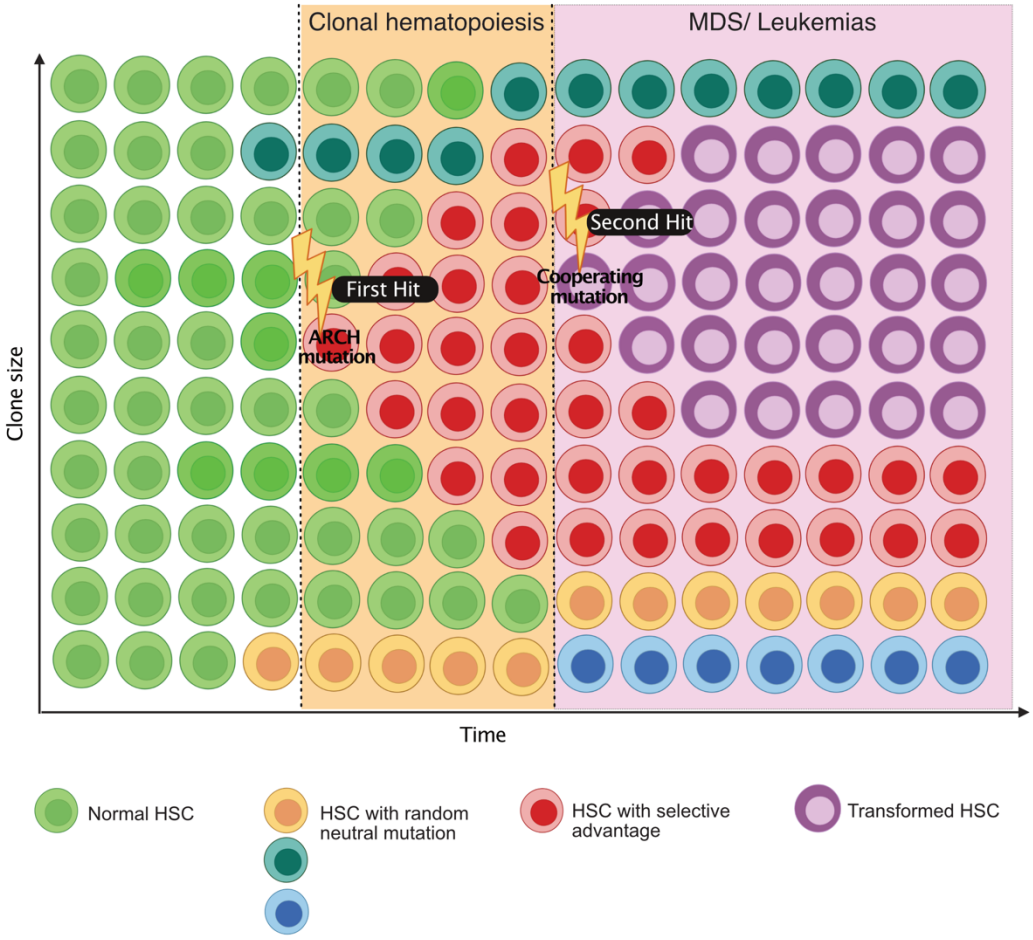

Figure 1.6. Clonal evolution of hematologic malignancies, with ARCH as an intermediate. The first hit represents a mutation that leads to uncontrollable expansion of the clone, such as the ones occurring in TET2 and DNMT3A genes. The second hit represents a cooperating mutation that facilitates transformation into myelodysplastic syndrome (MDS) and leukemias. Figure created with BioRender.com.

1.5 The bone marrow niche

The bone marrow is a critical anatomical environment that hosts adult HSCs; however, its role extends beyond merely housing these cells. It functions as an ecosystem where multiple cell types coexist and interact, influencing each other's functions. Historically, hematopoiesis and blood disorders studies largely overlooked the bone marrow niche or stroma. Yet, its influence on the function of the hematopoietic system has begun to be appreciated by research underlying its importance in blood health and disease[95,96].

1.5.1 Non-hematopoietic cellular components and molecular signals

The homeostatic bone marrow niche encompasses a complex network of hematopoietic and non-hematopoietic cell types, each playing a crucial role in orchestrating hematopoiesis[96,97]. Within this environment, there are multiple micro-niches, each specialised to support specific functions[96,98,99]. Central to the bone marrow niche are the mesenchymal stromal cells (MSC), a heterogeneous population that is believed to include the niche's stem cells. MSCs produce various niche components such as fibroblasts, osteolineage cells, adipocytes and chondrocytes[96,97,100]. Notably, MSCs are wrapped around blood vessels -arterioles and sinusoids- with the latter being the preferred micro-niche for resident HSCs, found closer to the endosteum. The characterisation of MSCs is still evolving, while attempts to describe it using mainly transgenic mouse models have resulted in the observation of CXCL-12-abundant reticular (CAR) cells, Nestin-GFP+ cells, Leptin-receptor positive (LepR+) cells and CD51+, platelet-derived growth factor receptor α (PDGFRα+) subfractions[96,97,100]. These subpopulations display distinct functions and differentiation potentials and occupy distinct micro-niches. Their relationship is also not unravelled yet[96,97]. Despite this complexity, MSCs are pivotal in regulating HSC maintenance, numbers and localisation. They exert these functions because they primarily produce critical cytokines such as CXCL12 and stem cell factor (SCF). They additionally produce angiopoietin 1 (ANGPT1), osteopontin (OPN), interleukin-7 and vascular cell adhesion molecule 1 (VCAM-1). These molecules support the regulation of quiescence, lymphopoiesis and homing of HSCs either directly or indirectly by controlling intermediate cell types[96,97,100]. It is important to note that the presence of various MSC subfractions in distinct micro-niches within the bone marrow underscores the nuanced nature of this environment. Their isolation and study effectiveness often depend significantly on the methodologies used to capture them (i.e., flushing of the bone or enzymatic digestion)[100].

Another critical cell type in proximity to HSCs is endothelial cells, lining the interior of the blood vessels. Endothelial cells communicate with HSCs both in direct contact and by soluble mediators. They produce lower levels of CXCL12 but support the system with SCF, Notch ligands such as Jagged-1, pleiotropin, ANGPT1 and vascular-endothelial growth factor A (VEGFA), promoting hematopoietic regeneration[96,97]. The sympathetic nervous system (SNS) also innervates the bone marrow niche. Adrenergic signals from SNS control the retention or

egress of HSCs in circulation, which displays circadian behaviour. Furthermore, if neuroprotective drugs are supplied to guide this rescue, the SNS can boost the system's regeneration after genotoxic stress, such as chemotherapy and irradiation[96,97,101]. Finally, osteo- and adipo-lineage cells are also essential niche components. They are likely the direct progeny of CARs, but they localise to different environments after the differentiation. Osteoblasts and osteocytes are found at the endosteum, while adipocytes are scattered around the marrow[97,100]. Although there is still a debate regarding their influence on HSCs, osteoblasts do not present concrete evidence that they impact HSCs directly. Instead, they focus on maintaining lymphoid progenitors. Conversely, adipocytes secrete adiponectin Q (ADIPOQ), which is a negative regulator of HSPC proliferation *in vitro*. At the same time, bones with a higher fat content usually do not support hematopoiesis, giving the impression of negative hematopoietic regulators[96,97,102].

The bone marrow niche is a dynamic environment with diverse micro-niches designed to support hematopoietic function. Although this section focused on the non-hematopoietic niche fraction, HSCs also engage in feedback loops with their progeny. Therefore, both hematopoietic and non-hematopoietic stromal fractions finely regulate hematopoiesis through physical contact and molecular signaling[97].

1.5.2 Age-driven niche remodeling

The ageing of the hematopoietic system involves complex interactions that extend beyond the cell-intrinsic ageing of HSCs. A significant aspect of this process is the influence of the niche, which changes with age and exacerbates many ageing-related phenotypes in blood formation[97].

One critical change observed in the ageing bone marrow is the altered localisation of HSCs. In young organisms, single HSCs are positioned close to sinusoids along with MSCs to optimize blood cell production and HSC maintenance. However, the sinusoidal network undergoes extensive remodeling with age, causing HSC clustering and mislocalisation[98,103,104] . The general vascular network within the bone marrow deteriorates with age, impairing the transport of essential nutrients and signals necessary for effective blood formation. This impairment is compounded by a decrease in vital signaling molecules such as OPN, CXCL12, SCF, and JAG1, all of which are crucial for maintaining robust hematopoietic communication and function[97,105].

Concurrently, the bone marrow experiences a shift in the differentiation potential of MSCs. With age, these cells increasingly favor the formation of adipocytes, which expand at the expense of active hematopoietic tissue. This adipogenic shift reduces the space available for hematopoiesis and leads to a decline in osteogenesis, which is critical for maintaining bone health[96,97,102]. Additionally, ageing bone marrow shows reduced neural innervation, vital for regulating the hematopoietic process. The decline in neural signals further disrupts the functionality of the hematopoietic system[97].

Parallel to these structural and functional changes, there is an increase in inflammatory activity within the bone marrow and throughout the body. Elevated levels of cytokines such as CCL5 or RANTES, TNFα, IL-1, and IL-6 are common. Within the bone marrow, these signals promote a shift towards myeloid cell production by HSCs. Generally, though, they are also typical of SASP, secreted by all the senescent cells of the body, increasing their systemic levels[105].

By dissecting these changes, we gain valuable insights into how the stroma regulates ageing hematopoiesis. Leveraging a deeper understanding of this matter can one day facilitate effective bone marrow rejuvenation approaches.

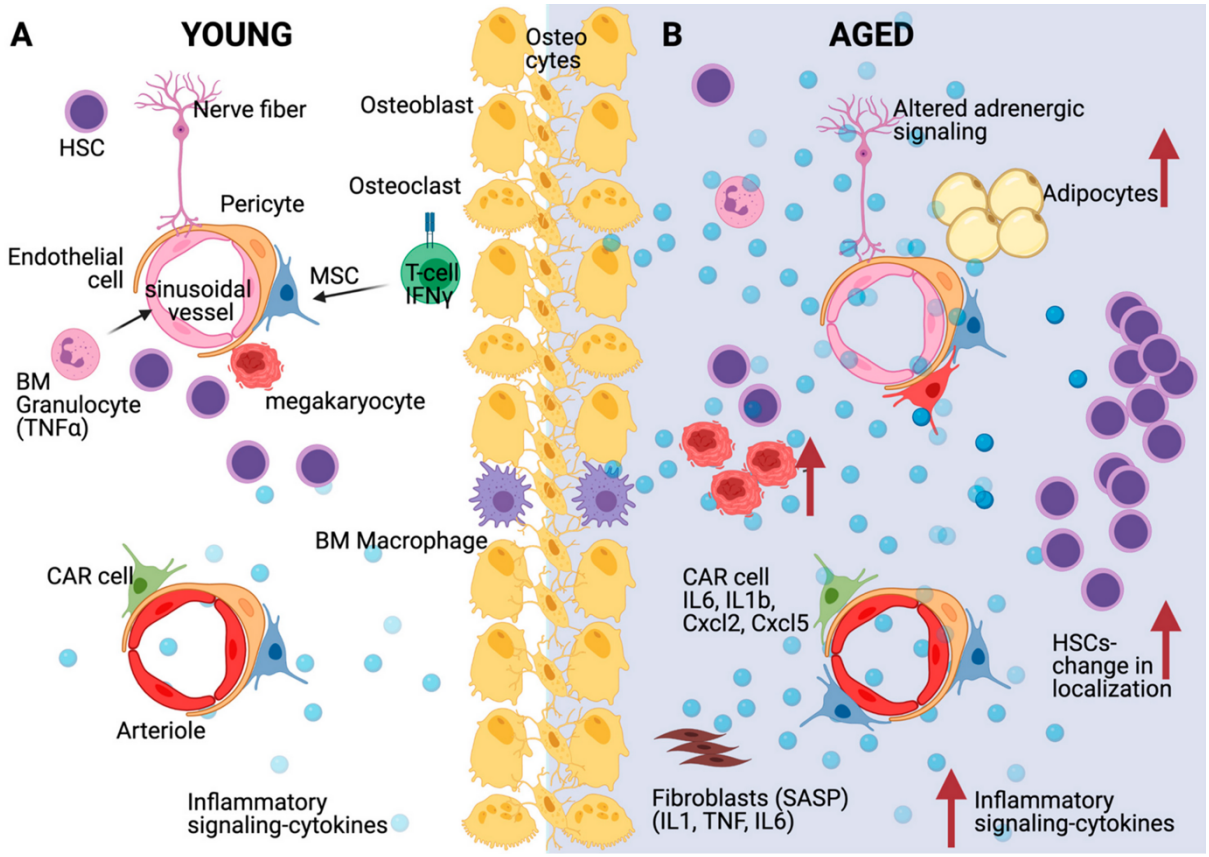

Figure 1.7. The bone marrow niche in A) young homeostatic conditions and B) advanced age. Taken from Bousounis, P., Bergo, V., & Trompouki, E., *Cells* (2021)[105]. Reprinted under a Creative Commons Attribution 4.0 International License: http://creativecommons.org/licenses/by/4.0/.

2 Aims (Project 1)

This part of my thesis aims to unravel the endogenous mechanisms that fuel the accumulation of somatic variants within the HSC population over time. Prior studies have meticulously assessed the mutational burdens harbored in human HSCs. Yet, the complexity of dissecting a precise mechanism within human subjects -owing to their variable genetic backgrounds and the environmental influences they are exposed to- poses a significant challenge. To offer a more controlled environment for investigation, I leveraged the power of mouse models, and I wished to address the following topics:

1. **To assess the age-related somatic mutation accumulation in murine HSCs.** Since this process in murine models had yet to be interrogated, I sought to establish a foundational understanding of somatic mutagenesis in murine HSCs during normal ageing. This "sanity check" step was crucial for validating the model as a reliable proxy for human HSCs, ensuring that my findings were grounded in a model that recapitulated the human phenotype.

2. **To investigate the role of apoptosis in managing mutational acquisition.** In pursuing this second aim, I focused on whether apoptosis serves as a protective measure to preserve genomic integrity by eliminating potentially harmful HSCs. Given the lifelong importance of HSCs, it was critical to understand if apoptosis acts as a gatekeeper, preventing damage propagation within the entire system.

3. **To understand the impact of cellular state dynamics on genomic integrity.** As a third aim, I directed my focus towards investigating the consequences of the cellular state transitions, from quiescence or dormancy to an active cycling state, for the HSC genome. It has been suggested that HSCs exhibit different susceptibilities to DNA damage depending on their state. Based on this, I hypothesised that they might also display distinct mutational landscapes.

4. **Acceleration of mutation acquisition.** Building upon the insights gathered from the previous aims, in this final objective I wished to explore the possibility of artificially accelerating the mutation acquisition in HSCs within a compressed timeframe. With this ambitious goal, I aimed to investigate whether I could enforce age-related mutagenesis on HSCs and understand its connection to age-associated stem cell attrition.

3 Results (Project 1)

3.1 Deciphering mutagenesis in single murine HSC genomes by interrogating their clonal progeny

To tackle the challenge of sensitively detecting variants within the rare population of HSCs, researchers over several years have leveraged the capacity of these cells to form clones in liquid cultures following single-HSC sorting[61]. Laboratories such as those led by Dr. Peter Campbell (Wellcome Sanger Institute, UK) and Dr. Ruben van Boxtel (Princess Maxima & Oncode Institute, Netherlands) have been at the forefront of employing this approach to investigate mutagenesis in human HSCs.

While studying human subjects offers invaluable insights into our biological makeup, it is important to acknowledge the presence of uncontrollable variables in such research, including exposures to different environmental stimuli and diverse genetic backgrounds, capable of skewing results. To focus on understanding the intrinsic mechanisms affecting the age-associated mutagenesis in HSCs under physiologic conditions, it was crucial to employ murine models. This option offered more controlled conditions in the study, as well as genetic manipulation. This approach builds upon the established methodology of studying mutagenesis in HSCs through their *in vitro* clonal progeny, adapted for murine models. As detailed in her thesis, Dr. Megan Druce dedicated significant efforts to optimise the pipeline of studies for the murine system and set a solid basis for the present study[106].

Briefly, the experimental workflow of this study involved the purification of bone marrow, followed by the sorting of single LT-HSCs (identified by the marker combination Lin- cKit+ Sca-1+ CD48- CD150+ CD34- and herein referred to as simply "HSCs") into individual wells of 96-well plates. The cells were cultured under hypoxic conditions for 10-14 days in a serum-free expansion medium (SFEM) that supported cell growth and stimulated differentiation towards the erythrocytic, megakaryocytic and myeloid lineages. Subsequently, DNA material was extracted from the resulting colonies for library preparation and WGS 150 bp paired-end (PE), achieving a minimum coverage of at least 30X (Figure **3.1A**). This level of coverage was carefully considered as the threshold at which the majority of variants can be reliably identified -particularly in the case of clonal samples- as reported previously by Alioto et al.[66] and corroborated by benchmarking analysis conducted in the aforementioned thesis[106].

To focus solely on somatic variants accumulated in HSCs, I also performed WGS on DNA extracted from the tails of each mouse. This step enabled the exclusion of potential germline variants from the analysis (Figure **3.1B**). Furthermore, to characterise only the variants that remain in the HSC pool *in vivo*, excluding those that arose during the culturing step, was

necessary[67]. This objective was easily achieved by implementing a VAF cutoff equal to 0.3[67]. The justification for this cutoff is shown in Fig.**3.1C**, which explains that a heterozygous somatic mutation present in an HSC prior to its isolation would be inherited by its entire colony, resulting in a VAF of 0.5. *In vitro*-occurred mutations, however, would be represented in sub-allelic fractions. For instance, a mutation arising during the first *in vitro* division would immediately reduce its VAF by 50%. Thus, setting the VAF cutoff between 0.5 and 0.25 effectively isolated those variants that represented the clone-initiating cell, allowing for a precise characterisation of the genetic landscape of HSCs *in vivo*[67]. The VAF distribution of SNVs after the application of the cutoff is provided in Supplementary Fig.**S1-S6**.

For somatic SNV detection, I employed *CaVEMan*, integrated within a comprehensive wrapper that further offers post-hoc filtering options (*cgpCaVEMan* wrapper)[107]. *CaVEMan* is an expectation maximimization (EM)-based tool that can predict somatic SNVs in each HSC clone by conducting a comparative analysis against the tail data and the reference genome (GRCm38 for *Mus musculus*)[107]. The identified variants listed in a variant call format (VCF) file were further filtered, as detailed in paragraph **8.6.2** of the Materials & Methods section, to ensure only high-quality calls. Subsequently, the number of variants retained after filtering was normalized to the callable genome size of each colony and finally scaled to the total length of the mouse genome (par. **8.6.5**, Materials & Methods).

For indels, I used *Pindel* wrapped within a comprehensive toolset as well (*cpgPindel* wrapper, v3.9.0)[108,109]. Utilizing a pattern growth algorithm, *Pindel* detects somatic indels through comparative analysis similar to *CaVEMan*'s, juxtaposing colony and tail WGS data and mouse reference genome GRCmm38[109]. The variants listed in the output VCF file underwent VAF and quality filtering as discussed in detail in the Materials & Methods section, paragraph **8.6.3**, with final normalization steps outlined in paragraph **8.6.5**, Materials & Methods.

Finally, I chose *Delly* for larger structural variants (SVs), including insertions, deletions, translocations, tandem duplications and inversions[110]. This tool employs a double-detection strategy based on the behaviour of the paired-end reads and split-read evidence[110] using short-read WGS data as template. *Delly*'s workflow, from execution to normalization of SV data per mouse genome, is detailed in paragraphs **8.6.4** and **8.6.5** of the Materials & Methods.

The aforementioned experimental and analytical methodology has been consistently applied throughout the entirety of this study.

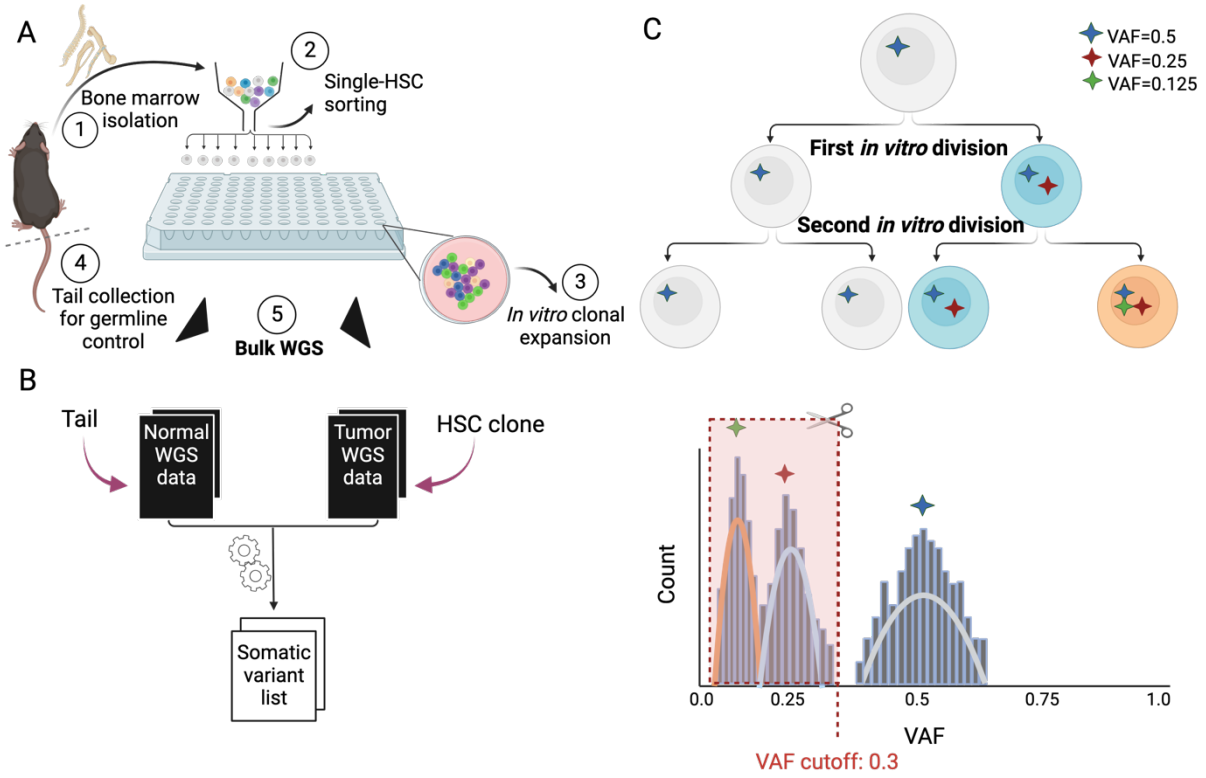

Figure 3.1. Workflow for the identification of somatic variants in normal murine HSCs. A) Experimental methodology to interrogate single murine HSC genomes through *in vitro* expansion. **B)** The analytical strategy for variant detection, mirroring techniques commonly used in cancer studies. Here, data from HSC clones were compared to a tail-derived germline control, treating the clones analogously to "tumor" samples to catalogue somatic variants unique to the HSC pool. **C)** The rationale behind the VAF cutoff of 0.3 that distinguished the variants existing in the initial clone-forming cells versus the ones emerging in the culture[67]. The figure was created with BioRender.com.

3.2 Detailed characterization of the age-associated mutagenesis in murine HSCs.

Previous investigations into age-associated mutagenesis within HSCs have posited a linear accumulation process, estimating the incorporation of approximately 15 SNVs per genome annually[68,69] alongside a slower accumulation of 0.71 indels per year[69]. Given the relative accessibility of human HSCs after their mobilization and blood collection, or even bone marrow aspiration, the characterization of age-related mutagenesis in murine HSCs has not been a focus of prior research. However, with the pivotal role of the mouse model in biomedical research and its particular relevance in this study, understanding the dynamics of somatic mutation acquisition with age in murine HSCs became essential and is thoroughly discussed in the following paragraphs.

3.2.1 Aged murine HSCs display increased SNV burdens

To explore the ageing mutational landscapes in murine HSCs, I analyzed colony-derived WGS data from young (8 months) and old (24 months) mice (Fig. **3.2A**). This data, acquired by Dr. Megan Druce[106], was collected from 4 colonies per mouse and for 3 mice per age group. Unfortunately, two colonies from the old group did not meet the quality control (QC) standards I set due to excessive duplication rates (>25%). Consequently, the study proceeded with a final analysis of n=12 colonies from the young group and n=10 colonies from the older group.

Similar to observations in human HSCs[68,69], older murine HSCs exhibited a notable increase in the number of SNVs accumulated in their genome. Building on the premise of a linear accumulation process, as previously supported by human studies[68,69], I calculated that approximately 3.7 SNVs are acquired by the autosomal genome per month, which translates to approximately 44 SNVs annually (Fig. **3.2B**). Despite the overall mutation burden in HSCs remaining modest, the SNV accumulation rate in mouse HSCs surpasses the one documented in humans[68,69], likely reflecting the inverse correlation between lifespan and somatic mutation accumulation rates observed across different mammalian species[72].

Old mouse HSCs did not exhibit a significant increase of indels in their genome (Fig. **3.2C**), contrary to patterns observed previously in humans[68,69]. This discrepancy leaves the question of indel accumulation during natural ageing in murine HSCs open for further investigation. Similarly, larger SVs were particularly scarce (Fig. **3.2D**). Taken together, these data underscore SNVs as the predominant mutation type amassed in the genomes of HSCs during natural ageing.

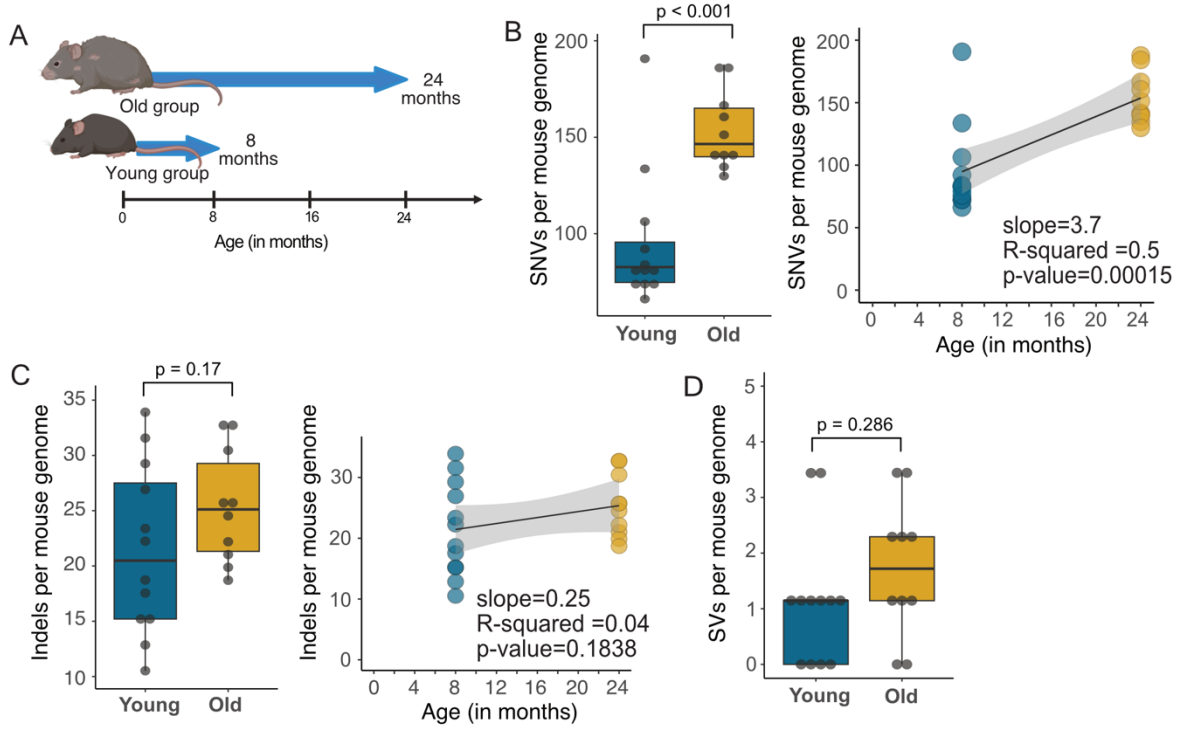

Figure 3.2. During ageing, murine HSCs acquire 3.7 SNVs per month. A) Overview of age groups. Created with BioRender.com **B)** SNVs were significantly increased in the old HSC genomes. Assuming a linear accumulation, linear regression analysis was performed to estimate the accumulation rate. The slope represents the number of SNVs acquired per month with statistical support indicated by the p-value directly on the plot and the 95% confidence intervals (CI) highlighted by the grey area. **C)** Age did not significantly impact indel frequency. **D)** Large SVs were particularly rare in the dataset.

Each dot in the figure represents an individual cell. Statistical analysis across panels B, C and D were conducted using Welch's t-test, with the p-value indicating statistical significance directly on the plot. Linear regression analysis was performed with the `lm()` function in R.

3.2.2 No mutational hotspots are evoked during ageing

To assess whether indels alter qualitatively with age, even though numerically, they remained stable, I inspected the types of indels accumulated in young and old HSCs. Regardless of age, the predominant indel types were deletions and insertions, with a negligible fraction being complex – an event caused by both an insertion and a deletion (Fig. **3.3A**). This finding further confirmed that the ageing process does not particularly influence indels.

Furthermore, the collective annotation of all the variants detected in the cells demonstrated that their majority occurs at non-coding regions of the genome, specifically in intergenic and intronic areas. Notably, this variant distribution remains unchanged with age (Fig **3.3B**). Among these variants, only 23 were predicted to exert tangible effects on the resulting transcripts or proteins. The impactful variants are displayed in Fig. **3.3C**; however, their scarcity precludes any substantive conclusion. In addition, a closer examination of SNV that accumulated significantly

with age, failed to identify any genomic regions subject to recurrent mutagenesis (Fig. **3.3D**). Collectively, these observations suggest that ageing does not predispose to specific mutational hotspots.

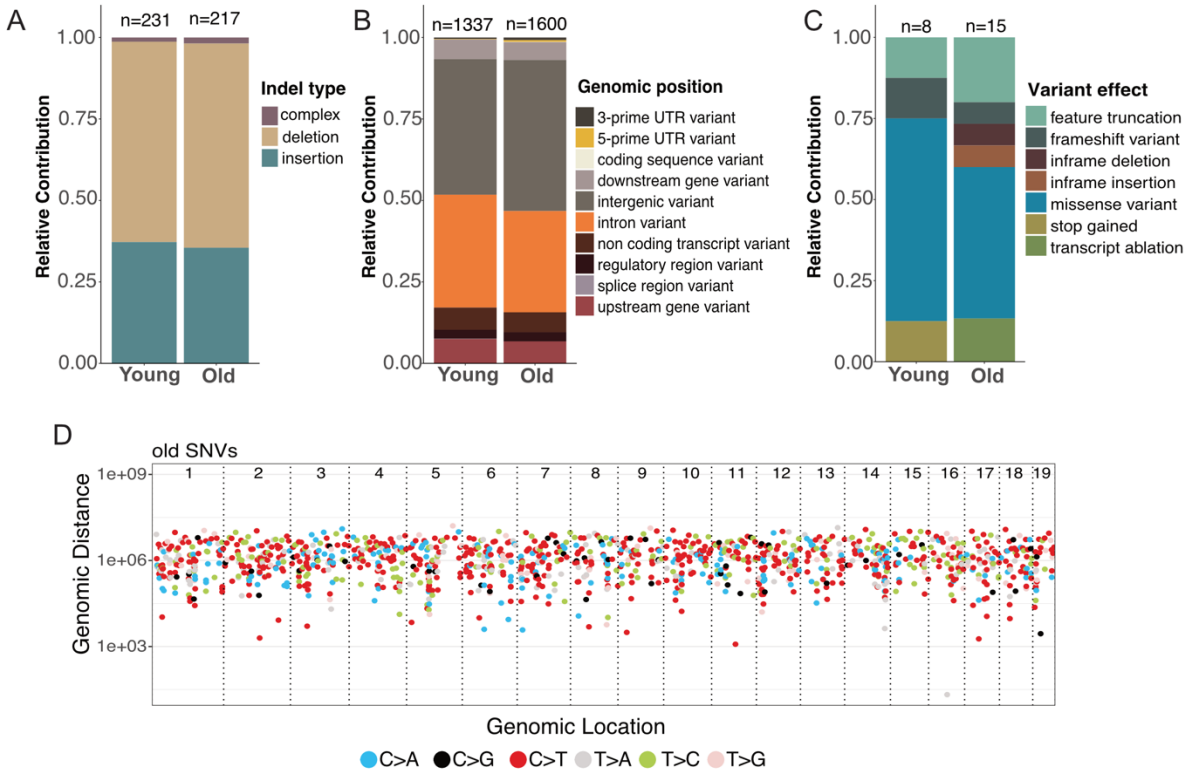

Figure 3.3. The genomic distribution of the variants is not influenced by age. A) Relative contribution of the different indel types detected in young and old HSC genomes. Analysis with chi-square test (p-value = 0.85) indicated no significant alteration with age. **B)** Annotation of all the mutation types detected in the cells, highlighting a predominant occurrence in non-coding regions. Analysis with chi-square test (p-value = 0.08) indicated no significant alteration with age. **C)** Identification of 23 variants with potential impact on transcripts or proteins. **D)** Rainfall plot illustrating the SNV distribution across autosomal chromosomes. Should an ageing-related hotspot emerge, it would manifest as a reduced genomic distance among a specific subset of variants.

3.2.3 The endogenous mutagenic processes between murine and human HSCs are analogous

To elucidate the underlying mutational processes contributing to the increased SNV load in old HSCs, I studied the mutational signatures within the dataset. These signatures represent distinct mutational patterns that can reflect specific mutagenic phenomena[82]. For this analysis, I merged the variants on a per-mouse basis and applied the *MutationalPatterns* R package[111,112] workflow. I began by assembling the mutational profile for each mouse by concatenating all the variants identified across their cells. This step considers not only each base substitution but also

the nucleotides flanking the resulting SNV, generating 96 different trinucleotide combinations, represented visually by trinucleotide plots. The trinucleotide plots provided in Fig. **3.4A,** though, depict the accumulated variants merged per age group to enhance visualization and facilitate comparison.

To mathematically dissect the mutational signatures composing the SNV profiles, I performed *de novo* signature extraction from the trinucleotide contexts using non-negative matrix factorization (NMF)[81113]. This extraction revealed three main signatures embedded within these profiles. Remarkably, one signature demonstrated significant similarity to one recently characterized in human HSPCs [68,88] (cosine similarity =0.87). The other two signatures did not match any known signatures and were thus designated as "SBSA" and "SBSB". Interestingly, the HSPC-like signature was more pronounced in the mutational profiles of the old group (Fig. **3.4B**), consistent with observations in old human HSPCs[68,114]. Additionally, SBSB was more prevalent in younger profiles, while SBSA was present in individuals across both groups. This observation suggests that both age-dependent and independent mutagenic processes are present in murine HSCs.

The fact that SBSA and SBSB did not show apparent similarities to previously reported signatures does not necessarily imply the discovery of novel patterns. It may rather indicate limitations in the algorithm's ability to distinguish signatures with minor contributions, which is often the case in normal tissues with low mutational burdens. To overcome this problem and further explore the nature of the two unidentified signatures, I proceeded with fitting known signatures into my dataset through bootstrapping[112]. After 150 iterations, the aforementioned HSPC signature, together with SBS1, SBS5, SBS8 and SBS18 from the COSMIC database,[80] established their presence in the dataset (Fig. **3.4C).** The patterns of each reported signature called are provided in Fig. **S7, S8**. First of all, the fitting confirmed the observations after the *de novo* extraction regarding the increase of the burden attributed to the HSPC signature (Fig. **3.4C, 3.4D**). Suppose the acquisition of HSPC mutations occurs in a linear fashion; the genome acquires 2.26 SNVs per month, annotating to 27 HSPC mutations annually (Fig. **3.4E**). In fact, this represents the majority of the yearly SNV accumulation. Next, SBS1 and SBS5 are two ubiquitous patterns that are active constantly throughout life. Specifically, SBS1 has been associated with the spontaneous deamination of 5-metC, which results in the fixation of thymine in the genome after a cell division, while the origin of SBS5 remains unknown[87]. Despite their clock-like nature, the absolute burden attributed to these signatures remained stable over time (Fig. **3.4D, 3.4E**), suggesting that their contribution to the mutational landscape of HSCs decreases with age (Fig. **3.4C**). Given SBS1's characterization as a mitotic clock[113], this observation likely underscores a tendency towards increased HSC quiescence with age[115,116]. Another signature of unknown origin, SBS8[80,82,86], often found in hematological studies[88] was detected in the dataset. Here, the SBS8 burden appeared significantly elevated in old HSCs (Fig. **3.4C**). Assuming that SBS8 also acts clock-like, it would account for 1.46 SBS8 substitutions per autosomal genome per month, equating to 18 SBS8 SNVs annually (Fig. **3.4E**). The last pattern

emerging in this dataset was SBS18, potentially indicative of ROS damage[80,82,86]. Intriguingly, young HSCs displayed a higher SBS18 burden than their old counterparts, likely suggesting variations in metabolic states (Fig. **3.4C**).

Collectively these data indicate that overall, the mutagenic processes affecting human and murine HSCs share similarities, encompassing age-dependent and constantly active mechanisms that contribute to the burdens of HSPC, SBS1, SBS5 and SBS8. Moreover, age-independent factors, likely reflective of differing metabolic states, are represented by SBS18. However, the main contributors of the old mutational landscape appear to be HSPC and SBS8, accumulating at a ratio of 3:2 of the total annual SNV burden.

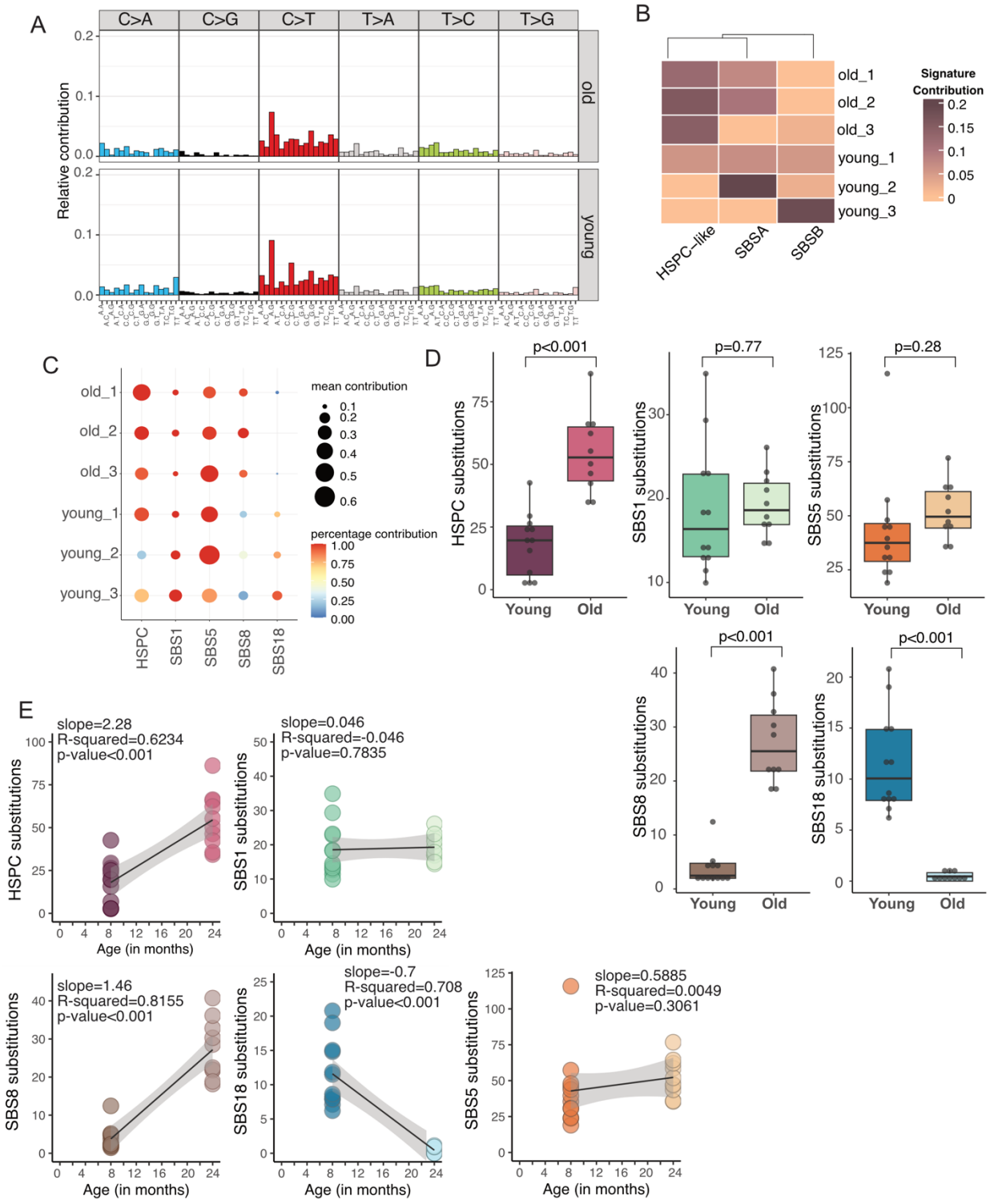

Figure 3.4. The aged mutational landscapes are composed of age-dependent and -independent signatures. (Legend follows on the next page)

A)Trinucleotide plots illustrating the integrated SNV spectrum of each age group. **B)** Heatmap showcasing the contribution of the three *de novo* extracted signatures (HSPC-like, SBSA, SBSB) to the mutational profile of each mouse. Each row represents an individual mouse. **C)** Dotplot summarizing the mean signature contributions across mice (rows), as determined by 150-run bootstrap fitting. **D)** Absolute numbers of SNVs attributed to each signature. Statistical significance across comparisons was assessed using Welch's t-test, with the p-values directly annotated on the relevant plots. **E)** Linear regression analysis using the `lm()` function in R to estimate the rates at which these signatures accumulate over time. Slopes indicate the SNVs accumulated per signature per month. The grey areas highlight 95% Cis, and the corresponding p-values are annotated on the plot.

3.3 Examining the role of intrinsic apoptosis as genotoxic guardian of HSCs during physiological ageing

Although the significance of apoptosis after stress-induced damage has attracted attention over the years, definitive conclusions regarding its role remain elusive. Furthermore, the mechanism's function in the absence of such strong stressors is not fully understood. It has been suggested that upon exposure to strong stimuli, such as IR, HSCs engage in the cell cycle with two possible outcomes: complete damage repair without accruing mutations or undergoing apoptosis[52]. Normal ageing exposes HSCs to numerous, albeit less severe, DNA-damaging events[27,45,46,52]. To determine if HSCs present low apoptotic thresholds even at homeostatic conditions, I blocked their ability to undergo caspase-dependent apoptosis.

3.3.1 Selective blocking of intrinsic apoptosis in HSCs in vivo

To disrupt the intrinsic-apoptosis pathway in HSCs, I used the Scl-Cre-ERT2 Bak $^{-/-}$ Bax $^{fl/fl}$ mouse model[117]. In this model, Cre recombinase is under the control of the Scl promoter, dictating expression in the very primitive hematopoietic compartment. At the same time, the ERT2 element triggers its expression after exposure to tamoxifen[118]. Cre expression results in the deletion of the homozygously floxed exons 2-4 of the Bax gene. Additionally, these mice were bred as complete homozygous Bak knock-outs (KO). Consequently, after administration of 20 mg/kg tamoxifen for 5 consecutive days, the concurrent KO of the pro-apoptotic factors Bak and Bax (hereafter referred to as Bak $^{-/-}$ Bax $^{\delta/\delta}$) inhibited intrinsic apoptosis in HSCs (Fig **3.5A**).

Anticipating that apoptosis offers genomic protection in stem cells; I hypothesized that Bak $^{-/-}$ Bax $^{\delta/\delta}$ HSCs would exhibit higher mutational burdens even at a young age, before the development of pathologies due to apoptosis deficiency could influence the results. Therefore, the Bak $^{-/-}$ Bax $^{\delta/\delta}$ mice were sacrificed at 8 months of age and compared against the wild-type (WT) young mice (Fig. **3.5B**). First of all, genotyping of HSCs confirmed successful Bax recombination in approximately 93% (51/55) of the sequenced Bak $^{-/-}$ Bax $^{\delta/\delta}$ colonies, as verified by inspecting the alignments on the *Integrative Genomics Viewer* (*IGV*)[119] (Fig. **3.5C).** Unrecombined colonies were not included in the analysis. Bak $^{-/-}$ Bax $^{\delta/\delta}$ mice showed increased

spleen size and white blood cell counts, indicative of hematopoietic cell accumulation, without affecting erythropoiesis (Fig. **3.5D**). Moreover, examination of the bone marrow via flow cytometry showed that the more primitive compartment that lacks lineage-specific markers (Lin- gate) was inflated in the Bak $^{-/-}$ Bax $^{\delta/\delta}$ mice compared to the WT, as shown after the t-distributed stochastic neighbor embedding (t-SNE) analysis (Fig. **3.5E**). Nevertheless, this Lin- inflation did not appear to be attributed evenly to all the premature populations. The LSK compartment identified by the markers Lin- Sca1+ c-Kit + containing the stem cells and the MPPs appeared significantly expanded, unlike the Lin- Sca1- cKit+ (LS-K) compartment containing the myeloid-restricted progenitors, which remained unchanged (Fig. **3.5F**). This observation suggests that the size of the LS-K population is not regulated by intrinsic apoptosis. Additionally, the inflation of the LSK compartment was partially driven by the increase in the HSC population, implying that the cells of interest were not eliminated by other cellular death mechanisms in the absence of intrinsic apoptosis (Fig. **3.5F**). Finally, the *in vitro* colony formation revealed that Bak $^{-/-}$ Bax $^{\delta/\delta}$ HSCs generated larger, yet similarly viable colonies compared to WT HSC, indirectly suggesting that the lack of apoptosis did not eventually lead to the attrition of the stem cells and the induction of proliferative senescence (Fig. **3.5G**). According to all the above, the Scl-Cre-ERT2 Bak $^{-/-}$ Bax $^{fl/fl}$ mouse model serves as a robust platform for investigating the role of intrinsic apoptosis in HSCs.

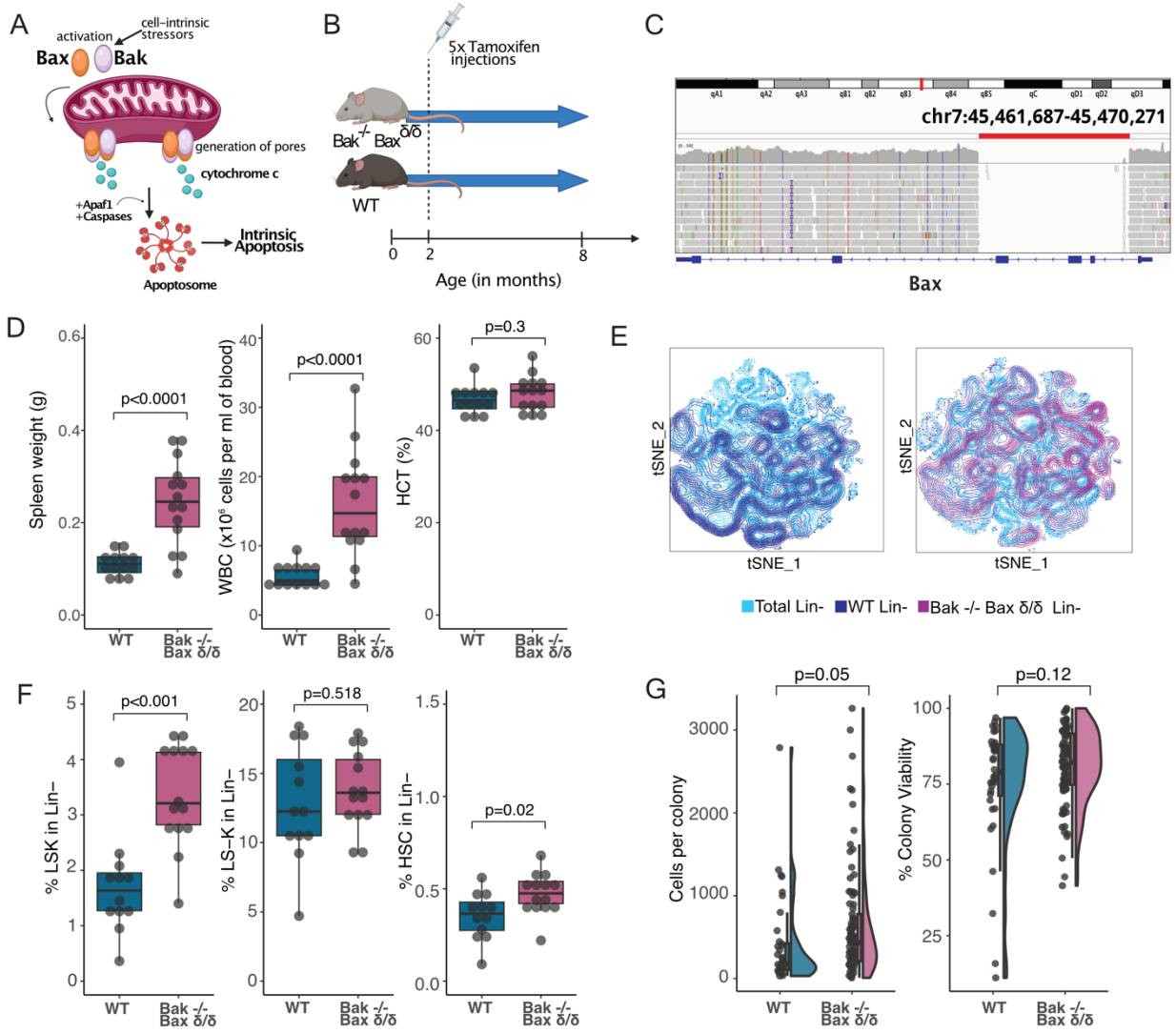

Figure 3.5. Phenotypic characterization of the Bak $^{-/-}$ Bax $^{\delta/\delta}$ mouse model. A) Representation of the cell-intrinsic apoptosis pathway initiated by the Bax and Bak proapoptotic factors. Created with Biorender.com. **B)** Overview of the experimental groups. The Scl-Cre-ERT2 Bak $^{-/-}$ Bax $^{f/f}$ mice were treated with tamoxifen at 2 months of age to induce the deletion of Bax. Both WT and Bak $^{-/-}$ Bax $^{\delta/\delta}$ were analysed at 8 months of age. The figure was created with Biorender.com. **C)** Genotyping of the Bak $^{-/-}$ Bax $^{\delta/\delta}$ colonies after WGS. The alignments were inspected on *IGV* to ensure successful recombination. **D)** Bak $^{-/-}$ Bax $^{\delta/\delta}$ mice displayed bigger spleens and significantly more leukocytes in their blood, although erythropoiesis was not affected by the KO. **E)** t-SNE plots highlighting the expansion of the Lin- compartment in Bak $^{-/-}$ Bax $^{\delta/\delta}$ mice. **F)** LSK and not LS-K cells accumulate in the bone marrow of Bak $^{-/-}$ Bax $^{\delta/\delta}$ mice. Additionally, the frequency of HSCs is increased compared to the WT. **G)** Raincloud plots supporting that Bak $^{-/-}$ Bax $^{\delta/\delta}$ HSCs were able to generate larger but equally viable colonies as WT HSC after 10 days in hypoxic culture.

Each dot represents an individual cell or a colony in the case of panel G. Statistical significance across comparisons was assessed using Welch's t-test, with the p-values directly annotated on the relevant plots.

3.3.2 Lack of apoptotic ability does not increase mutagenesis in HSCs

As mentioned earlier, to examine whether intrinsic apoptosis protects HSCs from genotoxic stress, I performed WGS with material collected from Bak$^{-/-}$ Bax$^{\delta/\delta}$ colonies, following precisely the same experimental and analytical strategy as explained earlier. Of note, in the case of one mouse (F3RR, Fig. **S3**), there was a mismatch between the sequenced germline and the colonies. The mismatch was evident by a considerably elevated mutational burden and the emergence of variants exhibiting VAF=1. To address this, I approximated the germline variant list by intersecting all the mutations shared across all the sequenced cells from this particular mouse, ensuring the usability of the data. For the WT proxy, 4 cells were sequenced per mouse, for 3 different mice in total (n=12, "young" group discussed previously). For the Bak$^{-/-}$ Bax$^{\delta/\delta}$ group, 1-6 cells were sequenced per mouse for 6 different mice (n=16).

Surprisingly, comparative analysis between Bak$^{-/-}$ Bax$^{\delta/\delta}$ and WT HSCs from age-matched mice revealed no significant quantitative differences regarding either SNVs or indels (Fig. **3.6A**). Moreover, the distribution of SNVs did not indicate any vulnerable genomic spots due to the absence of apoptosis (Fig. **3.6B**). Despite the unchanged numbers of indels, I observed a slight increase in the accumulation of complex indels within the apoptosis-deficient HSCs, compared to the WT ones (Fig. **3.6C).** However, it might reflect a by-product of the Cre-expressing transgenic system, rather than a biological effect of apoptosis on indels. Annotation of all the variants showed again that the vast majority of them occurred in intronic, intergenic and other non-coding areas of the genome regardless of the HSC genotype, while variants predicted to impact the downstream transcript or protein were as few as 22 (Fig. **3.6D, 3.6E**). These observations suggest that the absence of apoptosis does not appear to be catastrophic for the genomic integrity of HSCs. Instead, apoptosis-deficient HSCs exhibit similar burdens to those with intact apoptosis, implying that apoptosis could be a redundant mechanism in ensuring genomic integrity under physiologic conditions.

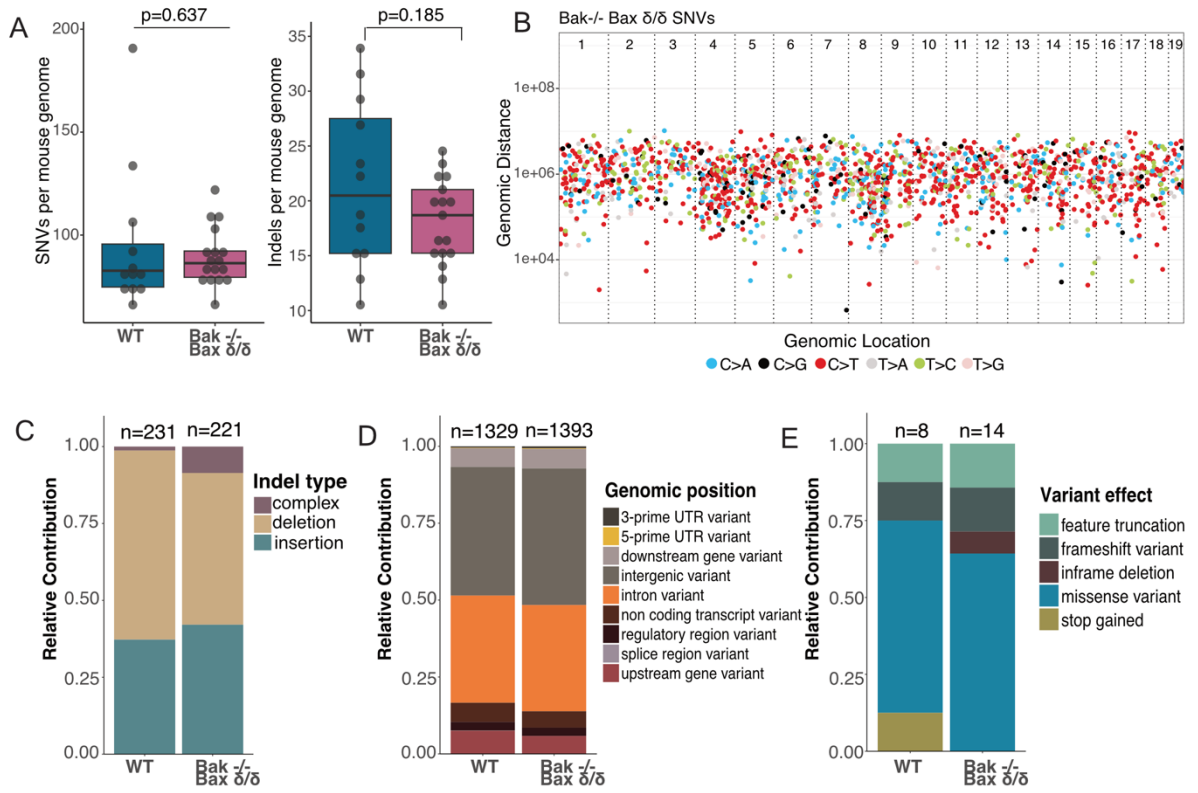

Figure 3.6. Lack of apoptosis does not compromise the genomic integrity of HSCs. A) Comparable SNV and indel levels between WT and Bak $^{-/-}$ Bax $^{\delta/\delta}$ HSCs from age-matched mice. Each dot represents one individual HSC. Statistical significance across comparisons was assessed using Welch's t-test, with the p-values indicated directly on the plot. **B)** Rainfall plot describing the genomic distance between the variants showed no signs of genomic hotspots. **C)** Relative contribution of the different indel types detected across the two genotypes indicated slight increase of complex indels in the Bak $^{-/-}$ Bax $^{\delta/\delta}$ genomes. Differences in the frequencies were assessed with chi-square test (p-value=0.0003). **D)** Annotation of all the mutation types detected in the cells, highlighting a predominant occurrence in non-coding regions, regardless of the HSC genotype. Differences in the frequencies were interrogated with chi-square test (p-value=0.55). **E)** Identification of 22 variants with potential impact on transcripts or proteins.

3.3.3 Apoptosis-deficient HSCs are governed by the same mutagenic processes as their WT counterparts

To examine whether, despite the numerically similar mutational loads to the WT cells, Bak $^{-/-}$ Bax $^{\delta/\delta}$ HSCs become subjects to different mutagenic processes due to the lack of apoptosis, I investigated the mutational signatures underlying their mutational profiles. To avoid masking low-contributing signatures or bleeding strong signals between WT and KO profiles, I analyzed the Bak $^{-/-}$ Bax $^{\delta/\delta}$ HSCs separately with *MutationalPatterns*. For a more robust analysis, I consolidated the analysis on a per-mouse basis, which ensures a higher mutational load per dataset. When data were available for fewer than 3 cells from a single Bak$^{-/-}$ Bax $^{\delta/\delta}$ mouse, I combined cells from different genotype-compatible mice to enrich the dataset. This approach

enabled the detailed interrogation of mutational signatures from three distinct apoptosis-deficient individuals and one additional combination of data from three separate mice (marked as "Bak$^{-/-}$ Bax $^{\delta/\delta}$_4").

Initially, the trinucleotide plots revealed subtle differences between genotypes, notably a reduction in C>T transitions within CpG islands in Bak$^{-/-}$ Bax $^{\delta/\delta}$ HSCs (Fig. **3.7A**). Subsequent *de novo* extraction of SNV signatures via NMF highlighted again an HSPC-like pattern bearing a high cosine similarity of 0.86 to the established HSPC signature[68,88,114]. Additionally, a low-contributing pattern was identified *de novo*, termed as "SBSC" since it diverged from known signatures (Fig. **3.7B**). To explore this SBSC signal further, I performed strict fitting of the known COSMIC signatures by bootstrapping. Intriguingly, the combination of signatures shaping the mutational landscapes of young and old WT HSCs -including HSPC, SBS1, SBS5, SBS8 and SBS18- also composed the mutational profiles of the Bak$^{-/-}$ Bax $^{\delta/\delta}$ HSCs (Fig. **3.7C**). This analogy indicated that the absence of apoptosis did not subject HSCs to distinct mutagenic influences. However, a notable difference emerged in the levels of SBS1 substitutions, with Bak$^{-/-}$ Bax $^{\delta/\delta}$ HSCs exhibiting fewer variants attributable to this signature (Fig. **3.7D**), aligning with the fewer C>T transitions at CpGs visualized by the trinucleotide plots. This indicates a lower proliferation rate among Bak$^{-/-}$ Bax $^{\delta/\delta}$ HSCs, potentially as a mechanism for controlling population size.

In summary, the analysis of SNV signatures affirmed that inhibiting cell-intrinsic apoptosis does not significantly transform the mutational landscape of HSCs, implying that these cells do not rely on this mechanism to maintain their genomic integrity during normal ageing.

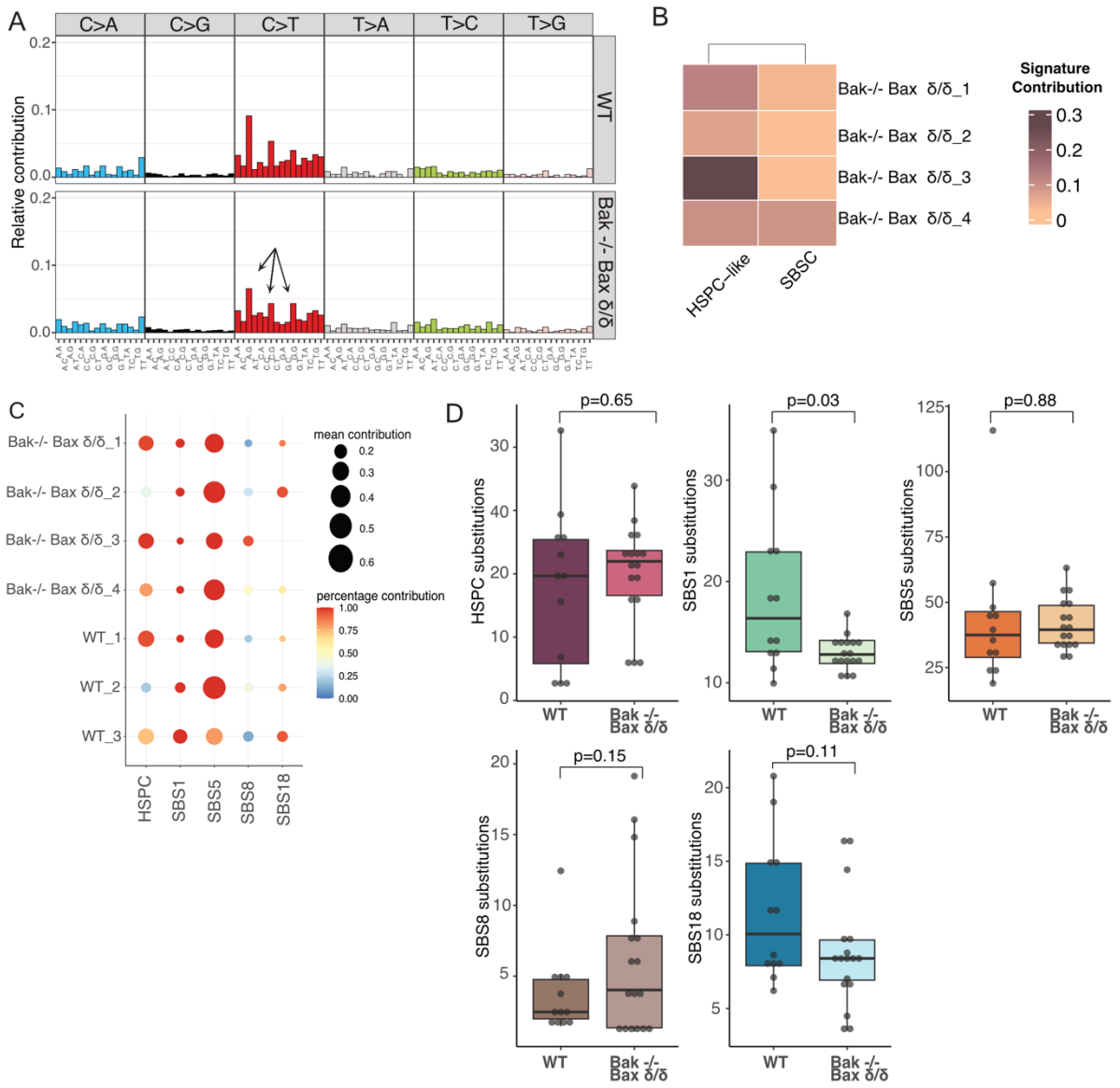

Figure 3.7. Inhibition of cell-intrinsic apoptosis does not subject HSCs to alternative mutagenic processes than their WT analogues. A) Trinucleotide plots representing all the SNV variants detected in WT and Bak $^{-/-}$ Bax $^{\delta/\delta}$ HSCs. The arrows indicate the C>T transitions at CpG islands that appeared reduced in Bak $^{-/-}$ Bax $^{\delta/\delta}$ HSCs. **B)** Heatmap indicating the relative contribution of the two *de novo* extracted signatures (HSPC-like, SBSC) to the mutational profile of each mouse (rows). **C)** Dotplot summarizing the mean signature contributions across mice, as determined by 150-run bootstrap fitting. The rows represent individual mice. **D)** Absolute numbers of SNVs attributed to each signature. Statistical significance was assessed with Welch's t-test and the p-values are annotated on the plots.

3.4 The impact of dormancy on the genomic integrity of HSCs

HSCs exist predominantly in a quiescent state in the bone marrow, remaining in the G_0 phase of the cell cycle. However, they reversibly engage the cell cycle, shifting into an active mode to contribute to tissue homeostasis. This activation occurs either as a response to the natural turnover of the mature cells or is prompted by stressors, including excessive blood loss and response to inflammation[26,27,120]. Studies have suggested that quiescent HSCs are susceptible to DNA damage, which can be efficiently repaired only after the cells activate their cycle[52,120,46]. This claim is based on the dependency of quiescent HSCs on NHEJ repair that shows decreased fidelity compared to HR, which is used by actively cycling cells to repair errors in their genome[120]. Moreover, it has been hypothesized that transcription is suppressed during quiescence; therefore, repair components are not sufficiently expressed in resting HSCs[46].

Cells that have remained in quiescence for extended periods are called dormant. Unlike quiescence, dormancy has been explored in the context of ageing, revealing its advantages for HSCs by preserving their stem cell fitness. Dormant stem cells occupy niches different from those of their active counterparts, exhibit a transcriptome akin to younger cells, and demonstrate superior regenerative capacity following transplantation[21,103]. Therefore, while quiescence is often thought to adversely affect the genomic integrity of HSCs, evidence suggests it also plays a role in sustaining their functionality long-term. Motivated by this paradox, I decided to investigate HSC mutagenesis, taking into account the cellular state of the cells.

3.4.1 Dormancy as a barrier against somatic mutation acquisition

To study the impact of dormancy on the HSC genome *in vivo*, I used WGS data collected previously by Dr. Megan Druce from Scl-tTA H2B-GFP mice[21], a model that segregates active from dormant HSCs based on green fluorescent protein (GFP) expression. More precisely, a fusion protein combining the human histone 2B (H2B) and GFP is constantly produced under the regulation of the Scl promoter, limiting its expression to HSCs. Additionally, the system incorporates a tetracycline-controlled transactivator (tTA) coupled with the Scl promoter, creating a tet-off mechanism. That translates as cessation of fusion expression in the presence of tetracyclines. Subsequently, active cells gradually dilute the GFP label as they divide and incorporate unlabeled H2B in their chromatin, while dormant HSCs remain GFP-positive and easily identifiable by fluorescence-activated cell sorting (FACS)[21]. Intriguingly, by ageing this mouse model for the first time in our lab, Dr. Ruzhica Bogeska, a former post-doctoral researcher in the group, uncovered that -despite the anticipation- HSCs in an aged bone marrow were not exclusively found in the GFP-negative fraction. Instead, a small reservoir of dormant cells was consistently present (Fig. **3.8B**), pinpointing the existence of cells that got activated never or very few times throughout the lifespan of the organism[103].

To generate the data used in the present study, doxycycline (Dox) was administered in a cohort of 4-month-old mice via their drinking water, initiating a continuous chase period of 18 months that concluded when the animals reached the age of 22 months. Subsequently, active and dormant LT-HSCs were purified from the same donor mice to allow for a detailed analysis of their mutational loads (Fig. **3.8A**). During the *in vitro* expansion, active and dormant HSCs were proven equally functional in generating clones. However, the active colonies appeared slightly smaller in size, hinting at dormant stem cell superiority (Fig. **3.8C**). Interestingly, the variant analysis showed that even though these cells were isolated from the same donors, dormant HSCs bore lower SNV burdens than their active counterparts. Meanwhile, indel frequencies remained unaltered across both cell states (Fig. **3.8D).** Relying on the linearity of the somatic mutation acquisition supported by the literature[68,69,72], linear regression analysis showed that throughout the lifetime of the mouse, the dormant HSC fraction acquires very few mutations, as opposed to the active fraction (Fig. **3.8E**). These observations underscored that, in fact, dormancy could be a protective state favoring more stable HSC genomes. Furthermore, the distinction of HSCs into active and dormant subpopulations highlighted the *in vivo* heterogeneity of mutation acquisition in HSCs, intricately linked to their cellular state.

Finally, to interrogate whether it is the lack of mitotic activity where dormancy attributes its protective role, I inspected the relationship between the median GFP intensity, recorded during the index single-cell sorting of LT-HSCs performed by Dr. Ruzhica Bogeska, with the normalized number of SNVs per mouse genome. However, no coherent correlation of these two metrics emerged (Fig. **3.8F**). This observation led to two possible interpretations: either that the genomic shield offered by dormancy extends beyond a mere reduction in cell division, or our mouse model might not accurately track divisions despite previous claims supported by the literature[121]. An important consideration that made me lean more towards the latter scenario is the uncertainty of whether all the cells express GFP at the same levels at the beginning of the lifecycle, potentially setting an unequal baseline. Consequently, accurately determining the relationship between the rate of somatic mutation accumulation and cell division frequency might be more complex than anticipated.

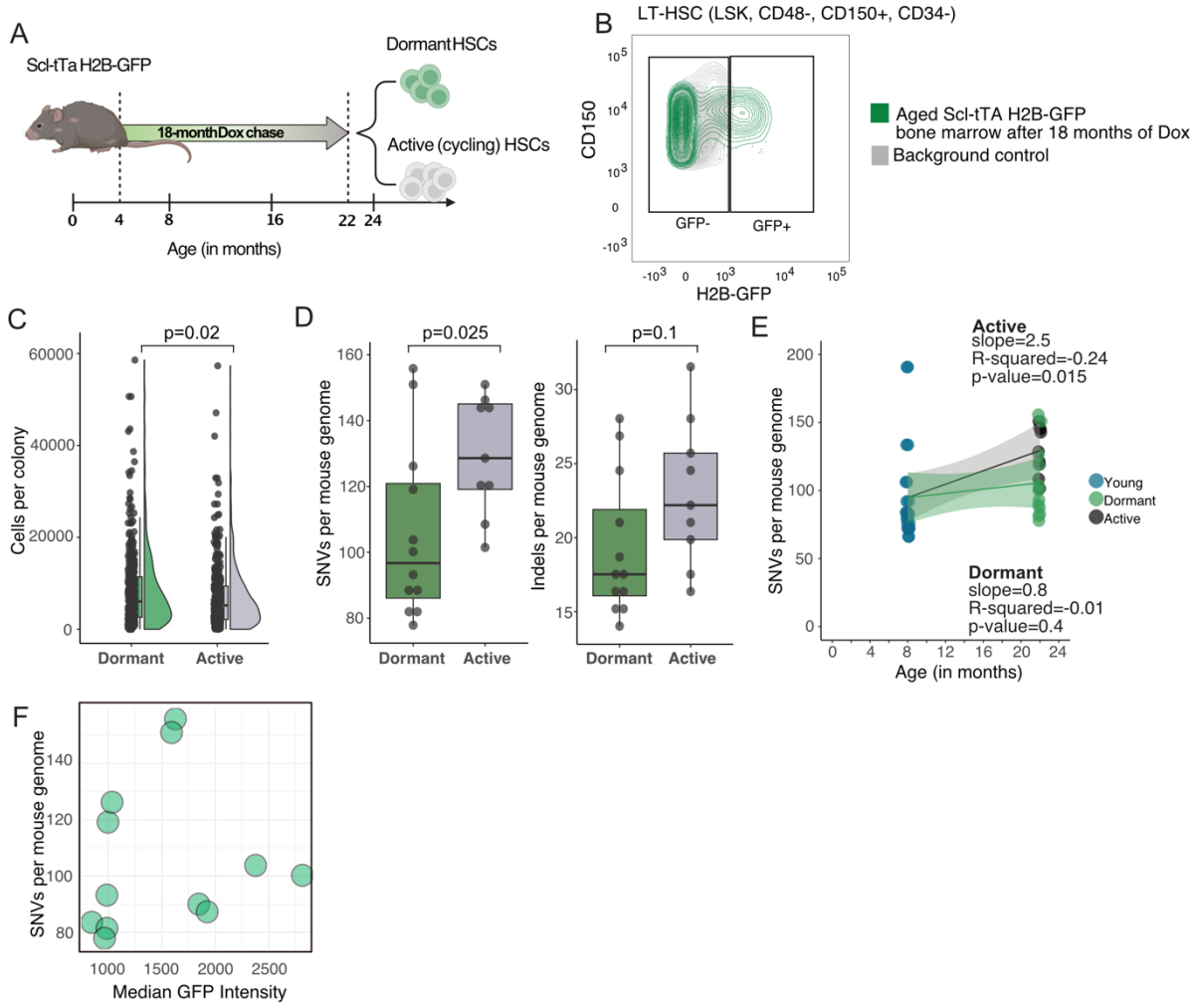

Figure 3.8. Dormancy restricts the acquisition of somatic mutations in HSCs during ageing. A) Experimental overview schematic created with Biorender.com. **B)** Typical example of the active and dormant HSC fractions, as observed in the bone marrow of an aged mouse. **C)** Raincloud plots describing the size of the colonies generated by single active and dormant HSCs after 14 days in culture. Each dot represents one colony. A comparison was performed using Welch's t-test to assess statistical significance, and the p-value is displayed on the plot. **D)** SNVs and indels as detected in the genome of dormant and active HSCs. Each dot represents one individual cell. The statistical comparison was performed using Welch's t-test; p-values indicated on the plot. **E)** Double linear regression between young-active and young-dormant groups using the `lm()` function in R. Significant increase appeared only from the young age to the active fraction. Grey areas highlight the 95% CI, and the p-values are annotated on the plots. **F)** Scatter plot suggesting no clear connection between the dormant cells' median GFP intensity, indicating their divisional history, and the SNV load presented in their genomes.

3.4.2 Mutational profiling suggests that mitotic latency protects the genome of dormant HSCs during ageing

Further inspection of the dormant and active variants revealed no differences regarding the types of indels accumulated (Fig. **3.9A**) nor the genomic loci affected (Fig. **3.9B**). Furthermore, the number of variants predicted to confer an effect on the gene expression product was extremely low, pinpointing once again that murine HSCs do not acquire deleterious mutations spontaneously (Fig. **3.9C**). However, trinucleotide analysis uncovered more C>T transitions at CpG islands in the genome of active HSCs, an expected outcome reflecting their proliferative nature (Fig. **3.9D**). Although dormant and active HSCs were subjected to the same mutagenic processes as the old bulk HSC population analyzed earlier, including HSPC-signature, SBSA and SBSB, there was not a clear distinction of these *de novo* patterns in the two HSC subpopulations (Fig. **3.9E**). Nevertheless, when I applied bootstrapping to fit known signatures into the dataset, I observed that active HSCs carried a greater SNV load attributed to SBS1 (Fig. **3.9F,3.9G**). HSPC and SBS8 signatures did not show any discrepancies between the two subpopulations, suggesting that their effects depend on the cells' chronological age. Additionally, accepting the suggestion that SBS5 represents background cellular damage[87], similar levels of SBS5 mutations in both dormant and active HSCs implied an equal capacity for coping with damage (Fig **3.9G**). Finally, SBS18 mutations were very limited, as observed also in the bulk HSC population (Fig. **3.4D, 3.9G**), which might indicate an age-dependent phenomenon. Collectively, these findings suggest that the mutational resilience observed in dormant HSCs can be primarily ascribed to their reduced divisional history, highlighting the protective role of stem cell dormancy against genomic instability.

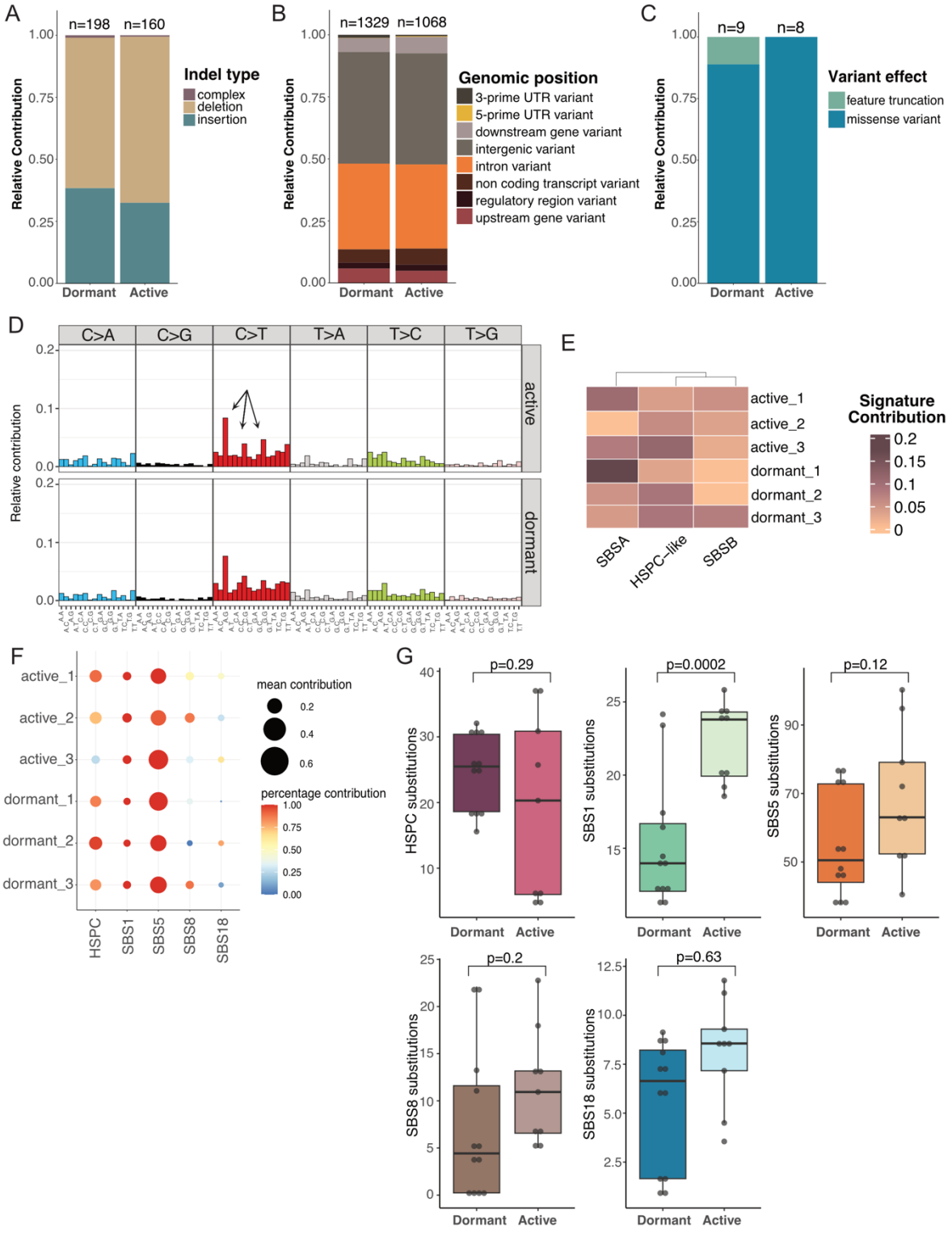

Figure 3.9. Active HSCs accumulate more mutations due to their self-renewal. (Legend continues on the next page)

A) Types of indels accumulated in dormant and active HSCs. Statistically significant differences in the frequencies were assessed with chi-square test (p-value=0.45). **B)** Genomic annotation of all the mutations detected in dormant and active cells. Statistically significant differences in the distribution of the variants were assessed with chi-square test (p-value=0.32). **C)** Variants predicted to confer a damaging effect on the transcript or protein. **D)** Trinucleotide plots displaying the SNV spectrum resulted from merging all the variants per group. The arrows pinpoint C>T transitions at CpG regions, a hallmark of SBS1. **E)** Heatmap showcasing the 3 different patterns underlying the mutational profiles of the cells, as extracted *de novo* by NMF. Each row represents one mouse. **F)** Contribution of known signatures after fitting with 150-run bootstrapping analysis. Each dot represents the average contribution of each signature as assessed by the bootstrapping iterations, and each row represents one mouse. **G)** Absolute counts of substitutions attributed to each signature fitted. Statistical comparisons were conducted using Welch's t-test; corresponding p-values are indicated on the plots.

3.5 Acceleration of cell division through HSC inflammatory response

Observing the significant discrepancy in mutational loads between dormant and active HSCs, notably influenced by the SBS1 signature, I hypothesized that forced cell division through system perturbations in younger HSCs could expedite mutagenesis. HSCs are known to initiate their cell cycle and undergo self-renewal and differentiation in response to inflammatory cues, such as interferons[122]. This process is not isolated to active HSCs; dormant cells are similarly roused by acute inflammatory challenges [26,27], that cause genomic damage[27]. Furthermore the observation that aged GFP- HSCs exhibit the most pronounced dysfunction, suggests that although self-renewal is essential, it might contribute to stem cell to attrition[103,121,123]. This attrition could be partly attributed to increased genomic instability. Thus, understanding how cell division shapes the mutagenic landscape of HSCs, opens up potential pathways to discern the age-related decline in stem cell functionality.

3.5.1 Induce HSC activation with pI:pC

In a first attempt to elucidate the genomic impact of inflammation-induced cell division in HSCs, Dr. Megan Druce used an intermittent treatment regimen with the double-stranded RNA molecule, polyinosinic:polycytidylic acid (pI:pC) [106], that has been well-established in the lab. As a toll-like receptor 3 (TLR3) synthetic agonist, pI:pC stimulates interferon response in the sensitive cell types, including HSCs, mimicking a viral infection in the body [124]. HSCs respond to this stimulus and activate their cell cycle[26]. This regimen requires 2 injections of 5 mg/kg pI:pC per week over 4 weeks, followed by a 4-week recovery period, constituting one round. The treatment is repeated for three rounds across 6 months, effectively maintaining HSCs in a state of continuous proliferation before allowing them to return to homeostasis (Fig **3.10A**). Mice begin treatment at 2 months, with the endpoint being at 8 months of age, which is compatible with the young age group in this study.

Our lab has recently detailed how pI:pC treatment precipitates HSC attrition and prematurely prompts the emergence of age-associated phenotypes[123]. An important finding from these experiments was a noticeable reduction in the *in vitro* clonogenic capacity of treated HSCs, resulting in fewer and smaller colonies[123] (Fig.**3.10C**). Consequently, this diminished capacity hindered the collection of adequate DNA material for our WGS pipeline, leading to unsuccessful library preparation or, in instances where libraries were produced, very few samples could eventually pass our custom QC criteria, as extensively discussed in the aforementioned thesis[106]. The significant reduction in the size of the pI:pC group prevents us from reaching any conclusions despite the absence of significant changes in SNV and indel levels post-treatment (Fig. **3.10B**).

Prompted by these observations, I explored the possibility that apoptosis plays a more pronounced role under stressful conditions, such as inflammatory stress, potentially explaining the diminished *in vitro* colony formation of HSCs. To test this hypothesis, I applied the pI:pC regime to Bak $^{-/-}$ Bax $^{\delta/\delta}$ mice, pre-treated with tamoxifen to induce the recombination. Interestingly, apart from observing larger spleen sizes in the treated group, there were no significant alterations in the hematologic phenotype between treated and untreated Bak $^{-/-}$ Bax $^{\delta/\delta}$ mice (data not shown). Moreover, and contrary to expectations, the subsequent variant analysis showed that SNV and indel levels remained unchanged post-treatment (Fig. **3.10D**), even though the cells had undergone division and incorporated C>T transitions indicative of mitosis (Fig. **3.10E**). In addition, when examining the *de novo* extracted signatures, no distinctive patterns emerged in the comparison of the two groups (Fig. **3.10F**). The only noticeable change, following strict fitting with bootstrapping analysis, was a reduced SBS5 burden in the apoptosis-deficient HSCs after chronic pI:pC treatment (Fig. **3.10G, 3.10H**).

In summary, the group of these observations suggested that neither inflammation nor consequent accelerated division of HSCs serves as a primary driver of mutagenesis in HSCs. Furthermore, even amidst inflammatory stress and its associated genotoxicity[27], apoptosis does not appear to be a dominant protection mechanism.

3.5.2 Exploring the actual genomic burden under inflammation in nano-scale

Extensive research has highlighted inflammation's role in diminishing HSC regenerative potential by inducing genomic damage through sudden cellular activation[27,123]. While inflammation may impact stem cells at various levels rather than altering the genetic information, the current analysis cannot provide clear answers, mainly due to the small sample size of the treated WT group. Moreover, recognizing the complexity of inflammation's impact on clone expansion *in vivo*[125] suggests that my standard sample size might be insufficient even in the case of treated Bak $^{-/-}$ Bax $^{\delta/\delta}$ HSCs. This belief persists despite the absence of any known driver mutations or, indeed, any coding mutations at all. To address these challenges, further delineate the actual mutational landscape following treatment in WT animals, and better understand apoptosis' role under stress, I decided to repeat the treatment experiments and change the analysis approach. The approach selected is the "Nanoseq" protocol, developed by the lab of Inigo Martincorena at the Wellcome Sanger Institute and introduced in Abascal et al., 2021[74]. Nanoseq is a refined duplex consensus sequencing approach that delivers single-molecule resolution results and is optimised experimentally and computationally to present the lowest error rates. Importantly, the pipeline needs as little as 1 ng of starting DNA material[74], making it ideal to interrogate even the smallest colonies generated by WT pI:pC-treated HSCs. Notably, the single-molecule resolution is achieved by barcoding each DNA strand separately during the library preparation, eliminating the need for *in vitro* culture. As such, I have sorted mini bulks of 1,500 LT-HSCs per mouse, for 10 mice per group, significantly increasing my sample size. To ensure comparable results, the same approach is also followed for treated Bak $^{-/-}$ Bax $^{\delta/\delta}$ HSCs

and the control group. Currently, the experiment is in the library preparation phase at the Sanger Institute, and therefore, the detailed outcomes of this work are not discussed in this thesis.

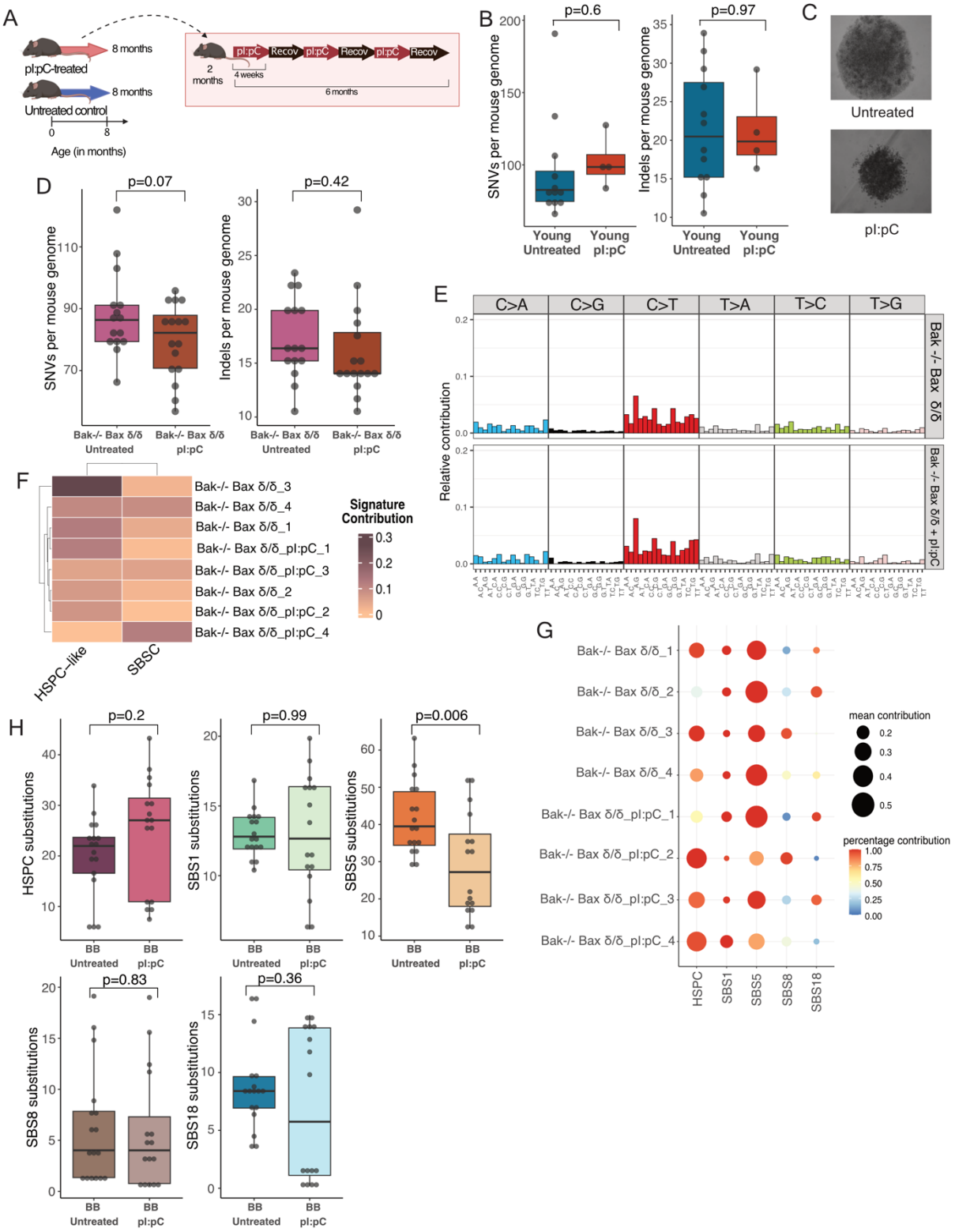

Figure 3.10. Inflammation-induced cell division does not mimic age-related mutagenesis. (Legend continues on the next page).

A) Overview of the chronic pI:pC treatment scheme applied to challenge HSCs into cycle intermittently. Figure created with Biorender.com. **B)** Normalized SNVs and indels detected in the HSC genomes of young untreated and young mice treated with pI:pC. Each dot represents one cell. The limited sample size of the treated group is attributed to the bad quality of the data due to the low DNA input collected from the colonies. Statistical analysis was conducted with Welch's t-test, and p-values are indicated on the plot. **C)** Typical examples of *in vitro* HSC clones from untreated and treated young mice. Photos taken by Dr. Megan Druce; 40X magnification. **D)** Normalized SNVs and indels detected in untreated and long-term pI:pC-treated apoptosis-deficient HSCs. Each dot represents one single cell. Statistical analysis was conducted with Welch's t-test, and p-values are indicated on the plot. **E)** Trinucleotide plots depicting the mutational spectrum resulting from merging all the SNVs per indicated group. **F)** De novo extracted signatures using NMF. No group clustering was observed, implying that all the samples, regardless of the treatment, were subjected to the same processes. Each row represents data from one mouse or a combination of treatment-compatible mice. **G)** Strict fitting of known signatures after 150-run bootstrapping analysis. Each row represents one mouse and the dots show the average contribution of all the boots performed for each mouse. **H)** Absolute SNV counts attributed to each signature fitted in the dataset. Statistical analysis was conducted with Welch's t-test, and the respective p-values are indicated on the plot. (BB=Bak $^{-/-}$ Bax $^{\delta/\delta}$).

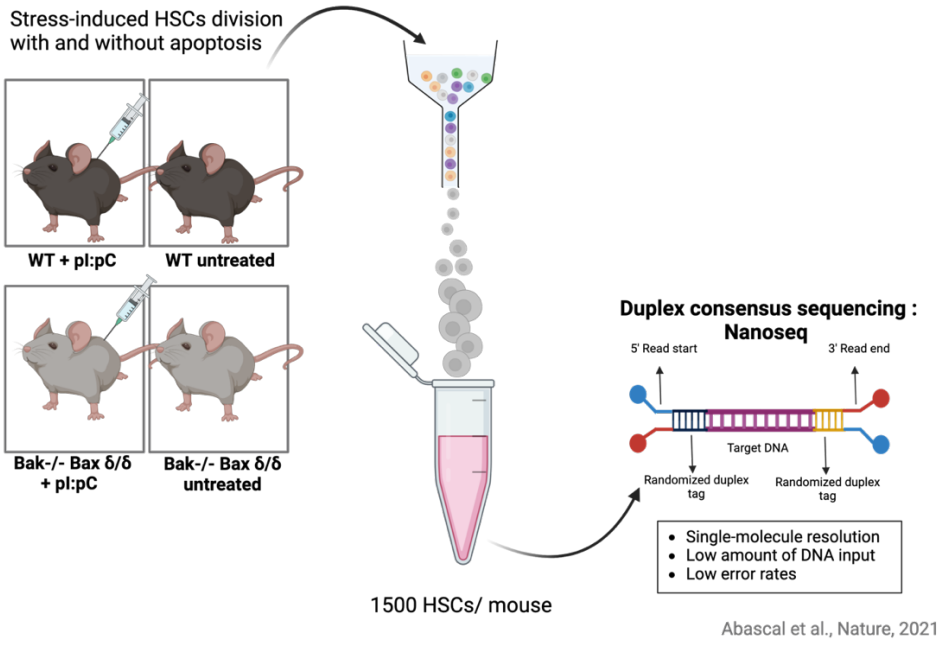

Figure 3.11. Exploring the genomic effects of inflammation in HSCs with Nanoseq. Schematic representation of the Nanoseq pipeline. The chronic pI:pC treatments have been repeated on both WT and Bak$^{-/-}$ Bax $^{\delta/\delta}$ mice, while the cells were sorted in mini-bulks of 1,500 LT-HSCs per mouse. The downstream Nanoseq pipeline is currently in progress, under the supervision of Dr. Alex Cagan. Figure created with Biorender.com.

4 Discussion (Project 1)

4.1 Exploring the endogenous age-related mutagenesis in murine HSCs

Age-associated somatic mutagenesis, universally observed across species, is a fundamental aspect of biological ageing. While it is a constant process[126,72], its implications -particularly in terms of cellular and organismal attrition- become pronounced only later in life, when evolutionary pressures to maintain optimal fitness diminish[69,72]. This delineation underscores the intricate balance between genomic integrity and longevity, revealing how the cumulative effects of mutations over time can influence the ageing process and lifespan[72].

Adult stem cells are central to tissue homeostasis over time, and therefore, accumulated damage and errors in their genomes can jeopardize tissue integrity during ageing[5,70]. Despite reports supporting that stem cells accumulate fewer mutations than their differentiated progeny[127,79], age-related genomic instability does not spare them[5]. The variability in the rates and patterns of mutational accumulation in stem cells, though, highlights a remarkable tissue-specificity influenced by factors such as cellular turnover, tissue architecture and environmental exposures[70,128].

HSCs, as progenitors of all blood cell lineages, play a pivotal role in lifelong hematopoiesis. Therefore, understanding the fundamentals of age-related somatic mutation acquisition within HSCs can offer valuable insights into how genomic errors can influence stem cell function, clonal expansion and predisposition to hematological disorders. Studies that have already addressed this topic in human HSCs from healthy donors suggested a linear accumulation of somatic variants, predominantly SNVs[68,69]. Despite the controlled environments and uniform genetic backgrounds, the age-related increase of SNVs is mirrored in murine HSCs, making them a reliable model to study the fundamentals of endogenous age-associated mutagenesis[68,128]. Based on the linearity of this accumulation[68,69], my analysis suggested an SNV accumulation rate of 44 variants per autosomal HSC genome per year, a process significantly faster than previously calculated rates in humans[68,69]. This finding aligns with the inversely proportional relationship between lifespan and mutation accumulation rates observed across mammalian species[72]. While somatic SNVs are common in most aged tissues, despite the lack of pathological signs[74,129–131], more complex variants such as SVs and copy number variations (CNVs) also accumulate with age, although rare and usually indicative of malignant entity development[132]. My findings support this rarity of SVs and reveal stable levels of indels, aligning with other human studies employing similar strategies of single-HSC clonal expansion[68,69].

The emergence of oligoclonality in normal aged tissues, with examples from but not limited to oesophagus[130], endometrium[133] and blood[91] is a clear indicator of the systemic ramifications of age-associated mutagenesis. This process, driven by mutations offering a competitive advantage to the carriers, underscores the complex dynamics of positive cell selection over time[89]. Nevertheless, despite the fact that clonal hematopoiesis is almost certainly present in individuals older than 70 years of age[69,89], mice do not develop such a condition spontaneously, as implied by the detection of no known drivers or hardly any coding mutations in my dataset. Yet, a study was able to show that driver mutations emerged when aged murine HSCs were subjected to transplantation stress[134]. Consequently, this observation underlined the crucial influence of environmental stressors on pathology manifestation, which is difficult to discern by studying only human material.

While the influence of environmental factors on age-associated mutagenesis is acknowledged, it falls beyond the scope of this study, which aims to delineate the endogenous baseline of this process. In this thesis, the mouse model has proven to be a valuable platform for understanding the intrinsic patterns of mutation accumulation with age, providing a solid foundation for exploration of the mechanisms that drive HSC ageing.

4.2 The complex mutational landscape of aged HSCs informs about divisional history, cellular state and metabolic dependencies

Somatic mutations are embedded in the genome due to replication errors or inefficient repair of acquired damage[6]. These mutations frequently form identifiable patterns or "signatures" associated with specific damage sources or repair processes[113]. Initially observed and deconvoluted in cancer datasets, it became quickly apparent that normal cells are also subjected to specific mutagenic processes depending on their nature and functions[70].

Previous studies in human HSPCs have unveiled a signature unique to these cells that likely encompasses mutagenic elements related to purine metabolism[68,88]. This signature is active primarily in adult HSPCs, while its contribution is limited in the mutational profile of cord blood HSPCs, marking a process that characterizes mainly the definitive bone marrow hematopoiesis[114]. My analysis indicated that the HSPC signature accounts for most of the annual SNV accumulation in murine HSCs, contributing 28 out of 44 variants. Furthermore, this signature exhibited a clear age-dependency, while its contribution was invariant across dormant and active HSC subpopulations, demonstrating that its accumulation in aged cells is not primarily driven by self-renewal.

The SBS1 signature emerges as a critical player in this study, defined by its typical C>T transitions at CpG doublets, a pattern largely attributed to the spontaneous deamination of 5-metC into thymine[86,87,113]. This ubiquitous signature is not only time-dependent but also serves

as a mitotic tracker, revealing correlations between SBS1 burden and the proliferative activity of both normal and cancerous cells[86,113]. Indeed, when aged stem cells were divided into dormant and active fractions, SBS1 was the main driver of the difference observed across the mutational loads of these two subpopulations, thereby reinforcing its role as a reliable mitotic clock and underscoring the significance of division-related mutagenesis. Additionally, my findings illuminated that by measuring SBS1 levels, a potential connection between HSC self-renewal and HSC population size was uncovered. More specifically, SBS1 contribution was slightly reduced in aged HSCs compared to their young counterparts, resulting in an equal SBS1 burden between the two groups in absolute SNV counts. Despite the claims about an increase of SBS1 signature in human HSPCs with age[68,79], my results were in accordance with the studies supporting increased quiescence within the aged stem cell pool[116]. Yet, interestingly, the HSC population expands significantly with age[15,17,45,61,135]. Moreover, HSC expansion, coupled with decreased SBS1 contribution as observed in Bak $^{-/-}$ Bax $^{\delta/\delta}$ HSCs, suggests an inverse correlation between HSC reservoir size and self-renewal frequency, indicating a sophisticated negative feedback mechanism. The influence of division on mutagenesis, though, needs a cell-type-specific context in order to be understood. For example, neurons acquire mutations over time even though they are post-mitotic, indicating altered underlying mutagenic mechanisms[74,136]. Furthermore, the impact of differentiation remains to be elucidated. Although differentiation requires numerous divisions of the stem cells to generate mature progeny, this process does not uniformly escalate mutational burdens across all cell types. For instance, granulocytes exhibit comparable SNV loads to HSPCs[74]. Conversely, lymphocytes undergo mutagenic processes specifically tailored to enhance their diversity, resulting in significantly higher burdens compared to their stem cell precursors[79].

Another time-dependent yet division-independent signature virtually present in all cell types is SBS5[86]. Although of unknown origin, its ubiquitous presence led to the suggestion that SBS5 is the outcome of "background endogenous DNA damage" not countered by the repair capacity intrinsic to each cell type[87]. Characterized as a "flat signature", SBS5 incorporates a broad range of substitutions[88]. Despite its clock-like nature, SBS5 did not appear to be the main driver of age-associated mutagenesis, as it only showed a slight uptick from young to old age, without reaching statistical significance. Interestingly, though, even though literature supports that resting HSCs in quiescence do not resolve their routine DNA damage[120,46], long-term quiescent or dormant HSCs did not show differences in SBS5 levels compared to their active counterparts, suggesting that in terms of genomic integrity, active HSCs do not necessarily exhibit a repair advantage over the dormant reservoir.

According to my analysis, SBS8 was also a prominent force of age-related mutagenesis, predominantly manifested through C>A and T>A mutations[82,86]. Although its origin remains elusive, this signature usually emerges in hematological contexts, including malignancies[88], suggesting its potential significance in blood cell dynamics, albeit its current underexplored status. In this dataset, SBS8 displayed a behavior similar to the HSPC signature, linked to the chronological age of the cells rather than the cellular state or the ability to undergo apoptosis. In

this study, the annual burden of SBS8-derived substitutions was calculated to 17 SNVs, underscoring its substantial contribution to the mutational profile of aged HSCs.

Finally, the last signature in this dataset was SBS18, a C>A-focused pattern strongly believed to reflect damage caused by ROS[82,86,137]. Notably, SBS18 mutations were significantly fewer in older HSCs. ROS levels typically increase during HSC activation, when the metabolism switches from anaerobic glycolysis to OxPhos[22]. This observation supports the hypothesis that aged HSCs adopt a more quiescent state than their younger counterparts. Yet, the anticipated differences in SBS18 mutation loads between dormant and active HSCs did not materialize, with both states showing similar levels of SBS18 mutations. This unexpected observation could stem from limitations of the Scl-tTA H2B-GFP mouse model, that sets an imprecise cutoff between dormancy and active state solely based on the GFP detection. This implies that GFP- cells might not be actively dividing, but it rather suggests that they have previously undergone sufficient division to dilute the GFP fluorescence.

This signature investigation illuminated the major endogenous players of age-associated mutagenesis affecting HSCs. Importantly, the signatures identified in this murine study resembled the results from previously reported human studies and reveal a valuable cross-species analogy.

4.3 HSCs do not trust their genomic integrity on apoptosis over time

The apoptotic cell death has been identified as a pivotal mechanism for addressing extensive DNA damage in the genome of HSCs, primarily through the intrinsic pathway initiated by the BAX and BAK proteins[138]. This mechanism is traditionally considered essential for maintaining population size[63] and preserving HSC genomic integrity, especially when subjected to severe environmental stressors, such as radiation exposure[52]. However, the genomic significance of apoptosis under steady-state conditions has not been explored. To delve into this question, I used the Scl-Cre-ERT2 Bak $^{-/-}$ Bax $^{f/f}$ mouse model, designed to specifically inhibit the apoptotic pathway in HSCs. The central hypothesis driving this research was that if apoptosis indeed influences the genomic stability of HSCs, inhibition of the pathway should reveal its importance early in life. This decision was further prompted by the fact that after induction of the double KO, all the mature progeny becomes anti-apoptotic as well, potentially increasing the system's susceptibility towards pathologies, such as immune autoreactivity or development of leukemias[117,63].

During this investigation, I observed that LSKs and, more specifically, HSCs expanded in size, as opposed to the LS-K population, suggesting that the most primitive compartment but not the committed progenitors are dependent on the intrinsic apoptotic pathway as a regulator of their population mass, recapitulating observations seen before by Bcl-2 overexpression in murine

HSCs[63]. Moreover, the ability of apoptosis-deficient stem cells to produce *in vitro* clones indicated that they did not succumb to senescence. Nevertheless, apoptosis did not appear to be a determinant for the genomic integrity of HSCs after scrutinizing the entirety of their genome, likely because endogenous processes are not able to induce such extensive damage during steady-state hematopoiesis. However, in this study, I assumed that the role of apoptosis remains constant throughout life. However, this notion has been challenged by an investigation supporting that the impact of apoptosis could evolve throughout life, with older HSCs potentially exhibiting resistance to apoptotic death[139].

On the other hand, differentiation should also be considered an alternative mechanism for safeguarding the HSC genome. A significant body of observations, including other systems such as skin, supports that differentiation could act as a natural sieve, removing potentially harmful mutations from the stem cell reservoir by passing them down to the temporary progeny[140–143]. In fact, this mechanism sounds like a possible scenario considering the behaviour of Bak $^{-/-}$ Bax $^{\delta/\delta}$ HSCs from mice treated with pI:pC, showcasing no inflation of the population size nor increased mutational burden. By differentiation means, though, mutations are pushed outside of the stem cell pool. Therefore, it doesn't represent a candidate mechanism of age-associated somatic mutation accumulation within the stem cell compartment.

Taken together, my data suggested that the loss of the apoptotic ability did not detrimentally affect the HSC genome in baseline conditions, indicating that it might be unnecessary. The fact that the mutational burdens did not appear to be elevated in apoptosis-deficient HSCs even after inflammatory exposure suggests the implication of potentially other overlapping mechanisms taking care of the genomic integrity of HSCs. Therefore, the complexity of stem cell regulation mechanisms is highly acknowledged, and the possibility of unexplored factors being significant responders against genotoxic stress cannot be ruled out.

4.4 Genomic stability is another advantage of dormant HSCs

In this investigation, the aged HSC reservoir was split into a dormant and an active subfraction according to the expression of the H2B-GFP following 18 months of Dox chase. It is our lab that, for the first time, aged this model and observed that a dormant fraction of HSCs is consistently present in the aged bone marrow, holding on average up to approximately 10% of the aged HSC population[103]. The list of the numerous benefits of dormancy on HSCs includes better regenerative potential of the dormant HSCs as assessed through transplantation assays, maintenance of cell polarity, young-like transcriptome, slow metabolism that prevents genotoxic stress and occupation of very specific sinusoidal niches within the bone marrow that likely protect them from damage[21,27,103]. The results of this study further showcased that genomic stability is another characteristic attributed to dormancy, as it was calculated that dormant HSCs acquire less than 10 SNVs per autosomal genome per year (Fig. **3.8E**).

For this study, the distinction between HSC quiescence and dormancy is important. Quiescence refers to a reversible state of cell cycle arrest in G_0, preventing cell exhaustion and sparing self-renewal capacity. Quiescent HSCs can dynamically re-enter the cell cycle in response to physiological demands[21]. Nevertheless, these quiescent cell cycle pauses have been considered error-prone due to their metabolically and transcriptionally inactive status[46]. In contrast, I focused on dormancy, which describes a deeply quiescent state that remained predominantly inactive throughout the entire lifespan of the mouse, thereby creating a small safety reservoir of highly functional stem cells. It is, therefore, likely that many different levels of quiescence exist between a dormant and a fully active HSC state that remains to be elucidated. A past study using a similar label-retention system estimated that deep dormancy is 4 divisions away from losing the GFP label that marks HSC functional attrition[121]. However, my results showed that this label-retention system is not an accurate division tracker, preventing precise calculations of SNVs accumulated per self-renewal or the number of SNVs potentially associated with stem cell attrition. What seems to be the case, though, is that HSCs do not divide following a uniform pace *in vivo*; instead, each cell's unique divisional history partly determines its mutational burden.

The existence of dormancy in human HSCs remains a challenging area of research, primarily due to technical limitations such as the inapplicability of *in vivo* label-retention systems. Despite these challenges, transcriptome information reveals a continuum of quiescent states within the human HSPC population[144,145]. The identification and characterization of markers specific to dormant HSCs are essential next research steps towards harnessing their therapeutic potential, particularly in enhancing the efficacy of transplantation therapies. To this end, progress on this topic has pinpointed the GPRC5C orphan receptor as a promising marker of dormant stem cells in both mice and humans[145]. Additionally, despite the previous association with myeloid bias, $CD61^{high}$ LT-HSCs were recently reported to potentially mark a functionally superior and predominantly quiescent HSC fraction[146].For sure, though, many aspects of dormancy and its regulation remain to be elucidated in order to open new horizons in regenerative medicine.

4.5 Inflammation-driven HSC attrition is potentially not exerted through increased mutational burdens

Understanding the genomic impact of inflammation has been proven the most challenging part of this project. Originally, the goal was to enhance the HSC self-renewal cycles to determine if replication is the primary driver of mutagenesis during ageing. However, the influence of inflammation extends beyond, rendering the cells non-clonogenic *in vitro*. Initially attributing this phenomenon to apoptosis, I repeated the experiment with $Bak^{-/-}$ $Bax^{\delta/\delta}$ mice ending up detecting similar loads between WT untreated, $Bak^{-/-}$ $Bax^{\delta/\delta}$ untreated and $Bak^{-/-}$ $Bax^{\delta/\delta}$ mice treated with pI:pC, despite the blockade of a major cell death pathway and the enforced self-renewal.

Although there is evidence of DNA damage accumulation in HSC genomes after inflammatory exposure[27,47], it is possible that cells can repair it reliably upon their activation, minimizing the accumulation of mutations[120]. It is, therefore, unclear whether inflammation promotes *de novo* mutagenesis. Nonetheless, inflammation has been noted to favor the expansion of mutant clones in both non-malignant and malignant settings, such as TP53[125,147], through mechanisms that we do not fully understand yet. One possible explanation is that the driver mutations confer different resistance against inflammatory cues to the bearing clones, and they eventually outcompete others within the HSC pool. This implies that inflammation may preferentially support the expansion of the most resilient cells, potentially obscuring its damaging effects[148]. Although no coding or even recurrent variants were observed across the different cells, the sample size is prohibitively small to extrapolate the genomic challenge that inflammation might impose on HSCs.

To delineate the influence of inflammation-driven replication on whole HSC genomes, the Nanoseq project stands as a pivotal extension to my current research, offering the potential to examine genomes at 100 times greater than my existing dataset. This ambitious plan aims to understand the genomic influences of inflammation, potentially providing critical insights into HSC ageing and mechanisms underlying disease progression.

4.6 Conclusions

In this project, I conducted a comprehensive analysis of WGS data from single-HSC-expanded clones. By leveraging the power of mouse models for genetic manipulation, I interrogated the endogenous mechanisms underlying the acquisition of somatic mutations within the HSC pool during natural ageing.

HSC mutagenesis is primarily driven by a unique to them signature, first observed in human HSPCs and termed likewise[68]. This signature shows dependency on chronological ageing, underscoring the profound impact of time on genomic stability. My findings further indicated that apoptosis does not provide genoprotection under physiologic conditions, contrary to previous beliefs. Instead, it appeared that HSCs rely on a state of dormancy to maintain stable genomes over time and preserve a potent stem cell reservoir. Dormancy, therefore, acts as a protective mechanism, shielding HSCs from accumulating mutations and ensuring the longevity of the stem cell pool.

On the contrary, active HSCs that have exited dormancy to participate in the tissue homeostasis accumulate higher loads of mutations. These mutations primarily arise due to replication, as evidenced by the increased SBS1 signature contribution. This finding presents a critical vulnerability for active HSCs, where the replication necessity introduces an inherent risk for mutation accumulation.

Together, the aforementioned insights unravel a complex interplay between the cellular states, the temporal dimension of ageing, and genomic fidelity. This study reaffirms the critical importance of comprehending the dynamics of the dual HSC nature in both homeostasis and disease. The key findings are highlighted in Fig.**4.1**.

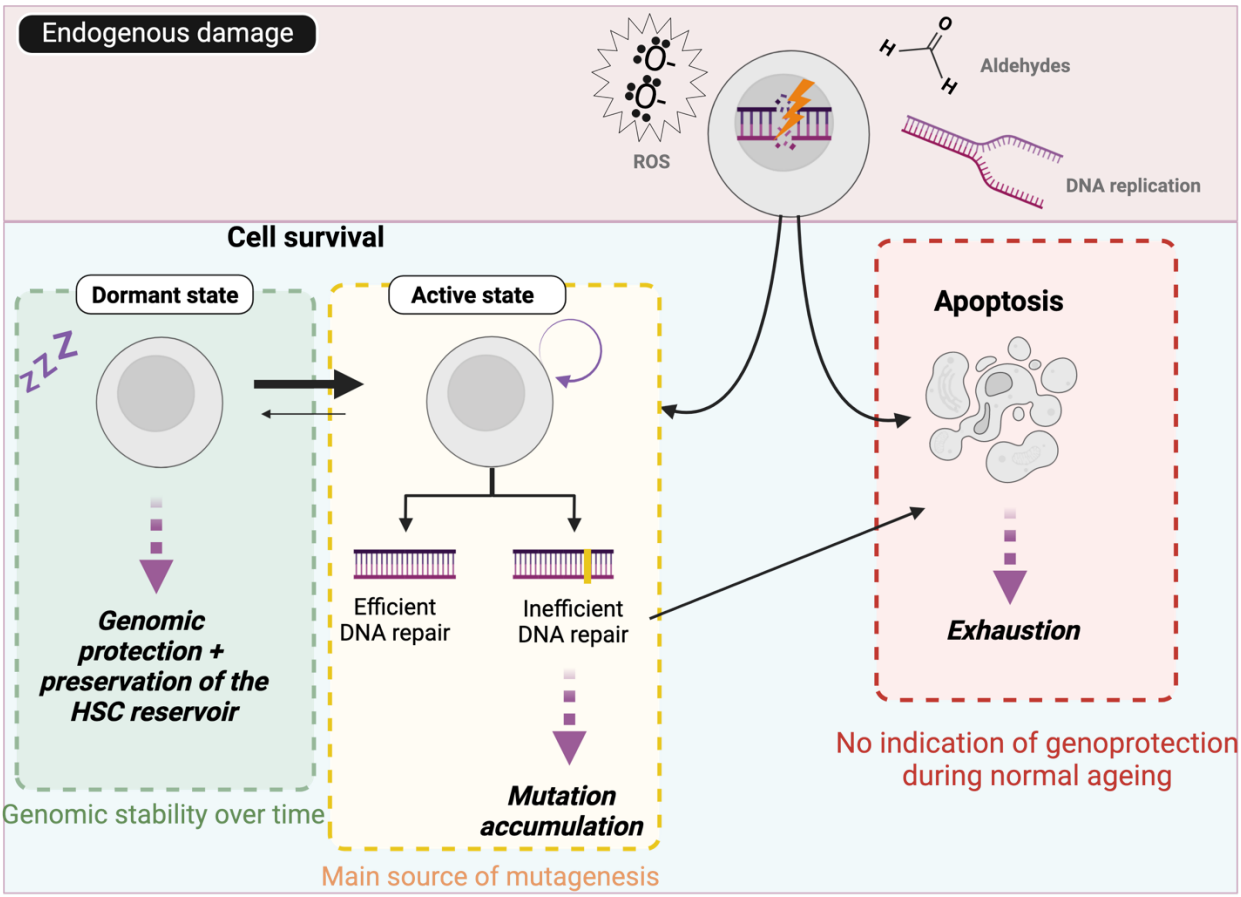

Figure 4.1. Graphical abstract of the conclusions. Figure created with BioRender.com

5 Aims (Project 2)

In this second part of my thesis, I expanded my investigation into the general phenotype of the aged hematopoietic system. This research aimed to illuminate the origins of its variability, a topic that remains largely unexplored. Like my previous project, I continued utilising mouse models with uniform genetic backgrounds and shared environmental conditions within the DKFZ animal facilities. This approach minimized extraneous influences and focused on the intrinsic biological aspects of the process. The specific objectives were the following:

1. **To generate a comprehensive murine dataset that describes the hematological profiles of multiple individuals.** Unlike typical ageing studies that perform group comparisons against younger controls, this study aimed to focus on the variability across the old individuals. By extensively analyzing hematopoietic tissues through flow cytometry, multi-omics, and bone histology, I sought to identify potential endogenous sources of heterogeneity and create a multi-parametric hematological profile for each mouse.

2. **To examine whether the classical age-associated metrics are interconnected.** After compiling the dataset, I sought to establish whether classical parameters associated with hematopoietic ageing are interconnected. The goal was to identify correlative relationships across commonly recognized critical indicators of this process.

3. **To unravel the role of the hematopoietic-niche cross-talk during normal ageing.** The bone marrow niche is crucial for sustainable hematopoiesis. Importantly, it is established that the niche also displays signs of ageing, challenging further the homeostasis of the hematopoietic system. To delineate the role of the niche during ageing, I used a large comprehensive scRNA-seq dataset generated for this study, encompassing hematopoietic and endosteal niche populations from 18 old and 12 young animals.

4. **To inspect for links across the multiple layers of information for interconnected parameters.** The ultimate goal was to synthesize information across various data layers to examine potential correlative links in-depth. By analyzing these links I aimed to identify distinct phenotypic patterns that could offer predictive insights into the ageing hematopoietic system

6 Results (Project 2)

6.1 Heterogeneity in hematological ageing is largely unexplored

Ageing hematopoiesis has attracted a lot of attention since the realization that HSCs are not immortal as was initially thought[135,29]. It is now established that the aged system is marked by an expansion of immunophenotypic HSCs[14]. Yet, the regeneration of the hematopoietic tree is often compromised, evident by reduced lymphoid outputs[14] and impaired erythropoiesis, typically indicated by low hemoglobin levels[149]. In parallel, there is a pronounced skewing towards myeloid cell production[14,37,150]. The HSC functionality during ageing has also been assessed through various transplantation settings. These investigations have revealed that aged HSCs, transplanted into young myeloablated recipients, exhibit a profound inclination towards the production of myeloid and megakaryo-erythroid lineages, while crucially, a large fraction of them is not able to reconstitute the recipient's hematopoietic system[33,32]. These observations led to a widely accepted hypothesis, that ageing is associated with an accumulation of defective, myeloid-biased HSCs, which disrupts the balance of mature cells output[32,37] and may play a pivotal role in the development of age-associated hematological disorders.

The alterations mentioned above have been broadly documented as average deviations compared to the system dynamics typically seen in young organisms. Nonetheless, little to no attention has been given to the variability of the aged phenotype[151,152]. Variability in human phenotypes is attributed to divergent genetic backgrounds and the array of environmental stimuli encountered by each individual[151–153]. In this study, I used inbred C57BL/6 mice housed under similar controlled conditions to discern whether ageing represents a programmed pathway leading to organismal decline or if it rather emerges as a stochastic phenomenon dictated by random events occurring at the cellular and molecular level.

6.1.1 Generation of a comprehensive dataset to explore the intricacies of the ageing process

To examine whether hematological ageing is a deterministic process or not, I designed a small epidemiological study, aimed at minimizing potential variability from genetic or environmental factors. For this purpose, I generated a multi-layered dataset using isogenic mice, with the ultimate goal to capture an exhaustive array of data out of each mouse (from now on mentioned as "experimental mouse") (Fig. **6.1**). This dataset contains information from 69 old (25 months), 24 middle-aged (18 months) and 41 young (2 months) WT mice. The primary data layer offers a detailed characterization of the cellular composition of hematopoietic tissues -including bone marrow, blood and spleen- as determined by flow cytometry. Importantly, this analysis spanned all three maturity

levels of the hematopoietic tree, providing information into the more primitive compartment, lineage-restricted progenitors and mature effector cell types (Fig. **6.1,** bullet **1**-all metrics measured are listed in Table **S1** of the Supplementary).

For the second tier of this dataset, I assessed the functionality of stem cells derived from experimental mice through competitive transplantations. This method required whole bone marrow (WBM) suspension from each experimental subject (donor) to be mixed in a 1:1 ratio with a common pool of WBM cells from young mice, called competitors. This mixture was then injected into the tail vein of a young, lethally irradiated recipient, establishing a 1 donor-1 recipient paradigm. By leveraging congenic mouse strains that express distinct isotypes of the pan-leukocytic marker CD45, I was able to track the transplantation outcomes and precisely assess the donor contribution across various cell populations using flow cytometry (Fig. **6.1,** bullet **2**).

To probe the extent to which interactions between hematopoietic cells and their bone marrow niche influence the overall aged phenotype, I produced single-cell RNA sequencing data from both compartments from 18 old and 12 young mice (Fig. **6.1,** bullet **3**). Additionally, to explore chromatin remodeling throughout the entire hematopoietic population spectrum but also within the cells of their interactive niche, I further generated single-cell Assay for Transposase-Accessible Chromatin with sequencing (ATAC-seq) data using 4 old and 4 young mice (Fig. **6.1,** bullet **4**).

Finally, another aspect under investigation is the increased adiposity within the bone marrow niche with age, a change whose impact on hematopoiesis remains debated[102]. To this end, one tibia from each experimental mouse was fixed, paraffin-embedded, and ultimately subjected to histological examination for adipocyte enumeration (Fig. **6.1,** bullet **5**).

In summary, this meticulously compiled dataset is a powerful tool for dissecting the fundamental mechanisms underpinning hematopoietic ageing. Generally, its foremost advantage lies in the multidimensional data obtained from each experimental mouse, able to unravel complex relationships across various factors. It is important to note, however, that this project is still ongoing, and bullets 4 and 5 will not be covered in this thesis due to their preliminary status.

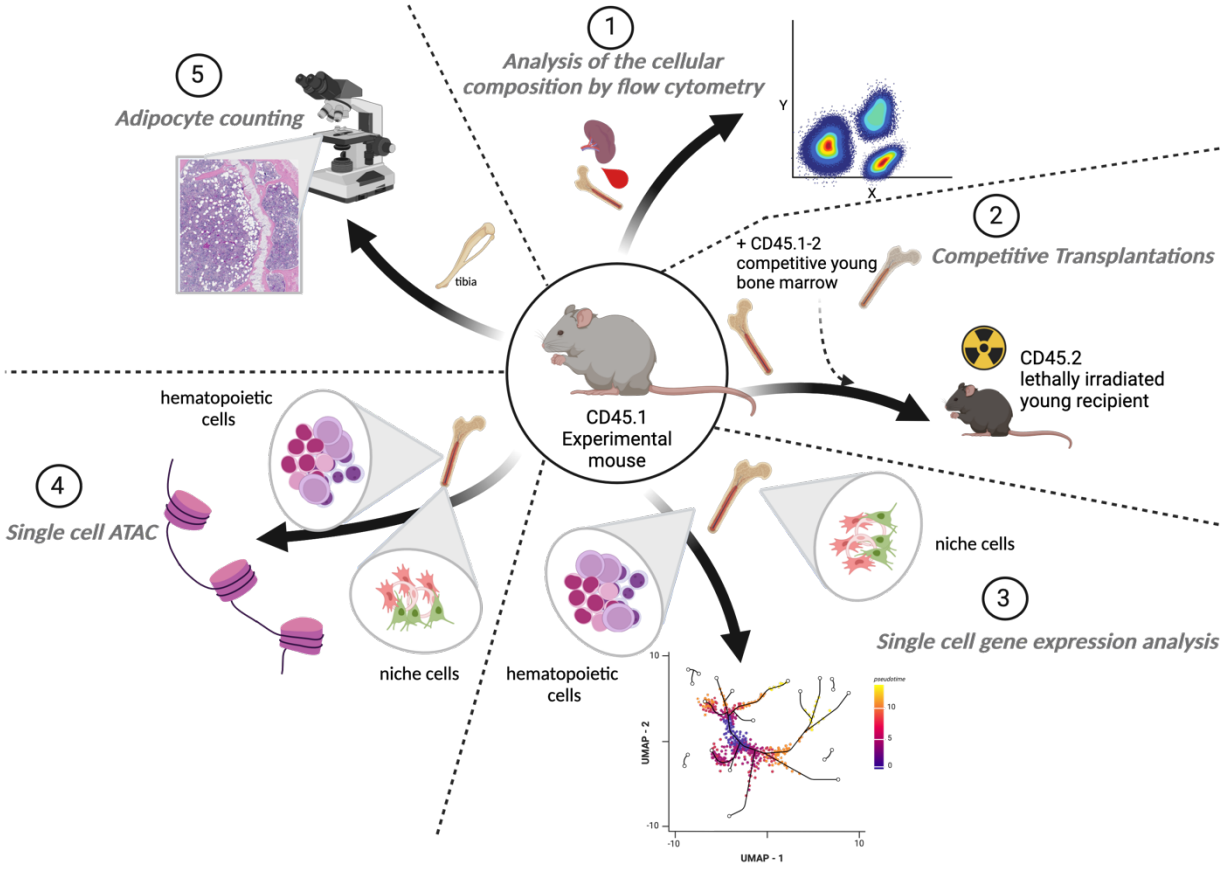

Figure 6.1. A comprehensive dataset to reveal ageing complexity. Overview of all the data tiers compiling the dataset. The figure was created with BioRender.com.

6.1.2 Phenotypic variance increases with age

To address potential diversity in my isogenic mouse dataset, I first examined several classical parameters indicative of hematopoietic ageing. Some of these parameters include hemoglobin levels and the ratio of myeloid (CD11b+) to lymphoid cells (sum of B cells and T cells) per ml of peripheral blood (PB) in the experimental mice. Additionally, the percentage of LT-HSCs in the LSK primitive compartment was measured in the bone marrow. Furthermore, widely recognized metrics of hematopoietic ageing can also be measured in the recipients' PB, such as the percentage of cells derived from the donor identified by the CD45.1 antigen (referred to as "donor chimerism"). Two more metrics that I inspected here were the donor chimerism explicitly measured in the myeloid compartment, addressing a potential myeloid bias and a more pronounced aged phenotype, and, once more, the myeloid-to-lymphoid ratio, serving as a gauge for tissue regeneration capacity.

In most of the classical metrics, a gradual change could be observed from young to old age, with the middle-aged group sustaining similar hemoglobin levels and myeloid-to-lymphoid ratio in PB as the ones presented by the young control group (Fig. **6.2A**). Conversely, the LT-HSC

population in the bone marrow of the middle-aged mice was inflated as much as in the older group, deviating dramatically from the levels observed in young mice (Fig. **6.2B**). Importantly, as observed in the figures, the consistency of the values displayed by young mice starkly contrasts with the variability noted in older and, occasionally, middle-aged groups, as evidenced by their variances (Fig. **6.2A, B**).

After the competitive transplantations, donor and competitor cells vie to reconstitute the recipient's hematopoietic system. Typically, superior performance in this competition usually indicates intact stem cell functionality, with young-like stem cell activity translated into approximately 50% ± 10% of donor chimerism, complementing the competitors' contribution. However, aged donors frequently underperformed compared to the young competitors, contributing less than 40% of the blood regeneration. Nonetheless, when analyzing the myeloid compartment specifically, the performance of aged donors was rescued, nearly matching the efficiency of young donors. Finally, the myeloid-to-lymphoid ratio in the PB of the recipient mice mirrored the ratios reported in their donors, suggesting that the young hosting organism cannot always alleviate the age-related flaws of the transplanted cells (Fig. **6.2C**). Notably, though, the variance in the recipient group that received old grafts, particularly in the chimerism cases, was dramatically elevated and displayed bi-directional extremes.

Next, I wanted to investigate whether there were any linear correlations across these classical parameters, whether they remained stable throughout time, and whether they could ultimately be sources of variance. Since age is a strong factor driving correlation and masking weaker connections, I inspected for correlations in young and old samples separately. Intriguingly, within the young dataset, a positive correlation emerged between the stem cell pool size and hemoglobin levels, potentially suggesting enhanced erythropoiesis with increasing numbers of LT-HSCs. On the other hand, larger LT-HSC populations correlated negatively with overall and myeloid-specific donor chimerism in PB, implying diminished post-transplantation performance with expanded stem cell populations. Remarkably, the total donor chimerism and the myeloid-specific chimerism presented by young donors exhibited a perfect correlation, highlighting the balanced reconstitution capabilities of young LT-HSCs (Fig. **6.2D** left panel**, 6.2E**).

The relationships identified in the young dataset were absent from the old dataset. Following the correlation analysis, only two metric pairs appeared linked: donor chimerism versus the myeloid-to-lymphoid ratio in recipient PB and total against myeloid-restricted donor chimerism. Notably, the correlation of the first pair was solely driven by one outlier, suggesting that no such correlation truly existed. The second pair displayed a strong correlation akin to that observed in young samples, indicating a linear relationship between overall donor chimerism and myeloid lineage contribution. An important distinction was that although the linear relationship in the young mice followed a $y=x$ trend, the aged donors' myeloid contributions consistently exceeded their total chimerism values, highlighting a mono-lineage potential (Fig **6.2D** right panel**, 6.2F**).

These findings collectively suggested that while literature-reported average changes are consistently observed, significant variability characterizes the aged hematopoietic phenotype absent from young individuals. Furthermore, the young system displays interconnected classical metrics, primarily implicating the stem cell pool size, indicative of a regulated system where stem cells maintain tissue homeostasis. Over time though, these relationships seem to dissipate, implying that hematological ageing is marked by a gradual loss of regulation, allowing stochasticity to dictate the fate of the system.

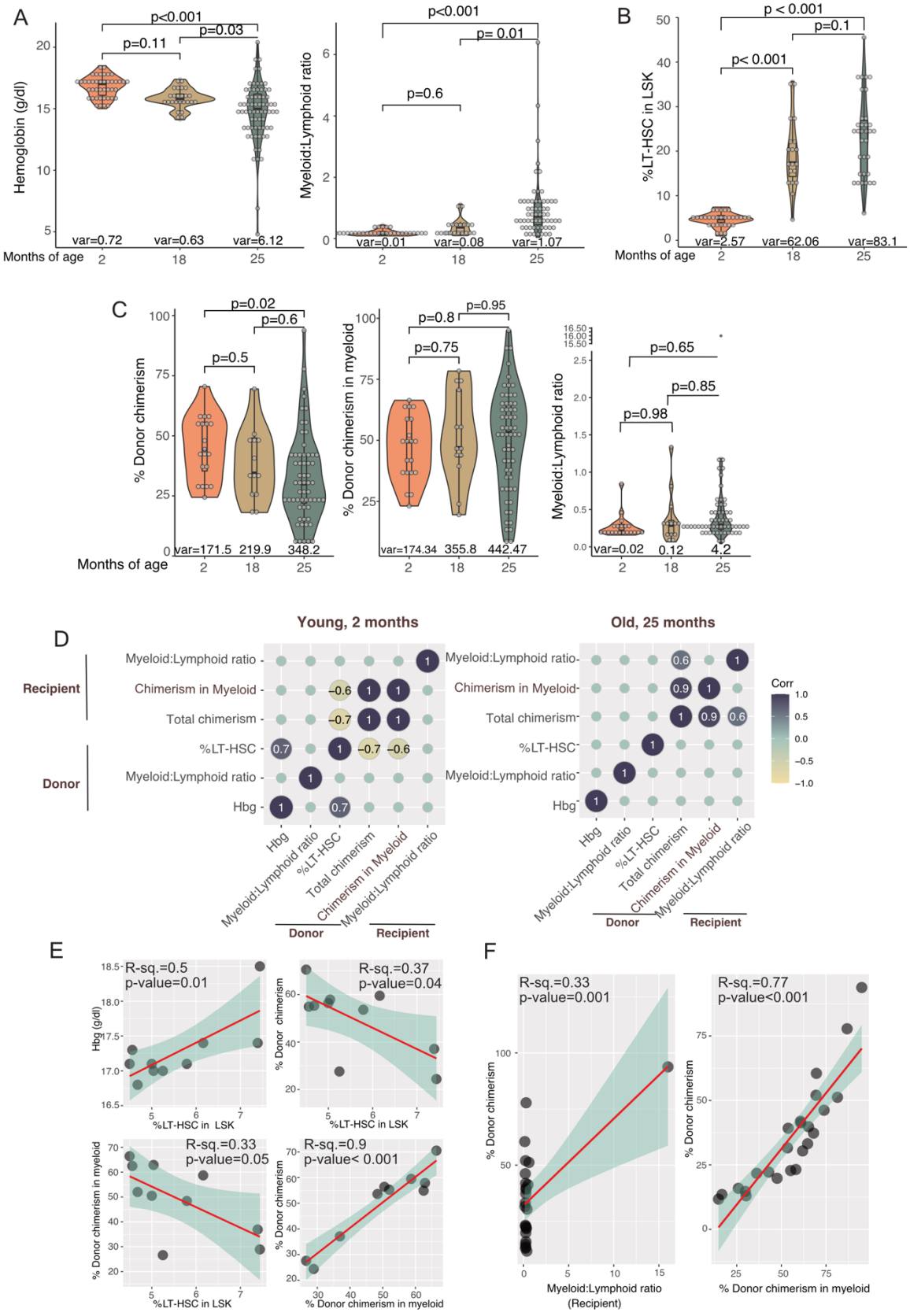

Figure 6.2. Increased variance and lack of connections across the classical parameters of hematopoietic ageing. (Legend continues on the next page).

A) Hemoglobin levels (g/dl) and myeloid: lymphoid ratio, as measured in PB of experimental mice. **B)** %LT-HSCs in the LSK compartment analyzed in the bone marrow of experimental mice. **C)** Transplantation metrics, measured in the blood of the recipients. Left: % donor chimerism indicated the total contribution of the donor in blood reconstitution, assessed by the percentage of CD45.1-expressing leukocytes. Middle: % donor chimerism specifically in the myeloid compartment (CD11b+ cells). Right: myeloid-to-lymphoid ratio measured in the PB of recipient mice. All comparisons in the panels mentioned above were conducted with One-way Analysis of Variance (ANOVA), followed by Tukey's honestly significant difference (HSD) test for multiple comparisons correction. Significance is denoted by the corrected p-values depicted directly on the plots. Each data point represents one individual mouse. The variance of each group is also mentioned directly on the plots. **D)** Linear correlations across the classical parameters of hematopoietic ageing for young subjects (left) and old subjects (right). Each significant correlation is denoted by its correlation coefficient. **E)** Scatter plots indicating the correlated parameters across the young subjects, as resulted from D (left). **F)** Scatter plots indicating the correlated parameters across the old subjects, as resulted from D (right). Linear regression for panels E and F was performed with the `lm()` function in R; p-value and adjusted R-squared are indicated directly on the plots. Green shaded areas indicate the 95% CI.

6.1.3 Ageing heterogeneity expands in all major tissues of native hematopoiesis

To broaden the investigation beyond the classical metrics discussed previously, I inspected the full range of variables recorded both in the native and recipient systems. To do so, I performed Principal Component Analysis (PCA) on a per-tissue basis, integrating most of the measured metrics for a holistic understanding.

In the native blood compartment, the first three principal components (PC) accounted for 64.1% of the total variation (Fig. **6.3B**). The major determinants of PC1, which represented the most significant age-associated alterations driving cluster separation, originated from the myeloid compartment and the CD8+ T cells, both of which typically increase in numbers with age[154]. Specifically, patrolling monocytes (CD11b+ Ly6C^{low}), memory (CD8+ CD44+ CD62L+) and effector T (CD4+/CD8+ CD44+ CD62L-) cell subpopulations contributed significantly to the variability explained by PC1 (Fig. **6.3C**). The PCA plot further revealed that young and middle-aged individuals formed more compact clusters, indicating relatively homogeneous phenotypes compared to their older counterparts. Interestingly, the old group blended partially with the middle-aged cluster, while a small fraction diverged across various directions on the plot (Fig. **6.3A**).

The native bone marrow analysis unveiled even greater heterogeneity within the old group, with the first two PCs accounting for 58.2% of the observed variation (Fig. **6.3E**). Here, the age-related dispersion implicated both PCs (Fig. **6.3D**). The most well-known age-associated changes, such as alterations in the stem cell pool size and myeloid lineage bias, primarily influenced PC1. In contrast, PC2 was associated with changes in megakaryo-erythropoiesis, the MPP5 population, and the CD4+ T cell compartment (Fig. **6.3F**).

Finally, I also inspected the spleen, normally characterized by its lymphopoietic capacity and subtle myeloid cell presence, mainly corresponding to tissue-resident monocytes[155].

According to my data, increased spleen masses were consistently observed with ageing, reflecting increased cellular load due to myeloid cell infiltration. Furthermore, although rare in the context of natural ageing, the spleen supports hematopoiesis under pathological conditions[156]. Therefore, characterizing the splenic cellular composition was also crucial. PCA using the splenic dataset showed complete overlap between young and middle-aged groups. However, a notable fraction of the oldest individuals deviated along the PC1 component, which accounted for 58.3% of the variation and highlighted increased myeloid cell infiltration and extramedullary hematopoiesis (Fig. **6.3G-I**).

Extending this analysis to recipient blood and bone marrow 24 weeks post-transplantation (pTx) revealed a significant overlap among the age groups. This observation suggested that the assay minimized strong age-associated factors. However, it's crucial to note that a lack of cluster density was observed across all age groups in blood. In contrast, in the bone marrow, this scarcity was predominantly evident in a small subset of aged individuals, similar to the native tissues (Fig. **6.3J**).

This analysis illuminated the growing heterogeneity and complexity of the hematopoietic system with age across all major tissues involved in the native organism. According to PCA, ageing did not manifest as a uniform process but appeared to be characterized by a broad spectrum of changes, affecting various cell populations differently across the studied tissues. Moreover, the transplantation studies revealed that, while certain age-associated features could be mitigated, underlying heterogeneity and complexity would still persist, potentially underscoring stem cell-endogenous alterations that occurred over time.

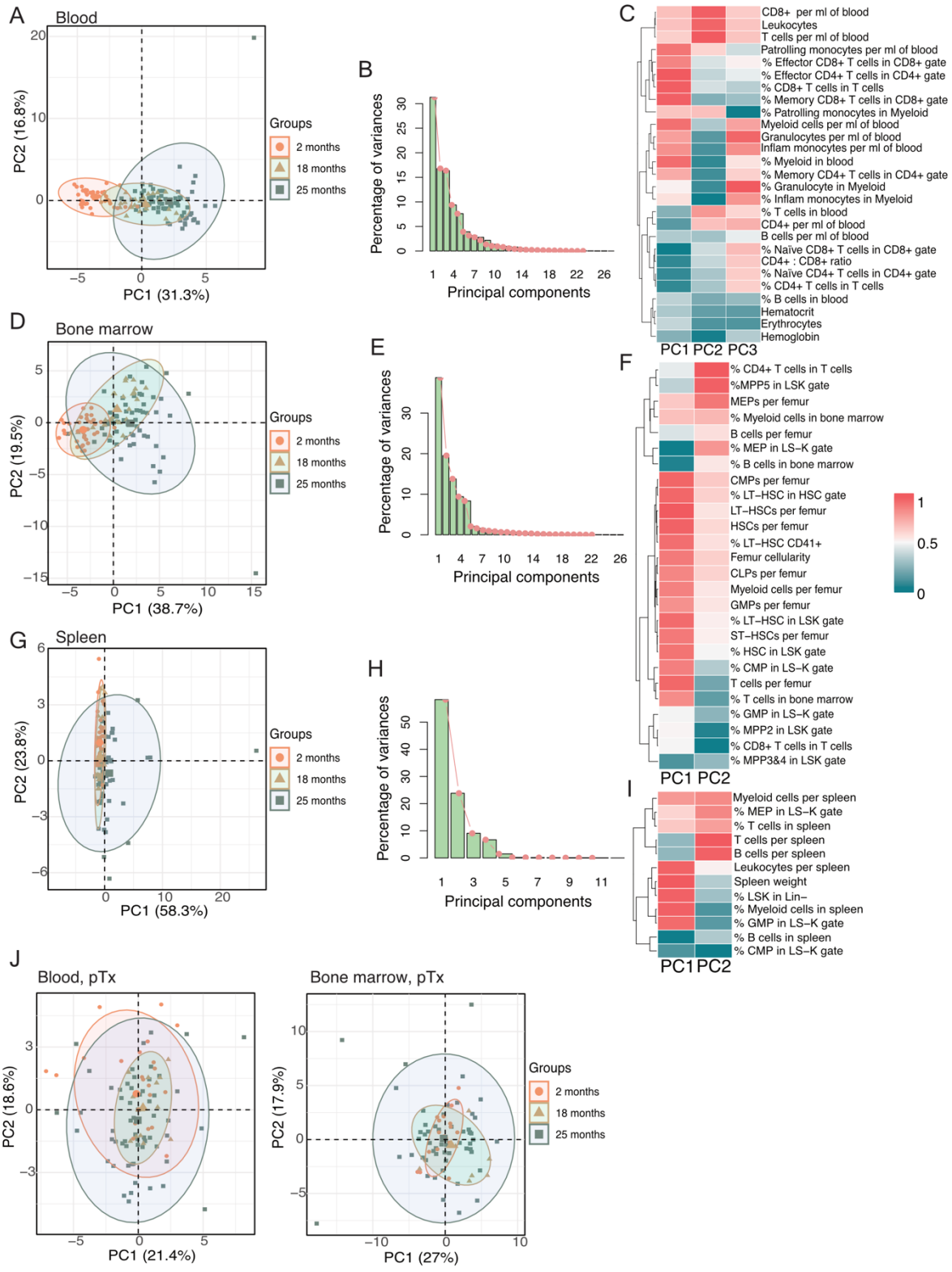

Figure 6.3. Heterogeneity as an element of the aged hematopoietic tissues. A) PCA plot depicting the blood phenotype of the experimental mice across different time points. Each dot represents an individual experimental mouse. **B)** Eigenvalues displaying the variance explained by each principal component in the blood dataset. **C)** Heatmap describing the scaled contribution of the blood metrics on the first 3 PCs. (Legend continues on the next page).

D) PCA plot depicting the bone marrow phenotype of the experimental mice over time. Each dot represents an individual experimental mouse. **E)** Eigenvalues displaying the variance explained by each principal component in the bone marrow dataset. **F)** Heatmap describing the scaled contribution of the bone marrow metrics on the first 2 PCs. **G)** PCA plot depicting the splenic phenotype of the experimental mice over time. Each dot represents an individual experimental mouse. **H)** Eigenvalues displaying the variance explained by each principal component in the splenic dataset. **I)** Heatmap describing the scaled contribution of the spleen metrics on the first 2 PCs. **J)** PCA plots describing the blood and bone marrow phenotype measured in the recipients at 24 weeks pTx.

6.2 Age-associated niche remodeling as potential influence of the overall phenotype

Despite variations observed in the old group pTx, some profound age-related alterations were alleviated, leading to overlapping clusters after the PCA. Given that transplantation provides a young niche for the old stem cells, I decided to explore the influence of the aged bone marrow environment on the overall hematopoietic phenotype by analyzing single-cell gene expression data acquired from both hematopoietic and niche populations in 2-month and 25-month-old mice. Hematopoietic cells were collected by sorting LSK, LS-K and CD45+ gates of the central marrow, after the leg bones were flushed. This strategy ensured a comprehensive representation of the hematopoietic tree. Moreover, for accurate niche representation, endothelial and endosteal stromal populations were collected from two generic sorting gates following digestion of the flushed bones. The experimental approach is detailed in paragraph **8.8** of the Materials & Methods section. The resulting dataset comprised approximately 110,000 high-quality cells in total. A concise uniform manifold approximation and projection (UMAP) is shown in Fig. **6.4A**, while the UMAP with the detailed cluster annotation is provided in Supplementary, Fig.**S9**.

6.2.1 Emergence of a new heterogeneous adipocyte-progenitor population in the aged niche

The gene expression analysis not only confirmed, in many cases, alterations in cellular composition with age, as supported by the existing literature, but also generally aligned with my flow cytometry results. In the most primitive hematopoietic compartment, represented by the LSK gate, there was a 9-fold increase of the LT-HSC population with age, while 2 MPP clusters reduced their size. Next, in the compartment of lineage-restricted progenitors collected by sorting LS-K cells, only the MEP cluster showed significant expansion, in accordance with the observations suggesting that aged stem cells favor megakaryo-erythropoiesis[33]. At the mature cell level, two notable findings were observed. The first was the accumulation of activated B cells in the aged bone marrow (`Activated_B_cell` cluster), a cluster characterized by enhanced expression of genes related to the major histocompatibility complex II (MHC-II) and components of the B-cell receptor (*Cd74, H2-Eb1, H2-Aa, Cd79a, Cd79b* and *Iglc* genes). The second finding referred to Natural Killer T cells (NKT), a small population crucial for defences against

infections[157,158]. These cells express invariable T-cell receptors (TCR) and recognize lipid antigens presented by CD1d rather than MHC molecules, typically associated with T cells[157,158]. Although NKT cells are frequently overlooked in ageing studies, I observed a significant accumulation of their population within the aged bone marrow (Fig. **6.4B**). Interestingly, similar observations have been reported in a previous study that also linked this accumulation to impaired adaptive immunity mediated by T-cells in aged organisms[159].

The niche populations captured contained cells with more primitive transcriptional profiles, primed towards either the adipocytic or osteocytic lineages. These populations likely represented MSCs and were named "Adipo-CAR" and "Osteo-CAR", respectively, following the terminology introduced by Baccin et al.[100]. The dataset also included larger fibroblastic and endothelial clusters, as well as smaller compartments with Schwann cells, smooth muscle pericytes and skeletal muscle cells.

The niche analysis also unveiled notable shifts in cell population dynamics within the aged bone marrow. Interestingly, there was a significant reduction in the size of clusters with fibroblastic profiles (`Fibroblasts_1-3`, `Fibroblasts_spe_1-4`, `Myofibroblasts`), a decline not widely discussed in the literature but observed in other organs such as the dermis[160]. Concurrently, as expected based on prior knowledge[96], adipocyte-related clusters (`Adipo_osteo_CAR`, `Adipo_CAR_1-5`) expanded with age, whereas osteocyte-associated clusters diminished (`Fibro_osteo_1-2`, `Osteoblasts`) (Fig. **6.4D**). These observations validated the reported MSC differentiation bias towards adipogenesis with age[96,123]. Finally, the composition of the endothelial compartment remained largely unaltered, except for an increase in the `Endothelial_1` cluster with age (Fig. **6.4E**).

A particularly intriguing finding was the identification of a cluster, specific to older individuals, named Adipo-CAR3. This cluster comprised a group of MSCs with an adipocyte-biased transcriptomic profile that further displayed expression of inflammatory genes such as *Cxcl9, Cxcl10, Ccl19, Ligp1* and *C3*, distinguishing it from other Adipo-CARs (Fig. **6.4C**). Additionally, this population displayed substantial heterogeneity in size across different old individuals, becoming one of the most variable niche clusters of the dataset (Fig. **6.4F**). The analysis of the niche transcriptome was conducted by Dr. Charles Dussiau, a post-doctoral fellow in our lab.

In this part of the study, we successfully mapped some of the well-characterized age-associated alterations of the hematopoietic system and its niche at the transcriptomic level. Notably, a completely new population was identified in the aged niche that demonstrated both age-dependency and considerable variance across the old individuals. The detection of Adipo-CAR3 underscores the complex remodeling that the bone marrow undergoes with age and may be pivotal for understanding the mechanisms that contribute to the variability of hematological ageing.

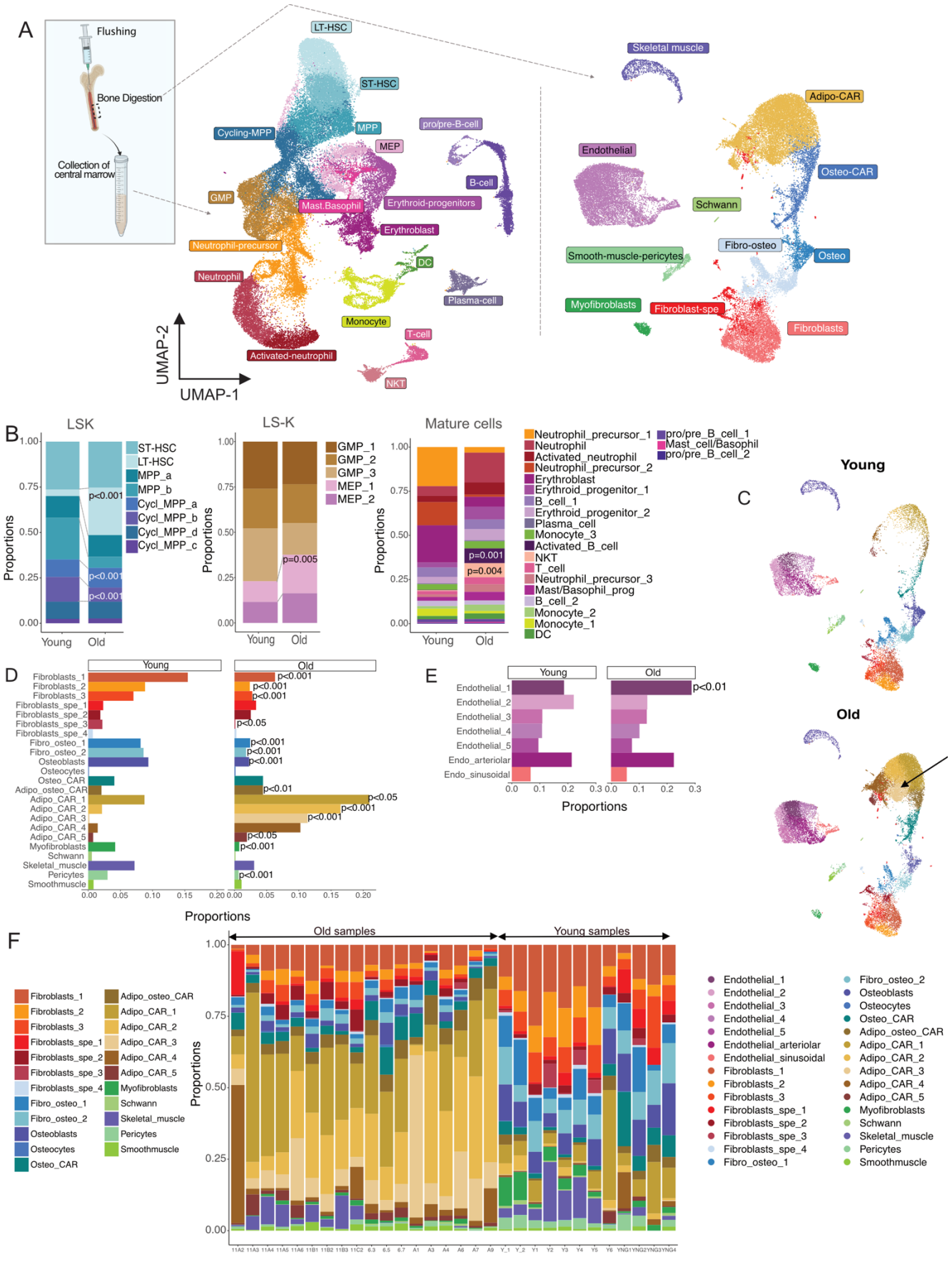

(Legend continues on the next page)

Figure 6.4. The Adipo-CAR3 cluster emerges during the age-associated niche remodeling. A) UMAP of the hematopoietic (left) and niche compartment (right). Hematopoietic cells were collected from the central marrow after flushing the leg bones, while the niche populations were collected after digesting the flushed bones. The figure explaining the experimental approach was created with BioRender.com. **B)** The cellular composition of each sorting gate used to collect hematopoietic cells. The significantly altered clusters are marked by the p-values calculated using t-test and Benjamini-Hochberg false discovery rate (FDR) correction (FDR<0.05). **C)** Detailed niche UMAPs, split by age group. The black arrow indicates the old-specific Adipo_CAR_3 population **D, E)** The cellular composition of each sorting gate used to collect bone marrow niche cells. The significantly altered clusters are marked by the p-values calculated using t-test and Benjamini-Hochberg false discovery rate (FDR) correction (FDR<0.05). **F)** The cellular composition of the stromal cell gate, displayed for each individual sample composing the dataset.

6.2.2 Adipo-CAR3 cells display a distinct inflammatory transcriptomic profile

To further elucidate the role of Adipo-CAR3 in the aged niche, Dr. Charles Dussiau investigated the activation of pathways relevant to hematopoiesis, inferred by the single-cell gene expression data using decoupleR[161] in junction with PROGENy database for pathway activity[162]. Initially, all Adipo-CAR clusters in the old group displayed a response to TNFα, evident by the upregulated expression of the associated genes (Fig. **6.5A**). Moreover, specifically within the Adipo-CAR3 cluster, interferon response via JAK-STAT signaling was detected, highlighted by the upregulated expression of genes, such as *Oas1a, Oas3, Rigi* and *Rsad2*[163–167](Fig. **6.5B**). Additionally, the old adipocyte progenitor clusters were marked by a pronounced expression of various chemokines, with peak expression levels observed in Adipo-CAR3 space (Fig. **6.5C**). This chemokine signature, including genes such as *Ccl5* (RANTES) and various Cxcl-members, suggested an inflammation-promoting role beyond mere inflammatory response. Such a behaviour highlights the potential influence of the old stroma on the age-associated phenotype of the hematopoietic system[168,169]. Lastly, Adipo-CAR3 displayed gene expression patterns associated with antigen presentation through MHC-II receptors, including receptor components, such as *H2-Aa, H2-Oa, H2-Eb1, H2-Ob, H2-Ab1*, the *Cd74* transporter and the transactivator *Ciita*[170–172]. Intriguingly, the niche-originated antigen presentation was restricted solely to the areas occupied by Adipo-CAR3 and Endothelial-Sinusoidal clusters in the old bone marrow (Fig. **6.5D**).

Collectively, these findings suggested that Adipo-CAR3 cells likely play a multifaceted role in the aged bone marrow environment, participating not only in inflammatory responses but also in subsequent antigen presentation and likely immune modulation. This complex population functionality suggested its potential impact on the diversity of phenotypes observed in hematological ageing.

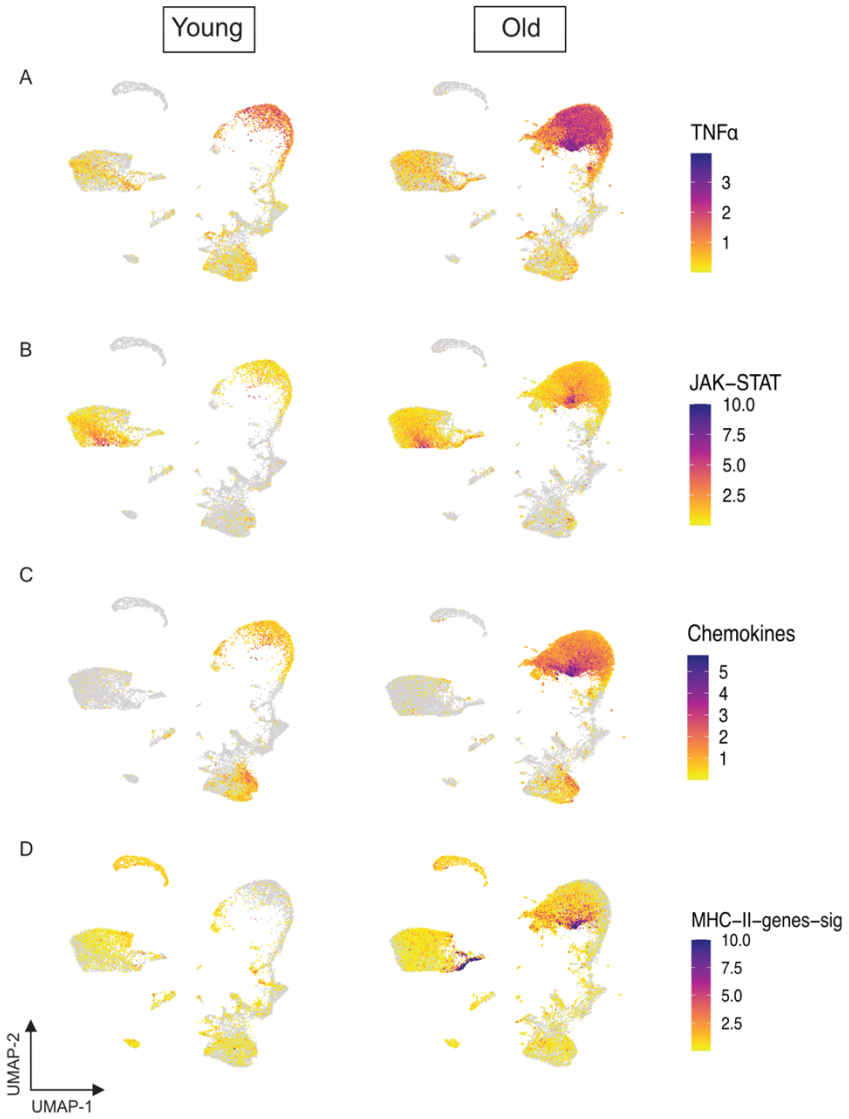

Figure 6.5. Transcriptomic profiles of old adipo-primed MSCs reveal inflammatory response and antigen presentation. Niche UMAPs depicting: **A)** Enhanced TNFα response by old Adipo-CAR clusters, resulted from pathway activity inference with decoupleR. **B)** JAK-STAT signaling originating specifically from Adipo-CAR3 cells, resulted from pathway activity inference with decoupleR. **C)** Old Adipo-CARs presented chemokine gene expression signature. **D)** Upregulated expression of MHC-II related genes in the Adipo-CAR3 and the Endothelial-Sinusoidal cluster, indicative of enhanced antigen-presentation capacity with ageing.

6.2.3 Formation of a Neutrophil-Adipo-HSC network in the aged bone marrow

Leveraging this extensive dataset, the study probed intercellular communications between hematopoietic cells and their surrounding environment. Dr. Charles Dussiau led this analysis, utilizing the MultiNicheNetR tool to assess the expression of ligand and receptor pairs at the pseudobulk level, considering also the expression of genes involved in the downstream pathways[173]. Eventually, each interaction was assigned a priority score to indicate its intensity.

Out of the first 50 interactions prioritized, 34 were present in younger subjects, while only 16 were detected in the old subjects, suggesting a decrease in the interaction intensity with age. Within the young bone marrow, 30 of the 34 interactions described a complex network of extensive communication among osteocytic clusters (`Osteo_CAR` and `Osteo` clusters), fibroblasts (`Fibroblasts` and `Fibro_osteo` clusters) and endothelial cells (`Endothelial` clusters). The remaining 4 interactions involved Adipo-CAR cells communicating within their group, with Fibro-Osteo and Osteo-CAR clusters, and with ST-HSCs via the *Kitl-Kit* axis, which consists of SCF and the c-kit receptor. Within the old bone marrow, the majority of interactions were still measured among osteocytes, fibroblasts and endothelial cells. However, activated neutrophils appeared to be initiating strong interactions, achieving communication with Adipo-CARs, LT-HSCs, and Osteo-CARs (Fig. **6.6A**).

Further examination of the interactions initiated by activated neutrophils towards the adipocyte progenitors revealed 4 upregulated communication axes with age. One such axis involved the increased expression of the IL-6 family member, oncostatin M (*Osm* gene), by activated neutrophils and its receptor, *Osmr*, by Adipo-CARs. Oncostatin M further stimulated the IL-6 cytokine family signal transducer, as detected by the upregulation of the *Il6st* gene in Adipo-CARs. Another noteworthy interaction between activated neutrophils and adipocyte progenitors involved IL-1β and its receptor IL-1R1, as shown by the upregulation of the respective genes. Interestingly, IL-1β was previously reported to originate from the aged stroma[104]. Lastly, the fourth axis involved the *Ifitm6* gene, encoding the Interferon-induced transmembrane protein 6 expressed by neutrophils, contacting the CD81 receptor on the surface of adipocyte progenitors (Fig. **6.6B**).

The analysis also highlighted that interactions driven by oncostatin M and IL-1β displayed higher priority scores than the IFITM6-CD81 pair. Oncostatin M influenced the expression of genes relevant to the complement (*C1s1, C3, Cfb*) and antigen presentation via MHC-II (*H2.M3, H2.Q10, H2.Q6, H2.T23*). Moreover, the predicted interaction of IL-1β with its receptor upregulated the expression of certain chemokine genes (*Cxcl1, Cxcl16, Cxcl9*) and decreased *Stat5a*, which encodes for the respective kinase, and *Vcam1*, which codes for a vascular cell adhesion molecule, critical for bone marrow intercellular interactions[174] (Fig. **6.6C**).

The analysis discussed so far pertained to interactions initiated by a specific cluster of activated neutrophils, named after a modest *Il1b* expression among its top markers. To investigate

whether these interactions differed from those involving other neutrophilic clusters, Dr. Charles Dussiau inspected the communication between the cluster of normal neutrophils and Adipo-CARs. Intriguingly, this pair exhibited a distinct interaction through the TNF axis, with *Tnf* expressed by neutrophils targeting the TNFR-II receptor, encoded by the gene *Tnfrsf1b*, on the surface of adipocyte progenitors (Fig. **6.6D**). This observation underscored how old adipocyte progenitors respond to multiple inflammatory stimuli from hyperactive innate immune cells.

In this context, the TNF axis between neutrophils and adipocyte progenitors upregulated genes related to inflammatory response, such as *C1s1, Cfb, Ctss, Cxcl1, Cxcl10, Irf7 and Ptges*. Conversely, it downregulated the expression of *Ccn2, Stat5a* and *Vcam1, as observed* with the previous axes stemming from activated neutrophils. Additionally, *Angpt1* and *Pappa* genes were also downregulated, with the former being involved in angiogenesis and the latter encoding the protein pappalysin 1, which contributes to the activation of the insulin-like growth factor (IGF) pathway[175] (Fig. **6.6E**).

Further inspections of the interactions focused on the communication between the adipo-primed MSC and the primitive hematopoietic compartment. It was revealed that three communication axes involving Adipo-CAR cells and ST-HSCs were notably weakened with age. The first axis of communication, observed for the first time in such a context, involved VCAM1 expressed by Adipo-CARs binding to integrin A4 (ITGA4) on the surface of ST-HSCs, encoded by the homonym gene. Additionally, a strong interaction in the young bone marrow between *Kitl-Kit* was also diminished with age; an interaction that has been suggested to be crucial for HSC maintenance[176]. Lastly, the axis Angpt2-Tie1 axis was found to be weaker in older individuals, although its impact is unclear given the TIE1 receptor's presumed redundancy in adult hematopoiesis[177] (Fig. **6.6F**).

This part of the study revealed significant alterations in the intercellular communication within the bone marrow as a result of ageing. The complex interactions across the stromal populations that characterize the young, healthy bone marrow appeared weaker with age. Conversely, in the old bone marrow, the most robust communications involved inflammatory mediators guided by the populations of the innate immune system towards the stroma and particularly adipocyte-primed MSCs. Adipo-CARs' response to these signals included, apart from inflammation, expression of MHC-II components and downregulation of interactive cues towards HSCs. This demonstrated the profound impact of ageing on bone marrow communication dynamics.

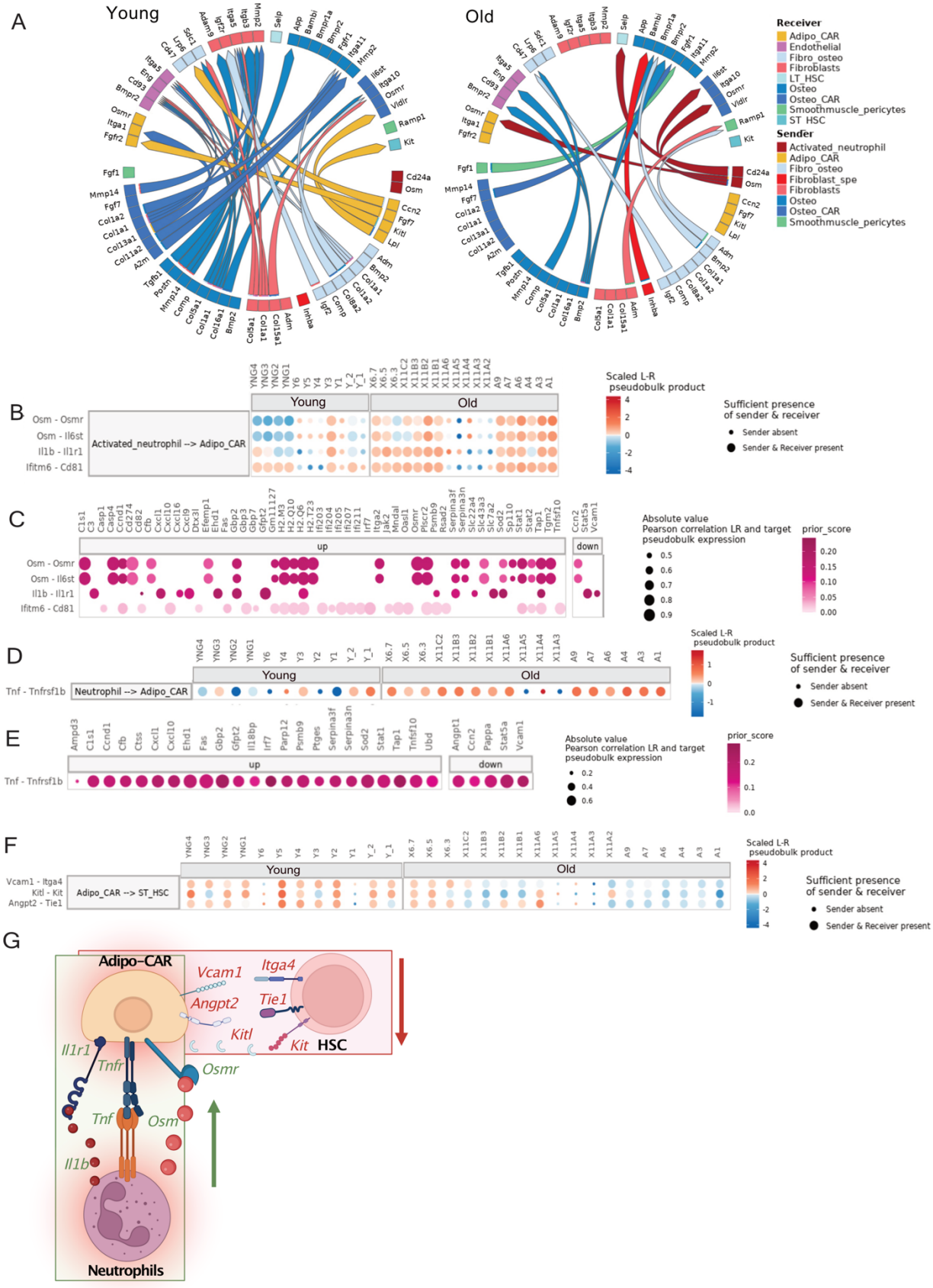

Figure 6.6. Adipo-CARs respond to inflammatory cues from the innate immune system and downregulate their communication with HSCs. (Legend continues on the next page)

A) Circos plots representing the top 50 intercellular interactions of the dataset, split by age group. **B)** Interactive pairs of ligands guided by activated neutrophils towards receptors expressed by adipocyte progenitors. Each column depicts one sample that corresponds to one individual mouse. **C)** Genes, the expression of which appeared affected within the target cells (Adipo_CARs) by the aforementioned interactions. The size of the dot describes the level of correlation between the expression of the interactive parts (ligand, receptor, LR) and the pseudobulk expression of the target cells. The color intensity depicts the priority score assigned by the tool to describe the level of interaction. **D)** Interactive pair of the ligand guided by neutrophils towards the receptor expressed by Adipo_CAR cells. Each row represents one sample that corresponds to one mouse. **E)** Genes, the expression of which appeared affected within the target cells (Adipo_CARs) by the interaction showed in (D). The size of the dot describes the level of correlation between the expression of the interactive parts (ligand, receptor, LR) and the pseudobulk expression of the target cells. The color intensity depicts the priority score assigned by the tool to describe the level of interaction. **F)** Interactive pairs of the ligands guided by Adipo_CARs towards receptors expressed by ST-HSCs. Each row represents one sample that corresponds to one mouse. **G)** Graphical representation of the newly discovered three-population network within the aged bone marrow. Schematic created with BioRender.com.

6.2.4 The old-specific inflammatory network does not explain the distinct aged phenotypes

Considering the influence of the niche on HSC behaviour and regeneration potential[104,178,179], I hypothesized that Adipo-CAR3 cells, which emerge only later in life and show variable proportions across individuals, could significantly influence the overall hematopoietic phenotype. To explore this, I performed another correlation analysis to examine possible linear relationships between the size of the Adipo-CAR3 population, the intensity of inflammatory transcriptional signals detected in the adipocyte compartment, and key metrics of hematological ageing. The metrics I interrogated included the blood composition and stem cell pool in the bone marrow of experimental mice, as well as their performance as donors after competitive transplantations.

Interestingly, the analysis revealed that most metrics remained utterly unrelated. Strong correlations occurred almost exclusively among the different chimerism measurements, as anticipated (Fig. **6.7A**). Specific metrics assessed through the single-cell gene expression analysis also showed connections. Precisely, the Adipo-CAR3 size was positively correlated with the chemokine and TNFα response signals measured in the entire population of Adipo-CARs, as it was the subcluster with the highest expression of the corresponding genes, as shown in Fig. **6.7A, 6.7C.** TNFα signaling was also positively linked with JAK-STAT signaling, suggesting intertwined pathways within the same cells[180]. Finally, the correlation matrix indicated a positive link between the JAK-STAT signaling and the MHC-II signal in adipocytes; however, a linear fit was inconclusive, implying that MHC-II upregulation might not be a direct response to this particular signaling (Fig. **6.7B**).

The critical question concerning the link between Adipo-CAR-related metrics and the overall hematopoietic phenotype in aged individuals remained elusive. Although the correlation

matrix hinted at a modest negative correlation between the Adipo-CAR3 population and T cell chimerism in recipients' PB, scatter plots and linear modeling showed poor fit and no observable connection. Interestingly, the same population was highly correlated with the ratio describing the proportions of myeloid cells over the lymphoid lineage in the native hematopoietic system. Yet, this appeared to be influenced by an outlier -a mouse with high myeloid content in its blood and a large Adipo-CAR3 reservoir in its bone marrow (Fig. **6.7C**).

In conclusion, the discovery of old-specific adipocyte-biased MSCs and their associated signaling suggests an additional layer of variability in hematological ageing, but without any clear links or causalities with the system's overall phenotype. The lack of deterministic explanations in this thesis underscores that ageing may predominantly be governed by stochastic events.

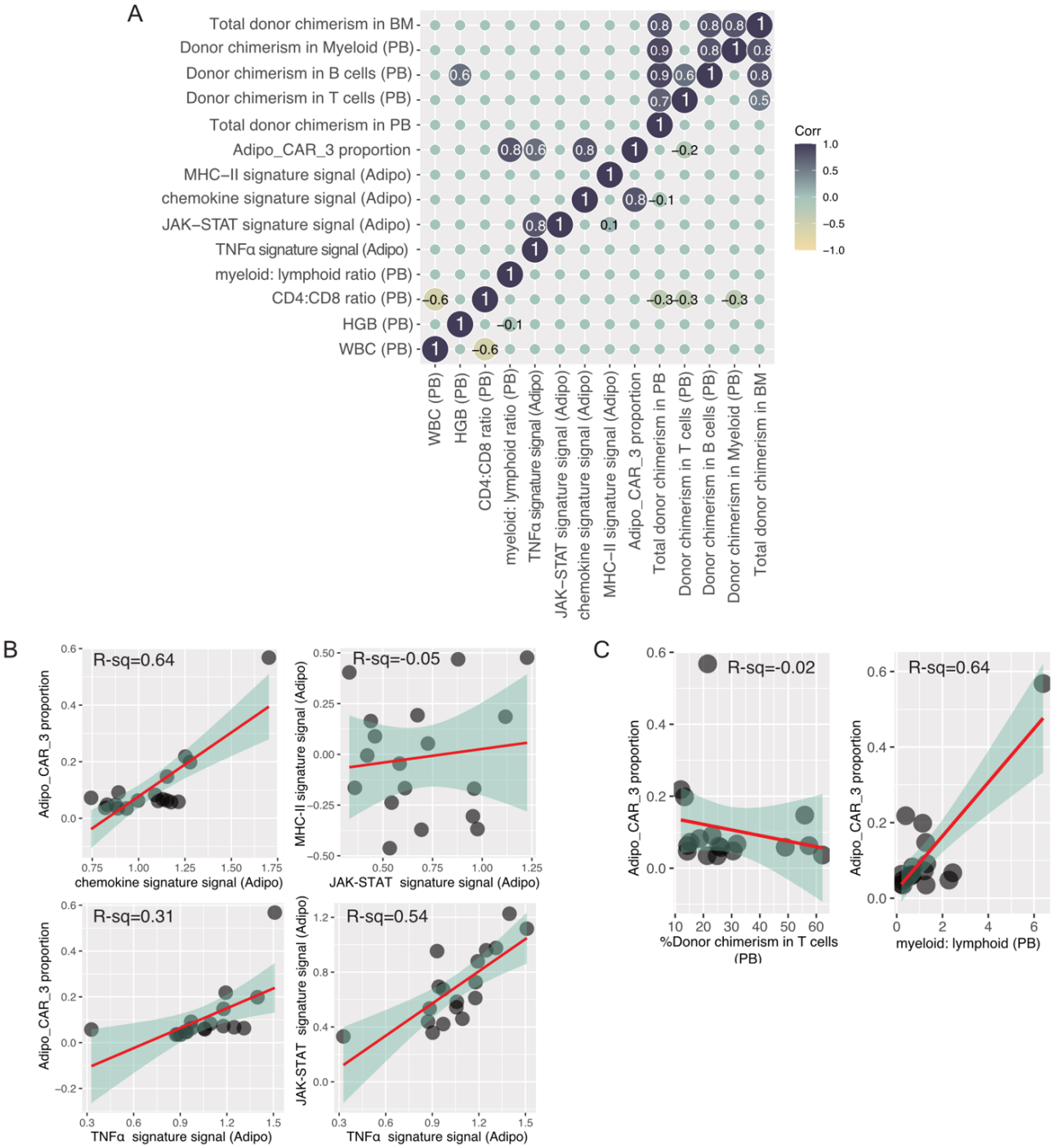

Figure 6.7. The old-specific Adipo-CAR3 population is not responsible for the overall hematological phenotype. **A)** Correlation analysis across classical ageing parameters alongside the newly discovered adipocyte progenitors and their emitted signals. The analysis was performed on the 18 old subjects from which scRNA-seq of the bone marrow was performed. Only significant correlations are shown, color-coded based on the correlation coefficient ("Corr"). P-values were adjusted for multiple comparisons using the Benjamini-Hochberg post-hoc test. **B)** Scatter plots indicating the correlations detected in A, between the parameters relevant to Adipo-CARs and their signaling, as detected during the scRNA-seq analysis. **C)** Scatter plots indicating the correlations detected in A, between adipocyte-associated parameters in the old bone marrow and classical aged hematopoietic parameters. Linear regression for panels B and C were performed using the `lm()` function in R. Adjusted R-squared are indicated directly on the plots. 95% CI are highlighted by the green areas.

6.3 Lifelong inhibition of critical inflammatory pathways does not prevent hematological ageing

IL-1 emerged as a critical mediator of the communication between aged neutrophils and adipocyte-biased MSCs. This interaction likely impairs the communication of these adipocyte progenitors with ST-HSCs, the HSC subfraction likely contributing to the faster restoration of tissue homeostasis. Studies have suggested that IL-1 is extensively secreted by the aged stroma[104], or the bone marrow myeloid cells as response to inflammatory cues[181], ultimately influencing the potential of HSCs. However, our results did not recapitulate stromal expression of *Il1b*. Furthermore, it has been claimed that treatments blocking the IL-1 signaling, such as anakinra, could have rejuvenative effects[104,181–183]. To investigate the role of IL-1 and its interactions during ageing, and to assess its impact on the overall phenotype and the observed heterogeneity, I characterized the cellular composition of blood and bone marrow in aged mice lacking the primary receptor for IL-1 ($Il1r1^{-/-}$; mentioned as "IL1R KO") using flow cytometry.

Another communication axis between neutrophils and adipocyte progenitors involved the TNFα pathway, also a critical age-associated signal. Despite the absence of direct evidence linking MSC-derived TNFα signaling to certain classical parameters of hematological ageing, I sought to explore the impact of its inhibition during ageing hematopoiesis. For this purpose, I employed the $Tnfrsf1a^{-/-}$ $Tnfrsf1b^{-/-}$ mouse model, lacking the expression of both TNFRI and TNFRII receptors, thereby preventing initiation of the signaling (referred to as "TNFR KO"). Lastly, to examine potential synergism between the aforementioned pathways and their cumulative effect on the ageing organism, I performed the same characterization for a mouse model that lacks the expression of *Il1r, Tnfrsf1a, Tnfrsf1b* (mentioned as "IL1R+TNFR KO").

6.3.1 Inhibition of TNF and IL-1 is not beneficial for the hematopoietic system

To characterize the native hematopoietic system in the absence of these critical signals, I studied 2-year-old mice with the aforementioned KO genotypes. Initially, I performed a survival analysis comparing KO strains to WT mice, which typically reach the endpoint of 25 months of age (that corresponds to approximately 108 weeks) with a survival probability of about 70 %. Intriguingly, the single KO strains exhibited better survival than WT mice until just before 100 weeks of age, after which their survival probability steeply declined to 50%. The double KO mice showed the poorest survival potential, with only 25% surviving to 100 weeks. According to the Cox Proportional-Hazards (PH) regression model that I used, IL1R KO and IL1R+TNFR KO animals displayed significantly shorter lifespans, likely due to the immunosuppression as an adverse outcome of the KO (Fig. **6.8A**). Thus, while there may be an early-life benefit to these genetic blockades, they do not extend lifespan.

Macroscopically, the WT, TNFR KO and IL1R+TNFR KO animals presented similarly aged phenotypes, including brittle white fur and increased subcutaneous fat. Interestingly, IL1R KO mice exhibited characteristics reminiscent of younger animals, such as more youthful fur, increased activity, and a leaner physique compared to the rest of the groups (Fig. **6.8B**). However, spleen sizes were comparable across all the aged mice, regardless of genotype (Fig. **6.8C**). Regarding the cellular composition in blood, leukocyte and hemoglobin levels were very similar across the different genotype groups. The myeloid-to-lymphoid ratios were also analogous although the variability within the KO groups was reduced, albeit with a smaller sample size than the WT group. Notably, the CD4+-to-CD8+ T cell ratio was higher in IL1R+TNFR KO mice, potentially indicating enhanced lymphoid potential and specifically improved regeneration of the CD4+ compartment in the absence of those signals (Fig. **6.8D**). Finally, regarding the age-related expansion of LT-HSCs in the bone marrow, only IL1R KO mice preserved a smaller stem cell reservoir. Although the TNFR KO group did not significantly control the size of the stem cell pool compared to the IL1R KO mice, both groups showed reduced expression of the CD41 marker on LT-HSCs, a megakaryocytic marker whose expression increases dramatically with age[150](Fig. **6.8E**)

In conclusion, lifelong blockade of TNF and IL1 signaling appears to prevent uncontrolled LT-HSC expansion with age and reduce the megakaryocytic-bias evidenced by the younger-like levels of CD41 expression in KO LT-HSCs. However, beyond the bone marrow compartment, KO mice did not exhibit tissue homeostasis comparable to that of younger animals. Taken together, my observations suggested that the effects of inhibition are primarily confined to the bone marrow and possibly the stroma[104]. The largely unchanged blood composition indicates that these pathways do not significantly affect the reconstitution potential of aged HSCs. Moreover, the trends observed in double KO mice were similar to those in single KO mice, indicating no distinct synergism between the associated signaling pathways, but rather overlapping influences. However, more experiments are necessary to increase the sample size and the power of these results.

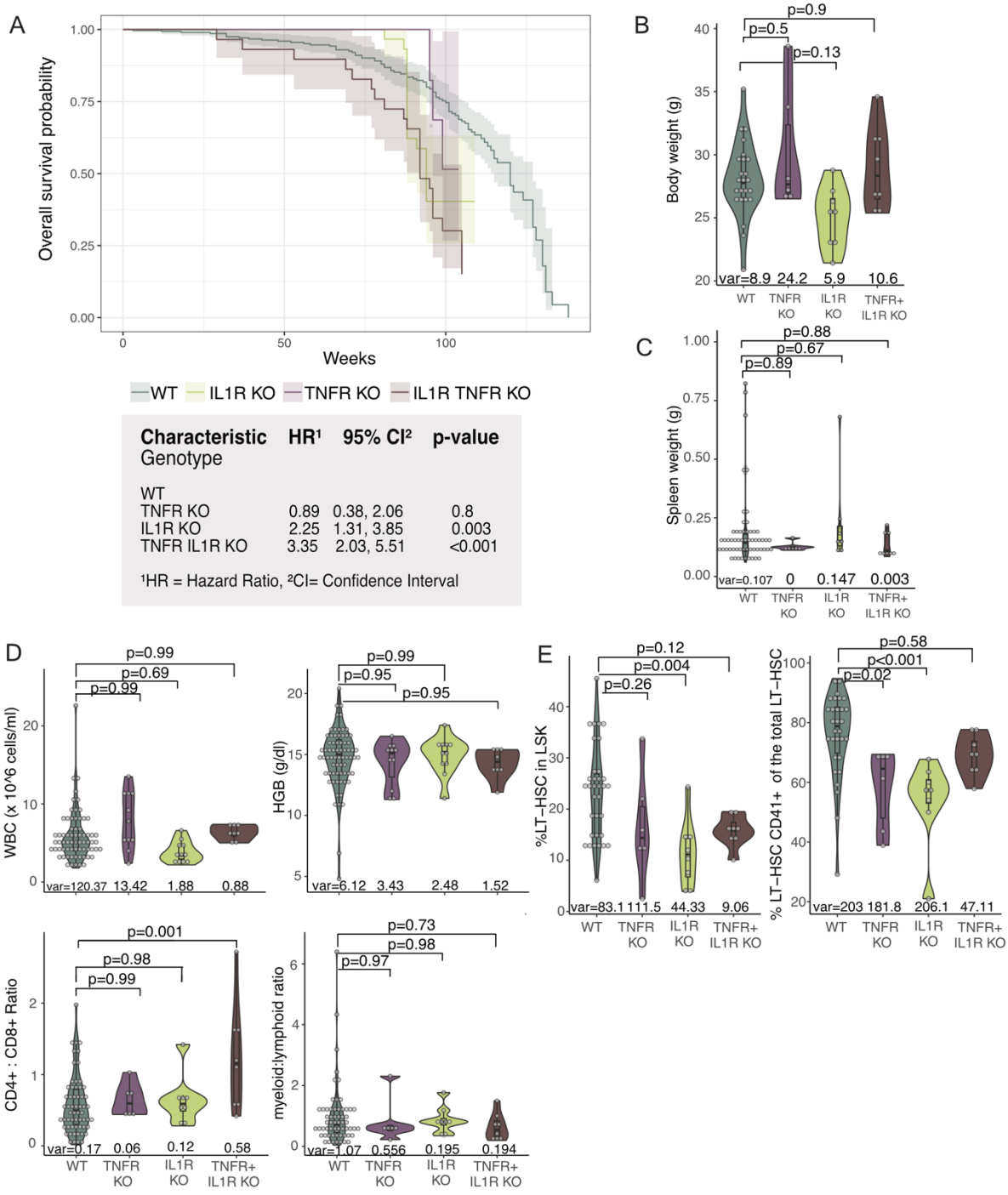

Figure 6.8. *Tnfr* and *Il1r* KO did not rescue hematological ageing. A) Kaplan-Meier curve describing the lifespan of each mouse strain in our facilities**.** The results of the Cox-PH regression model are summarized in the grey table**. B)** Body weight measurements on the day of the endpoint. **C)** Spleen weight. **D)** Hematological parameters. Upper left: white blood cells (WBC) per ml of blood; upper right: levels of hemoglobin. Lower left: ratio of CD4+ to CD8+ T cells; lower right: ratio describing the number of myeloid cells (CD11b+) divided to the sum of B and T cells per ml of blood. **E)** Stem cell pool size assessment within the aged bone marrow. Left: LT-HSC size measured as proportion within the LSK compartment. Right: size of the CD41+ LT-HSC reservoir relative to the LT-HSC population. Comparisons in the aforementioned panels were conducted with One-way Analysis of Variance (ANOVA), followed by Tukey's honestly significant difference (HSD) test for multiple comparisons correction. Significance is denoted by the corrected p-values depicted directly on the plots. Each data

point represents one individual mouse. The variance of each group is also mentioned directly on the plots.

7 Discussion (Project 2)

7.1 Minimal regulation during ageing exposes the hematopoietic system to randomness

The hematopoietic system functions as a tightly regulated hierarchical model with an exemplary dynamic capacity. In young organisms, HSCs, found at the apex of the hierarchy, are multipotent and able to promptly regenerate the tissue, responding to the body's fluctuating demands. To sense these demands, a sophisticated inter-organ communication network is essential, ensuring homeostasis[61]. Importantly, in young mice, the size of the HSC reservoir remains consistent across individuals, implying the existence of precise regulatory mechanisms. Moreover, findings from this thesis indicate that a slightly enlarged stem cell pool in young animals may signify dysfunction, as evidenced by its negative correlation with transplantation efficacy.

Like most regenerative tissues, time impacts the homeostasis of the hematopoietic system. As organisms age, the HSC pool, particularly LT-HSCs, expands uncontrollably. At the same time, the uneven reconstitution of the different cellular lineages instructs that multipotency does not typically characterize aged HSCs[14,15,61]. The aged phenotype has been reported as a collection of average changes in cellular composition compared to a younger organism. However, the kinetics of the system's functional decline remain elusive. In this study, I incorporated middle-aged (18-month-old) mice to investigate the trajectories of age-related changes over time. I observed that metrics in the blood of experimental mice showed a gradual trend of change, while the HSC expansion in the bone marrow remained unaltered after middle age. This implies that the bone marrow ages faster than blood, potentially due to a decline in age-sensitive signals critical for normal hematopoiesis, such as IGF1[178]. Furthermore, this finding further implies that 18-month-old animals have not yet manifested the most aged phenotype possible. Consequently, it is necessary to reconsider when C57BL/6 mice should be categorized as middle-aged rather than old, given the large body of research focused on characterizing the old phenotype in 18-month-old animals.

Older animals generally recapitulated the age-associated hematopoietic remodeling; however, there was a notable heterogeneity across the three relevant tissues -blood, bone marrow and spleen. This variability was not pronounced in 18-month-old mice, further supporting the argument that these are middle-aged animals that have yet to reach the ultimate aged phenotype. Moreover, the transplantation studies indicated that, to a large extent, the transplanted aged marrow fraction was equally functional as that from younger donors. Despite this, the overall transplantation efficacy varied, suggesting the presence of functionally diverse HSC populations accumulated within the aged bone marrow[16,33].

Understanding the sources of this heterogeneity is gradually gaining interest. The comprehensive dataset I compiled was carefully designed to reveal potential connections across metrics hidden in different layers of information, which could potentially present a predictive value for the observed phenotype. However, no significant relationships among different variables were observed, and even those identified in the younger dataset disappeared in the old mice. Although the analysis is still ongoing, it is possible that regulatory mechanisms may be too energy-consuming to justify maintaining an organism far beyond its "selection shadow"[184]. Therefore, from an evolutionary standpoint, ageing has no reason to be programmed; rather, an aged organism likely becomes a template upon which random events act, determining its fate.

Random events occur at various biological levels. For instance, at the genomic level, this can include the accumulation of DNA damage and somatic mutations, or at the epigenomic level, random chromatin remodeling is another such event[5,61]. These examples illustrate just a few of the myriad ways stochasticity can influence organisms. With the advent of single-cell technologies, another stochastic phenomenon has been revealed during tissue ageing: transcriptional noise. This phenomenon occurs independently of the accumulation of somatic mutations and epimutations and is particularly significant in the context of stem cells, where it may lead to fate drifts[185]. In the context of hematopoiesis, previous work conducted by my colleague involved in this project, has shown that differentiation itself is a random process. This was evidenced by the increased gene expression variability among multipotent cells at the time of differentiation[186]. More recently, it was also assessed that aged LT-HSCs exhibit more transcriptional noise than their younger counterparts[187]. This could imply that transcriptional noise may significantly impact the gene expression of various cell types orchestrating ageing hematopoiesis and triggering the diverse phenotypes I have recorded. The data I have collected provide a solid template for the analysis of such phenomena, presenting a promising future direction for this project.

7.2 Bone marrow reacts to stress by generating transcriptionally unique stromal populations mediating complex niche networks

The bone marrow is a sophisticated organ hosting various critical processes that intricately influence each other. Hematopoiesis and osteogenesis occur concurrently in the bone marrow, along with adipogenesis, which exerts endocrine functions[102,188]. MSCs constitute a critical component of the bone marrow stroma, exhibiting stem cell properties and producing fibroblasts, osteoblasts, chondrocytes and adipocytes[189,190]. Over time, the cellular composition of the niche changes, indicating that MSCs are subject to ageing. Similar to HSCs, MSCs favor adipocyte production later in life, while osteogenesis gets severely impaired[97]. This phenomenon was recapitulated in this study, which furthermore marked the first observation of a reduction in fibroblastic content within the aged bone marrow.

Baccin et al. described MSC subpopulations that were transcriptionally primed towards either osteocytic or adipocytic lineages, termed "Osteo-CAR" and "Adipo-CAR", respectively[100]. Notably, Adipo-CARs were proposed to be particularly active in cytokine production and allocated in sinusoidal niches, where typically HSCs reside[103,100]. Beyond these reported subtypes, my scRNA-seq dataset and Dr. Dussiau's analysis uncovered a novel, transcriptionally distinct Adipo-CAR cluster within the aged niche, Adipo-CAR3. This population owed its distinction against the rest of Adipo-CAR clusters to its particular inflammatory transcriptomic profile and an upregulation of genes associated with MHC-II antigen presentation.

Recent studies have explored bone marrow anatomy under various stressful conditions. Insightful findings from multiple myeloma patients revealed an adipo-primed MSC population with characteristics akin to our murine Adipo-CAR3, including their inflammatory profile, IL-1β and TNF response, and cytokine production[191]. Another significant finding involved the identification of a population marked by the CD90 cell surface marker, crucial in niche remodeling in AML patients[192]. These observations suggest that exposure to inflammatory stress could potentially lead to the formation of transcriptionally distinct adipocyte-primed clusters, which adaptively respond to changes within the tissue environment. Furthermore, prolonged inflammation -a hallmark of ageing- has been shown to upregulate the expression of MHC-II components in stromal cells *in vitro,* which subsequently exert immunomodulatory functions by activating CD4+ T cells[101,193]. In the aforementioned pathological contexts, the distinct stromal populations displayed contacts with T cells and subsequently immunomodulatory potential[191,192]. The MHC-II upregulation was notable in Adipo-CAR3 and sinusoidal endothelial cells in the niches of the old animals. Since these cells are likely in proximity to HSCs, which also increase MHC-II expression following ageing[183] (data not shown), it raises the possibility that they may orchestrate coupled immunomodulatory activities in the aged marrow.

It is now well established that the bone marrow consists of multiple micro-niches, each fulfilling distinct roles[98–100,194]. For this study, the niche compartment was isolated after enzymatic bone digestion, therefore, it is assumed that those transcriptionally primed MSCs are found mainly in the endosteal part of the bone marrow, as previously suggested[100]. An attempt to identify the Adipo-CAR3 via flow cytometry did not reveal any old-specific populations in either the bone lining or the central marrow (data not shown), leaving the precise identification of characteristic cell surface markers an open question. Utilizing spatial transcriptomics could potentially allow us to locate this newly-observed population accurately and to determine whether there are specific micro-niches within the bone marrow tailored to address stressors.

Inference of intercellular communication within the aged scRNA-seq dataset revealed downregulation of three potential axes of communication between Adipo-CARs and HSCs, including *Kitl-Kit*, *Angpt2-Tie1* and *Vcam1-Itga4* ligand-receptor pairs. MSCs normally provide essential signals, such as KITL or SCF, to HSCs to sustain their survival and support hematopoiesis[97,100,178,179]. Downregulation of this interaction was recently observed that it occurs much earlier than the age of the old group in this study[179], therefore it is unlikely that it

contributes to the overall variable aged phenotype. Similarly, while *Angpt2-Tie1* communication is known to be impacted by ageing, TIE1 is not essential for adult hematopoiesis[177]. However, alterations in the *Vcam1-Itga4* axis could potentially disrupt the localization of HSCs within their micro-niches, impacting their overall functionality. Although not covered in this thesis, it might be interesting to examine to what extent the intensity of the *Vcam1-Itga4* interaction is variable and whether it is linked with specific phenotypes observed in the aged bone marrow or blood.

This comprehensive examination of the bone marrow environment during ageing illuminated the organ's complexity once more. The identification of novel stromal populations, like Adipo-CAR3, along with the observed changes in cellular communication patterns, underscored the dynamic transformations that occur as the marrow ages. Notably, Adipo-CAR3 has not yet shown correlations with any metrics recorded in the dataset, yet its further characterization could still mark a significant advancement. Looking ahead, future investigations could prove invaluable if they focus on determining whether there is an equivalent population in aged human bone marrow, its localization and its direct role. Such insights would deepen our understanding of bone marrow biology and potentially reveal key regulatory mechanisms to counteract age-related declines in marrow function.

7.3 Revisiting the role of IL-1 and TNFα: Inhibition of two critical ageing-related pathways fails to decelerate its emergence

This study identified IL-1β and TNFα signals originating from neutrophilic populations as key instigators of the inflammatory response in Adipo-CAR3 cells. Both of these signals stimulate the activation of HSCs and their subsequent myeloid differentiation and have been strongly associated with ageing hematopoiesis[104,195,196]. A recent study suggested that stromal secretion of IL-1β and TNFα during ageing contributes to aged phenotypes in both niche and HSCs[104]. However, this finding is not validated in this thesis since *Il1b* and *Tnfa* expression was not detected in the niche-derived scRNA-seq data. It has also been proposed that increasing plasma cells with age enhances the production of the aforementioned cytokines within the aged marrow[197]. Although the hematopoietic scRNA-seq data analysis is incomplete and therefore not covered in this thesis, the increase in activated B cells found in aged mice might link to these observations. Furthermore, these signals have been proposed to influence the aged phenotype as a response to external stimuli, such as the intestinal microbiome entering the circulation through porous aged epithelia[181]. Lastly, these cytokines are thought to mediate Tet2-driven clonal hematopoiesis, often seen among older adults[198].

Due to the central role of IL-1 and TNF pathways in ageing, prospective rejuvenation strategies targeting these pathways have drawn considerable interest. Experiments using aged IL1R or TNFR KO mouse models claim that IL-1 is a more pivotal player, the inhibition of which primarily influences the regenerative capacity of HSCs[104] and mitigates the myeloid

skewing[181]. In reality though, the improvements were only modest. In line with this, my experiments demonstrated that the blood profiles of IL1R KO, TNFR KO, and IL1R+TNFR KO mice were similar to those from WT age-matched mice, with comparable myeloid-to-lymphoid ratios representing equivalent reconstitution potentials. Therefore, it becomes clear that these pathways are merely elements within a broader array of factors that regulate ageing, and their inhibition alone does not equate to viable rejuvenation strategies. The alleviating alterations were even more subtle when IL-1R antagonists, such as anakinra, were administered in old WT mice[104,181].

As shown in my KO experiments, the elimination of those pathways impacted the size of the stem cell pool and moderated the expression of CD41 in LT-HSCs. Previous observations showed that IL-1R KO or anakinra-treated old mice displayed better stromal homeostasis and restored osteogenic capacity[104], which is likely to influence the HSC population positively and prevent its uncontrollable expansion. However, a consistent uncoupling of marrow and blood profiles with age was observed throughout this study. For instance, middle-aged mice exhibited an expansion of HSCs within the bone marrow akin to that seen in older mice. Yet, the blood phenotype remained relatively stable and did not show dramatic differences compared to younger mice. This disconnection could be attributed to additional regulatory mechanisms active in other organs, such as thymic involution, contributing to reduced lymphopoiesis with age. This phenomenon could provide another explanation for the lack of correlations across the various metrics measured. However, considering that some intercompartmental relationships exist in young mice, it is fair to hypothesize that this uncoupling progresses over time. Exploring its ageing trajectory could certainly provide valuable insights into the regulatory complexities of the ageing process and its evolution over time.

In conclusion, the current investigation illustrated that while inhibiting IL-1 and TNFα pathways does not halt hematological ageing, it emphasizes their roles within the broader network of this time-dependent process. The revealed complexities illustrated that ageing is governed by a tapestry of interconnected systems composed by both intrinsic and extrinsic factors. Each layer of complexity may represent a substrate for stochastic events to occur, likely leading to the emergence of unpredictable phenotypic patterns. Delving deeper into the myriad layers of information associated with ageing could enable us to discern potential links across its variables, enhancing our ability to predict personalized trajectories.

7.4 Future perspectives

Despite the conclusion of my PhD, this part of my research remains ongoing, and several critical avenues remain to be explored. The scRNA-seq analysis presented in this thesis is incomplete, since the hematopoietic compartment has not been carefully examined yet. Additionally, the scATAC-seq dataset encompassing the same populations used for the scRNA-seq is another exciting frontier. To my knowledge, this dataset is the first comprehensive

scATAC-seq from healthy murine bone marrow, promising a holistic view of the chromatin accessibility landscapes characterizing these populations. Further work is also needed on the histological evaluation of the bone materials collected. This effort would aim to assess the adipocytic profiles across different specimens thoroughly. The continuation of this project will be led by my colleage, Dr. Charles Dussiau, who has collaborated closely with me over the past two years on this topic.

8 Materials & Methods

8.1 Mouse models

For all cohorts of wild-type mice, including old (22-26 months), middle-aged (18 months) and young (8 months for Project 1; 2 months for Project 2), C57BL/6 mice were used, bred and maintained on a CD45.1 background. Similarly, the transgenic mouse lines Scl-tTA, H2B-GFP, Scl-CreERT2 and Bak $^{-/-}$ Bax $^{fl/fl}$ were also bred and maintained with the same background, whereas Il1r $^{-/-}$ and Tnfrsf $\alpha^{-/-}$ $\beta^{-/-}$ mice were kept on the default CD45.2 background. Scl-tTA H2B-GFP mice resulted from crossing the Scl-tTA and H2B-GFP lines while Scl-CreERT2 Bak $^{-/-}$ Bax $^{fl/fl}$ resulted from the cross of the Scl-CreERT2 and Bak $^{-/-}$ Bax $^{fl/fl}$ lines. Competitor mice expressing both CD45 isotypes (CD45.1-2) resulted from the cross-breeding of C57BL/6-CD45.1 with C57BL/6J mice. All of the aforementioned mouse lines were bred and housed at the facilities of the DKFZ central animal laboratory following a specific pathogen-free (SPF) status. The CD45.2 young mice that served as recipients for Project 2 were purchased from Janvier and acclimated in the DKFZ facilities for at least 2 weeks before the transplantation experiments. The animals were caged in individually ventilated cages (IVC) in same-sex groups of maximum 5 individuals. They were offered food and water *ad libitum*. For Project 1, both female and male mice were used. However, only female mice were used for Project 2 due to the sexual dimorphism in ageing phenotypes. All the experiments were pre-approved by the Regierungspräsidium Karlsruhe under the license numbers G-117/17, G-284/18 (Project 1) and G-162/22 (Project 2). Any organ harvest *post-mortem* was sanctioned by the internal DKFZ357 license.

8.2 Animal treatment protocols and procedures

8.2.1 Label-retention assay

To inhibit the constant H2B-GFP expression in HSCs, 2 mg/ml doxycycline (doxycycline hyclate, Sigma-Aldrich; D9891), along with 20 mg/ml sucrose (saccharose, Sigma-Aldrich; S0389) was administered to 8-week-old Scl-tTA H2B-GFP mice through their drinking water. The doxycycline chase was kept uninterrupted for 18 months, concluding when the mice reached the age of 22 months.

8.2.2 Tamoxifen treatment

To induce the homozygous deletion of the floxed Bax gene in Scl-CreERT2 Bak $^{-/-}$ Bax $^{fl/fl}$ HSCs, mice received 5 intraperitoneal (i.p.) injections of 200 µl 10 mg/ml tamoxifen (Sigma-Aldrich; T5648). Tamoxifen powder was first dissolved in 10% absolute ethanol (Supelco; 1.00983) and 90% sunflower seed oil (Sigma-Aldrich; S5007).

8.2.3 Chronic polyinosinic : polycytidylic acid (pI:pC) treatment

At 8 weeks of age, mice were i.p. injected with 5mg/kg of pI:pC (Poly(I:C) HDW, InvivoGen; tlrl-pic) following 3 rounds of intermittent treatment. The pI:pC was first resuspended in sterile phosphate-buffered saline (PBS) (Dulbecco's Phosphate Buffered Saline, Sigma; D8537) according to the manufacturer's guidelines. Each treatment round involved two weekly injections for 4 weeks, followed by a 4-week recovery period. By the end of the regimen, the mice were approximately 8 months old.

8.2.4 Competitive transplantation assay

Young CD45.2 C57BL/6 mice (C57BL/6J) served as recipients in competitive bone marrow transplantation experiments for Project 2. To prepare these mice for transplantation, they underwent total body irradiation in two sessions of 500 Rad to eliminate existing host hematopoiesis, either on the day of the experiment or the day before as earliest. The two irradiation sessions were spaced by a four-hour interval and were conducted by the animal care staff at the DKFZ central animal facility. The bone marrow transplants consisted of a sterile and equal mix of experimental donor and young competitor bone marrow suspensions for a total of $5x10^6$ cells. Typically, bone marrow from 2-3 young competitor mice was mixed to create a common competitor pool for each experiment. Infrared lamps were used to dilate the tail vein of the recipient mice and then 200 ul containing the $5x10^6$ bone marrow cells were injected intravenously (i.v.) using an insulin syringe (BD, 324827). After the transplantation, to prevent irradiation-related infections, recipient mice received 90mg/kg of bodyweight per day sulfamethoxazole/trimethoprim through the drinking water for 3 weeks.

8.3 Sample collection

8.3.1 Blood collection

Bleeding of each mouse was achieved by puncturing the *vena facialis* with a 21Gx1'' hypodermic needle (BD Microlance 3). The blood was collected in an EDTA-coated tube (Microvette K3 EDTA; Sarstedt; 20.1278) to avoid clotting for a maximum volume of approximately 60 ul. Complete blood count checks were performed using a ScilVet-abc Plus+ veterinary counter (Scil Animal Care Company Gmbh).

8.3.2 Bone marrow collection

On the designated endpoint, the mice were euthanized via cervical dislocation. Subsequently, tibias, femurs, hips, vertebrae and sternums were harvested from each mouse after removing any adherent flesh with a scalpel (Disposable scalpel No 20; Feather). The bones were flushed (only for leg bones) in PBS supplemented with 2 % fetal bovine serum (FBS) (Heat-inactivated FBS, Gibco; A5256801) or crashed in Iscove's Modified Dulbecco's Medium (IMDM; 12440053) using a mortar and a pestle. The resultant cell suspension was further filtered with a 40-um strainer (Easystrainer 40 um for 50 ml tubes, Greiner Bio-One; 542040) to eliminate bone fragments and then centrifuged at 1500 rpm for 5 min at 4 °C. After discarding the supernatant, the pellet was resuspended in PBS-2% FBS. Bone marrow cell counts were measured with a ScilVet-abc Plus+ veterinary counter.

8.3.3 Spleen collection and digestion

The spleens were dissected out of each mouse and their weight was initially measured and recorded. Afterwards the organ was cut in two pieces: one for histology examination and the other for flow cytometry (FC) analysis. The weight of the FC piece was measured and recorded to calculate the ratio `FC piece weight (g)/total spleen weight(g)`. To prepare for the FC, the spleens were mechanically digested in IMDM, against a 40-um strainer using the flat part of the plunger from a 2.5 ml syringe (BD; 309646). The cell suspension was further centrifuged 1500 rpm for 5 min at 4 °C and later the cell pellet was resuspended in PBS-2% FBS. The spleen cell counts were measured with a ScilVet-abc Plus+ veterinary counter.

8.3.4 Tail collection

To capture the genomic variations of the germline for each mouse used in Project 1, a 2-3 cm segment of the tail was cut *post-mortem*. These tail samples were then placed in 1.5 ml tubes (Eppendorf; 12682) and stored in -20 °C until future DNA extraction.

8.4 Clonal expansion of single LT-HSCs

8.4.1 Depletion of mature cell lineages

The bone marrow cell suspension was first centrifuged at 1500 rpm for 5 min at 4 °C. Following this, the resulting cell pellet was resuspended in 115 ul of lineage biotinylated antibody cocktail (Table **8.1**) for every 10^8 bone marrow cells; and incubated for 30 mins at 4 °C on a rolling platform. Post-incubation, the antibody cocktail was washed off by centrifugation and the pellet was then resuspended in 3 ml PBS-2% FBS. To this suspension, 1 ml of pre-washed magnetic Dynabeads (Thermo Fisher; 11415D) was added and the samples were allowed to incubate for another 45 min at 4 °C on a rolling platform. After the incubation, the tubes containing the cell-

bead mixtures were positioned on a magnetic rack to separate the supernatant, containing the most primitive cells, for collection.

Antibody	Targeted cell type	Volume
Cd5 (BD Pharmingen; 553019)	T lymphocytes	250 ul
B220 (BD Pharmingen; 553084)	B lymphocytes	167 ul
Cd11b (Mac-1) (BD Pharmingen; 550282)	Myeloid cells	157 ul
Cd8a (BD Pharmingen; 550281)	T lymphocytes	250 ul
Gr1 (Ly6G & Ly6C) (BD Pharmingen; 550291)	Granulocytes	143 ul
Ter119 (BD Pharmingen; 553672)	Erythrocytes	157 ul
Total		1124 ul

Table 8.1. Recipe of the biotinylated lineage antibody cocktail to eliminate mature-lineage populations from the bone marrow.

8.4.2 Single-LT-HSC sorting

The mature-lineage-depleted cell suspension was centrifuged at 1500 rpm for 5 min at 4 °C. The cell pellet was resuspended in 250 ul of staining master mix consisted of PBS-2%FBS and the list of antibodies indicated in Table **8.2**; and incubated for 30 min at 4°C in the dark. To halt any further reactions, 1 ml PBS-2% FBS was added to the mixture after the incubation and the samples were then centrifuged at 1500 rpm for 5 min at 4 °C. The pellet was once more resuspended with 1 ml of PBS-2% FBS and filtered into FC tubes with cell strainer snap cap (Falcon; 352235). Single LT-HSCs were sorted using Aria I or II sorters (BD) and collected into round-bottom 96-well plates (Cellstar, Greiner Bio-One; M9436-100EA) filled with 200 ul/well of serum-free expansion medium (SFEM) (Table **8.4**). In the case the experiment involved Scl-tTA H2B-GFP mice treated with Dox, the antibody panel shown in Table **8.3** was used for bone marrow staining instead of the one in Table **8.2**. Additionally, the sorting was indexed. At least three 96-well plates were used for each mouse involved in Project 1.

Cell Surface Marker Antibody	Fluorochrome
Lineage antibodies: CD4 (eBioscience; 48-0041-82) CD8a (eBioscience; 48-0081-82) CD11b (eBioscience; 48-0112-82) B220 (eBioscience; 48-0452-82) Gr1 (eBioscience; 48-5931-82) Ter119 (eBioscience; 48-5921-82) Streptavidin (eBioscience; 48-4317-82)	eFluor450
cKit (Cd117) (Biolegend; 105835)	BV711
Sca-1 (BD Biosciences; 560654)	APC-Cy7
CD150 (Biolegend; 115912)	PE-Cy5
CD48 (Biolegend; 103424)	PE-Cy7
CD34 (eBioscience; 11-0341-82)	FITC
Dead cells	7AAD (Invitrogen; A1310)

Table 8.2. Antibody panel for single LT-HSC sorting from WT and Bak-/- $Bax^{\delta/\delta}$ mice

Cell Surface Marker Antibody	Fluorochrome
Lineage antibodies: CD4 (eBioscience; 25-0041-82) CD8a (eBioscience; 25-0081-82) CD11b (eBioscience; 25-0112-82) B220 (eBioscience; 25-0452-82) Gr1 (eBioscience; 25-5931-82) Ter119 (eBioscience; 25-5921-82) Streptavidin (eBioscience; 25-4317-82)	PE-Cy7
cKit (eBioscience; 17-1171-83)	APC
Sca-1 (BD Biosciences; 560654)	APC-Cy7
CD150 (Biolegend; 115912)	PE-Cy5
CD48 (eBioscience; 12-0481)	PE
CD34 (eBioscience; 48-0341-82)	eFluor450
Dead cells	7AAD (Invitrogen; A1310)

Table 8.3. Antibody panel for single index LT-HSC sorting from Scl-tTA H2B-GFP mice

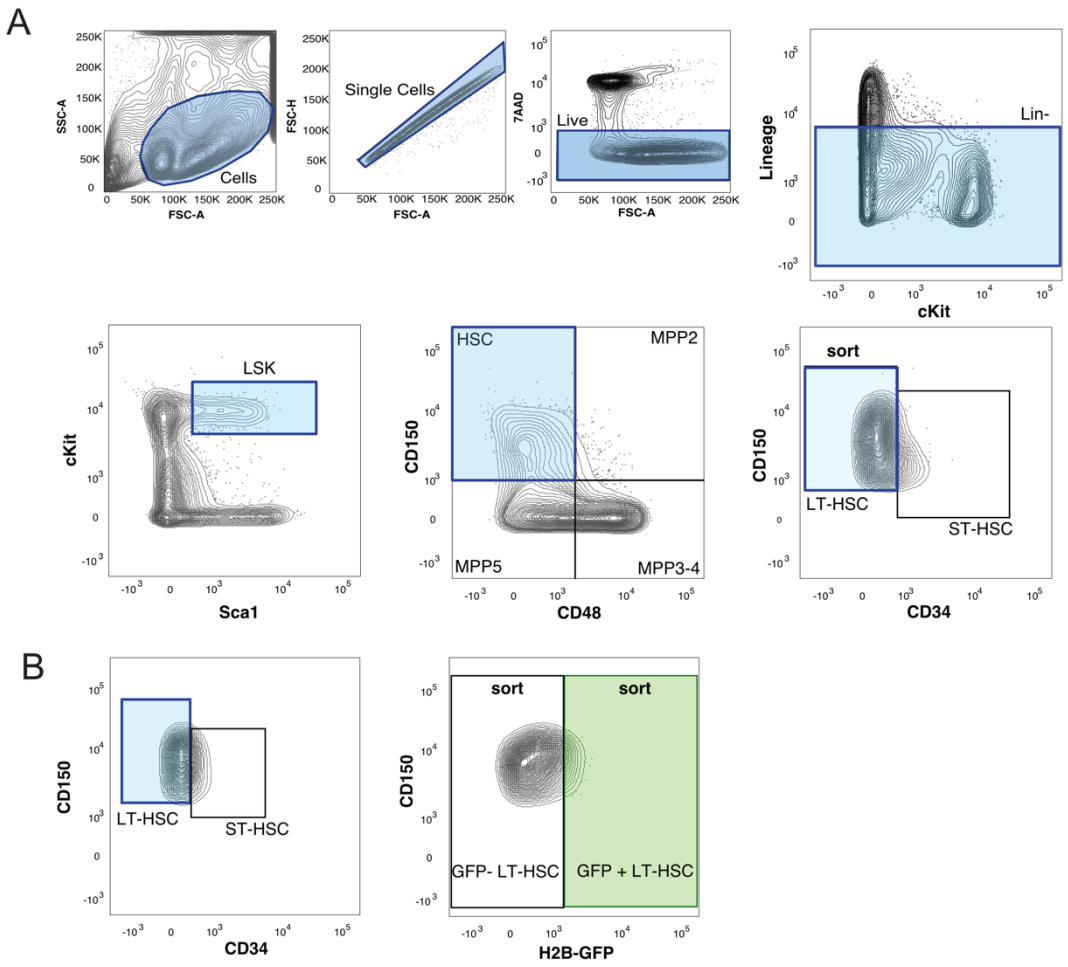

Figure 8.1. Gating strategies for single LT-HSC sorting. A) Strategy employed for WT and Bak-/- Bax$^{\delta/\delta}$ mice, depicting the initial exclusion of multiplets and dead cells, with LT-HSC identification route highlighted by the blue gates**. B)** Segregation of LT-HSCs in the Scl-tTA H2B-GFP mouse model into dormant and active based on H2B-GFP expression.

8.4.3 *In vitro* clonal expansion of single LT-HSCs

After sorting, the plates were transferred to an incubator to expand under hypoxic conditions (5% O_2, 37°C, 5% CO_2). The cells were left to produce progeny for 10 days without any medium change or supplement addition. During this period, essential cytokines provided through SFEM (Table **8.4**) supported the cells' growth and differentiation towards erythroid, megakaryocytic and myeloid lineages. At the end of the incubation period, the plates were observed under a light microscope (Nicon Eclipse TS100) with 10x or 40x magnification to score the clonogenic efficiency of the cells (`colony formation wells/total number of wells`). Ultimately, selected colonies from each individual (approx. 30 colonies per mouse) were collected for WGS by transferring the liquid colony into 1.5 ml Eppendorf tubes. These tubes were centrifuged at 1500 rpm for 5 min at 4 °C. After discarding the supernatant, the cell pellets were snap-frozen using liquid nitrogen and stored at -80 °C, preserving them for subsequent DNA extraction.

Cytokines	Final concentration
Penicillin/Streptomycin (Sigma-Aldrich; P4458)	1%
L-Glutamine (Gibco; 25030081)	1%
Recombinant human (rh) Flt3-ligand (PeproTech; 300-19)	10 ng/ml
Recombinant murine (rm) Stem Cell Factor (SCF) (PeproTech; 250-03)	50 ng/ml
Rm Thrombopoietin (TPO) (PeproTech; 315-14)	10 ng/ml
Rm Interleukin-3 (IL-3) (PeproTech; 213-13)	5 ng/ml
Rm IL-11 (PeproTech; 220-11)	10 ng/ml
Rh Erythropoietin (EPO) (ERYPO®, Janssen)	0.3 IU/ml
Rm IL-7 (PeproTech; 217-17)	22.2 ng/ml

Table 8.4: SFEM recipe for the proliferation of single LT-HSCs in liquid culture.

8.4.4 Colony size and viability assessment

The remaining colonies were processed to assess their size and viability. Initially, the plates underwent centrifugation at 1500 rpm for 5 min at 4 °C, followed by the removal of the supernatant. Each cell pellet was then resuspended in 100 ul of PBS-2%FCS solution containing 1:200 7AAD to evaluate cell viability. Finally, the plates were analyzed using the high-throughput sampler (HTS) option of an LSR-Fortessa analyzer (BD) equipped with a 96-well plate reader, to determine the cell count and viability within each colony.

8.5 WGS library preparation

8.5.1 DNA extraction

Genomic DNA was extracted from the frozen colony pellets using the QIAamp DNA mini kit (Qiagen; 56304), following the manufacturer's guidelines. The only deviation from the standard protocol was the elution step, where DNA was eluted in a significantly reduced volume of 30 ul water instead of the recommended 200 ul, resulting in more concentrated DNA samples. In the case of the tails, segments up to 2 mg were processed by adhering to the DNeasy Blood and Tissue Kit (Qiagen, 69504) protocol. The DNA concentration of each sample was measured with a Qubit ® 3.0 Fluorometer (Life Technologies; Q33216) using the Qubit dsDNA HS (High Sensitivity) Assay kit (Life Technologies; Q32854).

8.5.2 DNA shearing with sonication

Shearing of the DNA purified from the samples was achieved through sonication using a Covaris M220 focused-ultrasonicator (Covaris, 500295). According to the Illumina TruSeq Nano protocol that was followed for the library preparation, a minimum of 100 ng of DNA was initially required for the fragmentation. However, as mentioned in her thesis[106], Dr. Megan Druce optimized the sonication procedure, demonstrating that as little as 25 ng of DNA could be effectively fragmented by modifying the sonication duration. Based on this, I adjusted the sonication time depending on the available DNA quantity, as outlined in Table **8.5.** The shearing of the DNA was validated by analyzing the samples with a Bioanalyzer 2100 (Agilent) using High Sensitivity DNA chips (Agilent; 5067-4626) according to the manufacturer's instructions.

DNA input (ng)	Sonication duration (s)
100	65
95	75
60	85
55	88
50	90
45	93
35< (sample DNA) <40	95
30< (sample DNA) <35	98
25< (sample DNA) <30	100

Table 8.5. Tuning of the sonication duration according to the amount of DNA input for efficient fragmentation before the library prep.

8.5.3 WGS library preparation and sequencing

The libraries were generated using the TruSeq Nano DNA Low Throughput Library Prep Kit (Illumina, 20015964) with adherence to the provided manufacturer's instructions. Subsequently, 150 bp paired-end (PE) WGS was carried out at the NGS core facility of DKFZ utilizing either a Hi-Seq X10 or a NovaSeq 6000 sequencer. For samples sequenced by Hi-Seq X10, single adapters were used for each sample (TruSeq DNA Single Indexes, Illumina; 20015960 or 20015961), with each sample allocated onto a single lane on the flowcell. Conversely, for samples sequenced using the NovaSeq 6000, the libraries were double indexed (IDT for Illumina-TruSeq Unique Dual (UD) Index kit, Illumina; 20020590) and pooled in equimolar multiplexes of 8 for each lane of the S4 flowcell. Before sequencing, the final library constructs were validated with a Bioanalyzer 2100 with High Sensitivity DNA chips. A summary of all the samples used in this thesis together with some QC metrics are provided in the `QCsum_WGS_allsamples-FF-vol2-FF.xlsx` file provided in Gitlab: `https://git.dkfz.de/a012/hsc-mutagenesis.git`.

8.6 WGS analysis

8.6.1 Read alignment

Sequencing reads were mapped to the mouse reference genome GRCm38 utilizing the Burrows-Wheeler Aligner (version 0.7.15), while duplicate reads were identified and flagged using Sambamba (version 0.6.5). The alignment of reads and subsequent quality control tasks were carried out by the DKFZ Omics IT and Data Management Core Facility. For the sequenced clones from SclCreERT2 $Bak^{-/-}$ $Bax^{fl/fl}$ mice the alignments were inspected with the Integrative Genomics Viewer (IGV, version 2.13.2) to verify the effective deletion of the Bax gene by the recombinase.

8.6.2 SNV calling

SNVs were identified using *CaVEMan* (*cpgCaVEManWrapper*, version 1.16.0). This expectation-maximization algorithm lists the putative somatic base substitutions after performing a comparative analysis between a tumor sample, its respective normal tissue as germline control, and the reference genome (here: GRCm38, mm10)[107]. In this study, I compared each aligned HSC clone sequence against the tail alignment of the same mouse in order to subtract the germline variants and list only the ones that are exclusively present in the clones. As shown in the *CaVEMan* submission script template provided on Gitlab, the run required additional inputs such as the `IGNORE_FILE`.This file is a tab-separated document listing repetitive and homologous regions in the mouse genome and instructs the algorithm to overlook these areas due to their high susceptibility to produce false positive calls (`genome.gap_v3.tab_` file on Gitlab). Other repetitive regions, such as centromeric and simple repeat regions, were also excluded from the analysis by guiding the tool to bypass them through a collection of Browser Extensible Data (BED) files downloaded from the University of California Santa Cruz (UCSC) Genome Browser (`https://genome.ucsc.edu/cgi-bin/hgTables`). Finally, an exclusion file of unmatched panels of normal mouse samples sequenced under similar conditions was used to identify common genomic regions prone to errors, such as mapping artefacts or polymorphisms. The ignore file and the unmatched panels of normal mouse samples were provided by Dr. Alex Cagan from the Wellcome Sanger Institute.

After the *CaVEMan* run and the generation of the Variant Call Format (VCF) files, I continued with more variant filtering steps as listed below and as explained in the script provided in the Gitlab (`Caveman_filtering_example.sh`):

-`PASS` filter: this is a flag given by *CaVEMan* to every call that meets its intrinsic filtering criteria[107]. Calls lacking this flag were removed.

-Sex chromosome filter: Sex chromosomes were removed since both male and female mice were included in the dataset and were unevenly distributed across the different experimental groups.

-Coverage filter: Variants found in coverage areas below 10X or above 100X were dismissed to eliminate the possibilities of calls-artefacts.

-Alignment filters: Variants of a read-adjusted median alignment score (ASRD) less than 0.94 as assessed by *CaVEMan* were omitted from the study. Additionally, variants supported by reads containing soft-clipped bases (Clipped Read Position Model, CLPM) were also filtered out (i.e. CLPM must be =0).
-VAF filter: Heterozygous somatic mutations in the originally sorted LT-HSC show a VAF distribution around 0.5, while the *in vitro* generated variants display sub-allelic fractions. This filter sets the VAF cutoff at 0.3 to isolate all the variants exclusively present in the single LT-HSC before its amplification. (Fig.**S1-S6**). Samples with no such distribution were not considered clonal and were eliminated from the study.

8.6.3 Indel calling

To identify small deletions (1-1000 bp) and insertions (variant size dependent on the read length, approximately 130 bp in my case), I utilized the pattern growth approach offered by *Pindel* in a comprehensive wrapper (*cgpPindel* version 3.9.0)[108,109]. Similar to *CaVEMan, Pindel* discerns somatic indels by contrasting the aligned sequences from each LT-HSC clone with their corresponding tail sequence alignments. During the run, exclusions were made again for centromeric and simple repeats by referencing the UCSC list. Additionally, a list of unreliable regions (`extremedepth_v2.bed.gz`) recorded by the Wellcome Sanger Institute was integrated into the script to omit them from the analysis. Following the approach with *CaVEMan*, I applied further filtering after the indel calling. Initially, the variants that failed to comply with *Pindel*'s own criteria (FF004, FF005, FF006, FF012, FF015 and FF016, all explained here: `https://github.com/cancerit/cgpPindel/wiki/VcfFilters`) were discarded. Subsequently and similar to *CaVEMan* calls, the sex chromosome, coverage, alignment, and VAF filters were also implemented. Additionally, a Phred score cutoff of 20 was applied.

8.6.4 SV calling

To explore larger structural aberrations, I chose *Delly*, a tool that leverages both pair-end and split-read techniques to detect larger-scale insertions, deletions, duplications, inversions and translocations[110]. During the first step of calling, *Delly* excludes areas of high repetition, such as telomeric and centromeric regions (`mouse.mm10.excl.tsv` file)[110]. In addition to the pairwise comparison of each colony with its corresponding germline control, *Delly* also screens potential somatic variants against a panel of normals (PON) generated from all the germlines of the dataset. This step helps to identify recurring sequencing errors and polymorphisms[110]. *Delly*'s inherent filters dismiss SVs supported by <3 reads either identified through paired-end or split-end evidence, or displaying a mapping quality <20. In the case of inter-chromosomal translocations, the threshold for read support of the SVs is raised to 5. Beyond these built-in filters, further filtering was employed based on coverage, VAF and sex chromosome considerations, as explained in paragraph **8.6.2**.

8.6.5 Callable genome estimation and variant normalization

To facilitate comparisons across samples and groups, the variants called were normalized based on the size of the callable genome of each sample. The per-base coverage was assessed with *mosdepth*[199] (version 0.3.3) splitting the data in regions of coverage levels 0-10X, 10-100X and 100X-infinite. Regions that displayed coverages belonging to the former and the latter coverage range observed in both colony and tail data were subtracted from the analysis using *BEDTools*[200] (version 2.29.2). From the remaining 10-100X coverage areas, any other regions ignored by the algorithms, variants that did not meet the alignment or quality criteria and recurring problematic regions from the PON were further subtracted. According to all the above, after the calculation of the callable genome from all the reliable regions per sample, the number of variants was normalized following the simple formula:

`(number of variants) x (reference autosomal genome size)/(callable autosomal genome size)`

8.6.6 Variant annotation

All the filtered variants, apart from breakends (BNDs), were annotated using the *Ensembl Variant Effect Predictor* (*VEP*, v102.0)[201]. I selected one primary consequence per variant listed by adding the flag `--flag_pick`. This option creates the column "PICK", marking the most severe consequence per variant as "1", while retaining all the secondary consequences for inspection at the same time. The most severe consequence per variant was selected according to *VEP*'s default ordered set of criteria.

8.6.7 Mutational profile and signatures analysis

To construct each sample's SNV mutational profiles and extract the underlying SBSs, I used the *MutationalPatterns* R package (v3.12.0)[111,112]. Before the analysis, VCF files containing only the filtered SNVs per cell were concatenated to generate one VCF file per mouse. This strategy aimed to enhance the analytical power, given the relatively low mutational burden per cell. Operating under the hypothesis that young, old, dormant and active cells were subjected to the same mutagenic processes, all of these samples were analyzed collectively. This approach aimed again to achieve analytical robustness and to prevent the masking of other processes that might emerge under specific conditions such as lack of apoptosis, or "signature bleeding" on the other scenario[88]. Additionally, all the apoptosis-deficient cells, both treated and untreated, were grouped and analyzed separately. The determination of the number of signatures present in the dataset was estimated through NMF. Following this, the extracted signatures were compared against those listed in COSMIC to perform fitting of the known signatures in my dataset. The "HSPC" signature was kindly provided by Lucca Derks (R. van Boxtel lab) and added to the dataset of known COSMIC signatures. The fitting was achieved through 150-run bootstrapping, using the function `fit_to_signatures_bootstrapped()`. The average contribution per signature per mouse was determined by averaging the results across all bootstrap iterations. The absolute

SNV counts per signature were estimated by multiplying the average signature contribution calculated per mouse by the normalized SNV counts per cell isolated from that specific mouse. The `signature_contributions_allsamples-20032024.xlsx` table on Gitlab summarizes the signature contributions calculated in absolute numbers per cell.

8.7 Flow cytometry analysis

8.7.1 Analysis of peripheral blood

To examine the cellular composition, 30 ul of blood was mixed with 70 ul of a master mix composed of PBS-2%FBS and all the antibodies listed in Table **8.6** (for the primary/donor mice) or Table **8.7** (for recipients). This mixture was incubated for 30 min at 4°C in the dark. Following this, 1 ml of ACK lysis buffer (Lonza; 10-548E) was added to each sample to lyse the erythrocytes and the samples were left to incubate for 10 min at room temperature (RT). After incubation the samples were centrifuged at 1500 rpm for 5 min at 4 °C and the supernatant was discarded. The cell pellet was washed with 1 ml PBS-2%FBS. Following the removal of the second supernatant, the cell pellet was resuspended in 200 ul of PBS-2% FBS and passed through a 40-um filter preparing it for cytometry analysis. The samples were then analyzed using either a LSRII or an LSR-Fortessa cytometer (BD) following the gate layout displayed in Fig. **8.2.**

Cell Surface Marker Antibody	Fluorochrome
CD4 (eBioscience; 12-0041-83)	PE
CD8 (eBioscience; 48-0081-82)	eFluor450
B220(eBioscience; 17-0452-83)	APC
CD11b (Mac-1) (eBioscience; 15-0112-82)	PE-Cy5
Ly6C (Biolegend; 128026)	APC-Cy7
CD62L (Biolegend; 104418)	PE-Cy7
CD44 (Biolegend; 103006)	FITC

Table 8.6. Antibody panel for analysis of mature cell populations in the blood of experimental mice (donors).

Cell Surface Marker Antibody	Fluorochrome
CD4 (eBioscience; 12-0041-83)	PE
CD8 (eBioscience; 48-0081-82)	eFluor450
B220 (eBioscience; 56-0452)	Alexa Fluor 700
CD11b (Mac-1) (eBioscience; 15-0112-82)	PE-Cy5
Ly6C (Biolegend; 128026)	APC-Cy7
CD62L (Biolegend; 104418)	PE-Cy7
CD44 (Biolegend; 103006)	FITC
CD45.1 (BD; 565212)	BUV395
CD45.2 (eBioscience; 17-0454)	APC

Table 8.7. Antibody panel for analysis of mature cell populations in recipients' PB. Antibodies against the two different isotypes of CD45 are added to separate the cells that originate from the donor versus the ones that stem from the competitor.

8.7.2 Bone marrow analysis

Bone marrow samples were evaluated for both HSPC and more committed hematopoietic progenitor cell populations with two separate antibody panels as shown in the following tables (Table **8.8**, Table **8.9**). For the HSPC analysis, 20 x 10^6 cells were aliquoted and spun down at 1500 rpm, for 5 min at 4°C. After discarding the supernatant, the pellets were resuspended in 200 ul of the HSPC master mix and incubated for 30 min at 4°C in the dark. Following incubation, the cells were very briefly treated with 1 ml of ACK lysis buffer for 5 min at RT to eliminate the erythrocytes, then centrifuged in the same conditions to discard the supernatant again. The cells were washed with 1 ml of PBS-2%FBS and centrifuged once more. The final stained pellet was resuspended in at least 300 ul of PBS-2% FBS and passed through a 40-um cell strainer in preparation for the cytometry. For the progenitor analysis, 10-15 x 10^6 cells were stained following the same procedures but with 150 ul of the progenitor master mix. All the bone marrow samples used in Project 2 were measured with an LSR-Fortessa cytometer (BD). When the bone marrow under investigation derived from recipient mice, the antibodies of CD45.1-BUV395 (BD; 565212) and CD45.2-APC (eBioscience; 17-0454) were added in the panels with no further alterations. The HSPC gating scheme is similar to the one used for the LT-HSC sorting, displayed in Figure **8.1.** The progenitor gating scheme is shown in Fig. **8.3.**

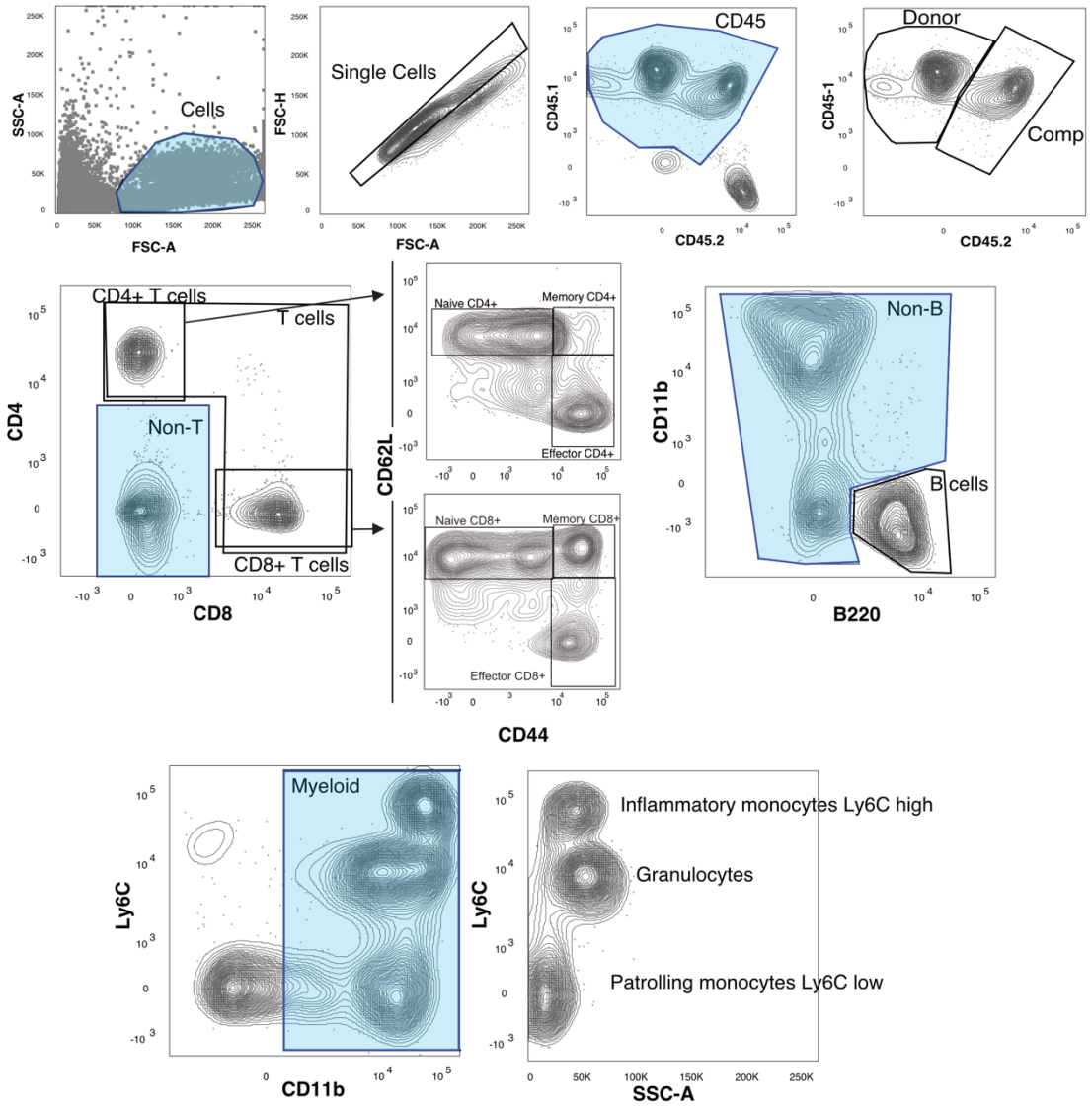

Figure 8.2. Gating strategy for the identification of mature cell populations (B, T, and myeloid cells). The scheme outlines the approach for analyzing recipient mice. It is noted that during the analysis of experimental (donor) mice, the CD45.1-CD45.2 plots are not included. The gating path is highlighted by the blue gates.

8.7.3 Analysis of splenic populations

Similar to the approach used for bone marrow samples (paragraph **8.7.2**), the splenic cell suspension was divided into different aliquots: 1) 20 x 10^6 cells for HSPC analysis, 2) 5-10 x 10^6 cells for progenitors and 3) a small aliquot of 0.5 x 10^6 cells to identify mature cell populations. The antibody panels employed for the spleen samples are similar to the ones listed above, in paragraphs **8.7.1** and **8.7.2.**

Cell Surface Marker Antibody	Fluorochrome
Lineage antibodies: CD4 (eBioscience; 48-0041-82) CD8a (eBioscience; 48-0081-82) CD11b (eBioscience; 48-0112-82) B220 (eBioscience; 48-0452-82) Gr1 (eBioscience; 48-5931-82) Ter119 (eBioscience; 48-5921-82)	eF450
cKit (Cd117) (Biolegend; 105835)	BV711
Sca-1 (BD Biosciences; 560654)	APC-Cy7
CD150 (Biolegend; 115912)	PE-Cy5
CD48 (Biolegend; 103424)	PE-Cy7
CD34 (eBioscience; 11-0341-82)	FITC
CD41 (eBioscience; 12-0411-82)	PE

Table 8.8. Antibody panel for identification of HSPCs.

Cell Surface Marker Antibody	Fluorochrome
Lineage antibodies: CD4 (eBioscience; 48-0041-82) CD8a (eBioscience; 48-0081-82) CD11b (eBioscience; 48-0112-82) B220 (eBioscience; 48-0452-82) Gr1 (eBioscience; 48-5931-82) Ter119 (eBioscience; 48-5921-82)	eFluor450
cKit (CD117) (Biolegend; 105835)	BV711
Sca-1 (BD Biosciences; 560654)	APC-Cy7
CD16/32 (eBioscience; 25-0161-82)	PE-Cy7
CD34 (eBioscience; 11-0341-82)	FITC
CD127 (ILRa) (eBioscience; 12-1273-83)	PE

Table 8.9. Antibody panel for the staining of the different committed progenitor populations.

8.7.4 Flow cytometry data analysis

All data obtained from the cytometers or sorters underwent an initial automatic quality control assessment using *flowAI* (version 1.30.0)[202], which identified and removed any anomalous events from the dataset. Subsequently, *FlowJo* (BD, version 10.9.0) was utilized to extract cell counts and other statistical metrics from the cleaned data. T-SNE analysis was also performed with the *Flowjo* feature. Additionally, the extraction of the GFP indices from the Scl-tTA H2B-GFP LT-HSC index sorting was performed with the *IndexSort* plugin in *Flowjo*.

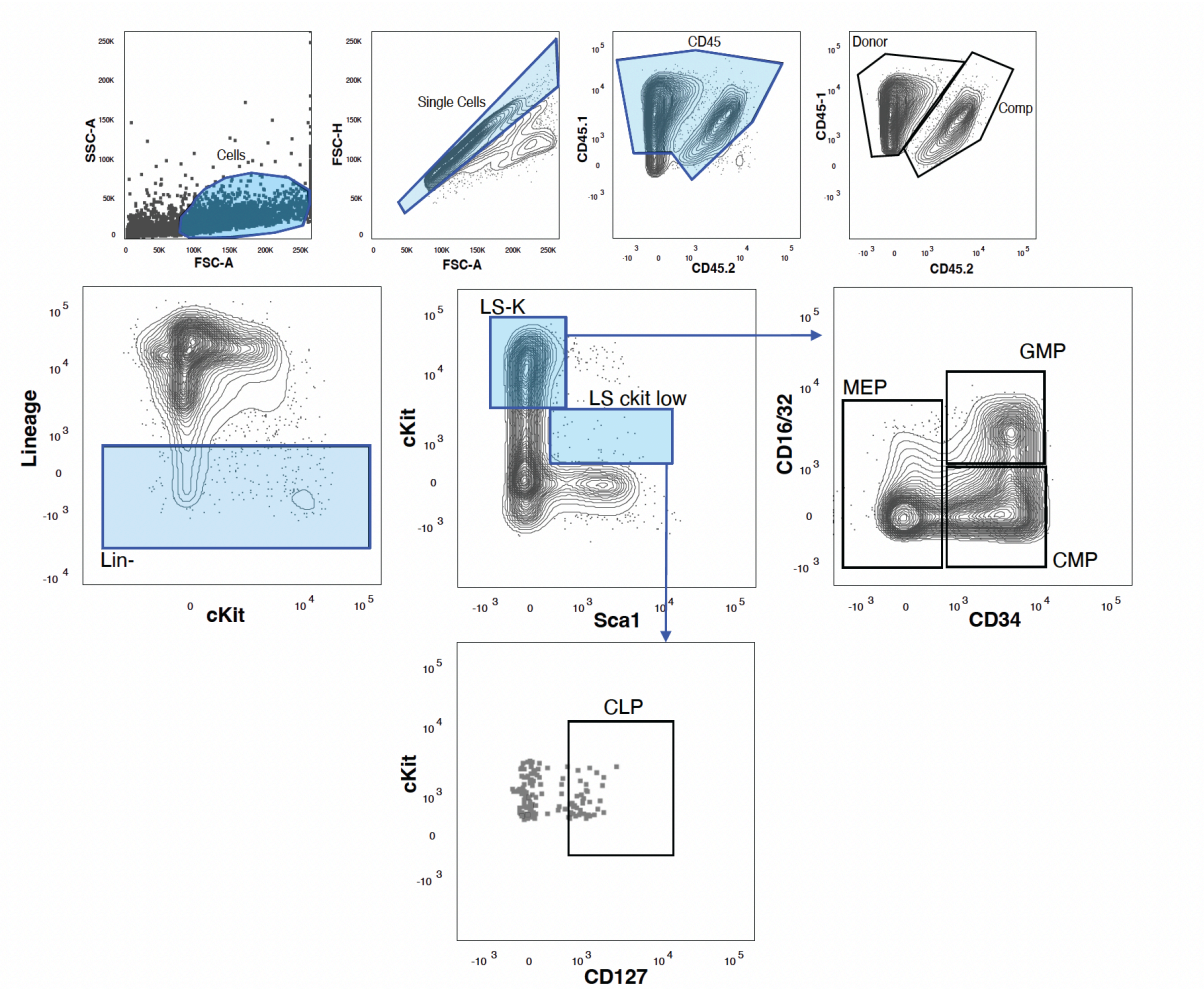

Figure 8.3. Gating strategy for the identification of committed progenitors: common-myeloid progenitors (CMP), granulocyte-monocyte progenitors (GMP), megakaryocyte-erythrocyte progenitors (MEP) and common lymphoid progenitors (CLP). The scheme outlines the approach for analyzing recipient mice. It is noted that during the analysis of primary (donor) mice, the CD45.1-CD45.2 plots are not included. The gating path is highlighted by the blue gates.

8.8 Single-cell RNA sequencing and gene expression analysis

8.8.1 Serial sorting of hematopoietic populations

To isolate hematopoietic and niche cells for scRNA-seq, leg bones (tibias, femurs, and hips) were first flushed into 2 ml of PBS-2% FBS. Cell abundance was then assessed using the ScilVet-abc Plus+. Following this, the cell suspension was divided into two parts: 2/3 of the cells underwent lineage depletion to prepare for HSPC staining (Table **8.10**), while the remaining 1/3 was stained directly with a CD45-FITC (eBioscience; 11-0451-82) antibody and Zombie Yellow (Biolegend; 423103) as viability dye. The undepleted marrow fraction contained high abundance of mature cell types expressing increased levels of CD45 and thus, was used for capturing the differentiated hematopoietic cell types. The lineage depletion and HSPC staining process are detailed in the paragraphs **8.3.2, 8.4.1** and **8.4.2**. Additionally, in a serial sorting process, 7000 CD45+ cells, 7000 LSK cells (Live, Lin-, cKit+ Sca-1+) and 7000 LS-K cells (Live, Lin-, cKit+, Sca-1-) were sorted using Aria I or II systems with 4-way purity mode, in the same 1.5 ml Eppendorf tube, containing 200 ul of StemSpan (Stem Cell Technologies; 09650). After the sorting the tube was centrifuged at 1500 rpm for 5 min at 4°C, and the supernatant was carefully removed ensuring approximately 30 ul of medium remained in the tube. This residual amount of medium was used to resuspend the cell pellet, which was then gently layered over the separately sorted niche populations as described in the paragraph **8.8.2**.

Cell Surface Marker Antibody	Fluorochrome
Lineage antibodies: CD4 (eBioscience; 56-0041) CD8 (eBioscience; 56-0081-82) CD11b (eBioscience; 56-0112) Gr-1 (eBioscience; 56-5931-82) Ter119 (Biolegend; 116220) B220 (eBioscience; 56-0452)	Alexa Fluor 700
cKit (CD117) (Biolegend; 105835)	BV711
Sca-1 (BD Biosciences; 560654)	APC-Cy7
CD150 (Biolegend; 115914)	PE-Cy7
CD48 (Biolegend; 103418)	Pacific Blue
CD34 (eBioscience; 11-0341-82)	FITC
EPCR (CD201) (eBioscience; 12-2012-82)	PE
Dead cells	Zombie Yellow (Biolegend; 423103)

Table 8.10. Antibody staining panel for bone marrow hematopoietic cells. Despite the sorting of more generic gates for the scRNA-seq (LS-K and LSK), additional markers have been incorporated to enhance data examination.

8.8.2 Bone digestion and purification of niche populations

The flushed bones from **8.8.1** underwent enzymatic digestion and depletion of CD45-expressing fractions as per a protocol developed in Dr. Marieke Essers' lab, Division of Inflammatory Stress in Stem Cells, DKFZ. Subsequently, the resulting cell suspension containing the niche populations was stained according to the antibody panel shown in Table **8.11**. A total of 5250 stromal (Live CD45-Ter119-CD41-CD31-CD71-) and 1750 endothelial (Live CD45-Ter119-CD41-CD31+) cells were serially sorted using Fusion I (BD) into the A1 well of a round bottom 96-well plate containing 5 ul of Dulbecco's Modified Eagle Medium (DMEM; Gibco, 12634028) supplemented with 15% FBS. The gating strategy is provided in Fig. **8.4**. The 30 ul of the hematopoietic cell suspension mentioned in **8.1** were mixed with the nice populations. From this final mixture, 5 ul were mixed with 5 ul Trypan blue (ThermoFisher; 15250061) and loaded into a Neubauer chamber to assess cell number and viability using a CytoSMART Lux platform (AXION Biosystems).

8.8.3 Single-cell gene expression library construction

The combined cell suspension, comprising hematopoietic and niche populations, became subject to the microfluidics-based platform of the Chromium Next GEM Single Cell 3' v3.1 workflow from 10X Genomics. Throughout the entire process of library preparation, the manufacturer's protocol was strictly followed. The libraries were finally validated with a Bioanalyzer using High Sensitivity DNA chips. The libraries were eventually sequenced on a NovaSeq 6000 platform using either S1 or SP flowcell. I targeted at least 30,000 reads per cell and accounted for an approximate 50% cell loss from the initial input in the 10X Chromium.

Marker	Fluorochrome
Lineage antibodies: CD45 (eBioscience; 11-0451-82) CD41 (BD; 561849) Ter119 (eBioscience; 11-5921-85)	FITC
CD200 (BD; 565546)	APC-R700
CD51 (BD; 740755)	BV711
PDGFRα (CD140α) (eBioscience; 25-1401-82)	PE-Cy7
Sca-1 (BD Biosciences; 560654)	APC-Cy7
CD31 (BD; 562939)	BV421
CD71 (eBioscience; 12-0711-83)	PE
Dead cells	Zombie Yellow (Biolegend; 423103)

Table 8.11. Antibody panel for the staining of bone marrow niche populations collected from digested bones Despite sorting more generic gates for the scRNA-seq, additional markers have been incorporated to enhance data examination.

8.8.4 Gene expression analysis

To process the raw FASTQ data through alignment, demultiplexing and ultimately obtaining the filtered count assignment, I used *cellranger*[203] (v7.1.0), the standard pipeline provided by 10X Genomics. Empty droplets were also excluded with *cellranger*. The dataset was further refined by removing ambient RNA and cell doublets with *SoupX*[204] (v1.5.0) and *scDblFinder*[205] (v1.16.0), respectively. The rest of the quality control, data normalization, clustering of the dataset and subsequent annotation of the cell clusters were achieved with *Seurat*[206](v4.3.0.1). This further quality control included elimination of mitochondrial and ribosomal genes, exclusion of the cells with fewer than 200 and more than 7500 unique molecular identifiers (UMIs = genes), removal of cells with over 25% mitochondrial genes and finally, removal of cells with low complexity as measured by *scCustomize* (v2.0.1). An initial clustering with resolution=0.5 was performed in order to split the dataset into its hematopoietic and niche fractions. For that, Dr. Charles Dussiau performed a gross automatic annotation. After the split of the dataset, the clustering was repeated for each fraction using the Leiden algorithm (*leiden* R package, v0.4.3.1). For the `RunUMAP()`, the number of dimensions was set to dims=30, and subsequently, the clustering resolution was 1.2 for the niche and 1.8 for the hematopoietic compartment. We manually annotated the two different compartments by examining the top 25 hematopoietic and top 10 niche marker genes per cluster supported by literature references. The estimation of population proportions was performed with the `propeller`[207] function from the *speckle* R package (v1.2.0) applied on each sorting gate separately. Gene expression signatures were analysed with *decoupleR*[161] (v2.8.0). Finally, cell-cell interactions between hematopoietic and niche cells were explored with *MultiNicheNetR*[173] (v1.0.1).

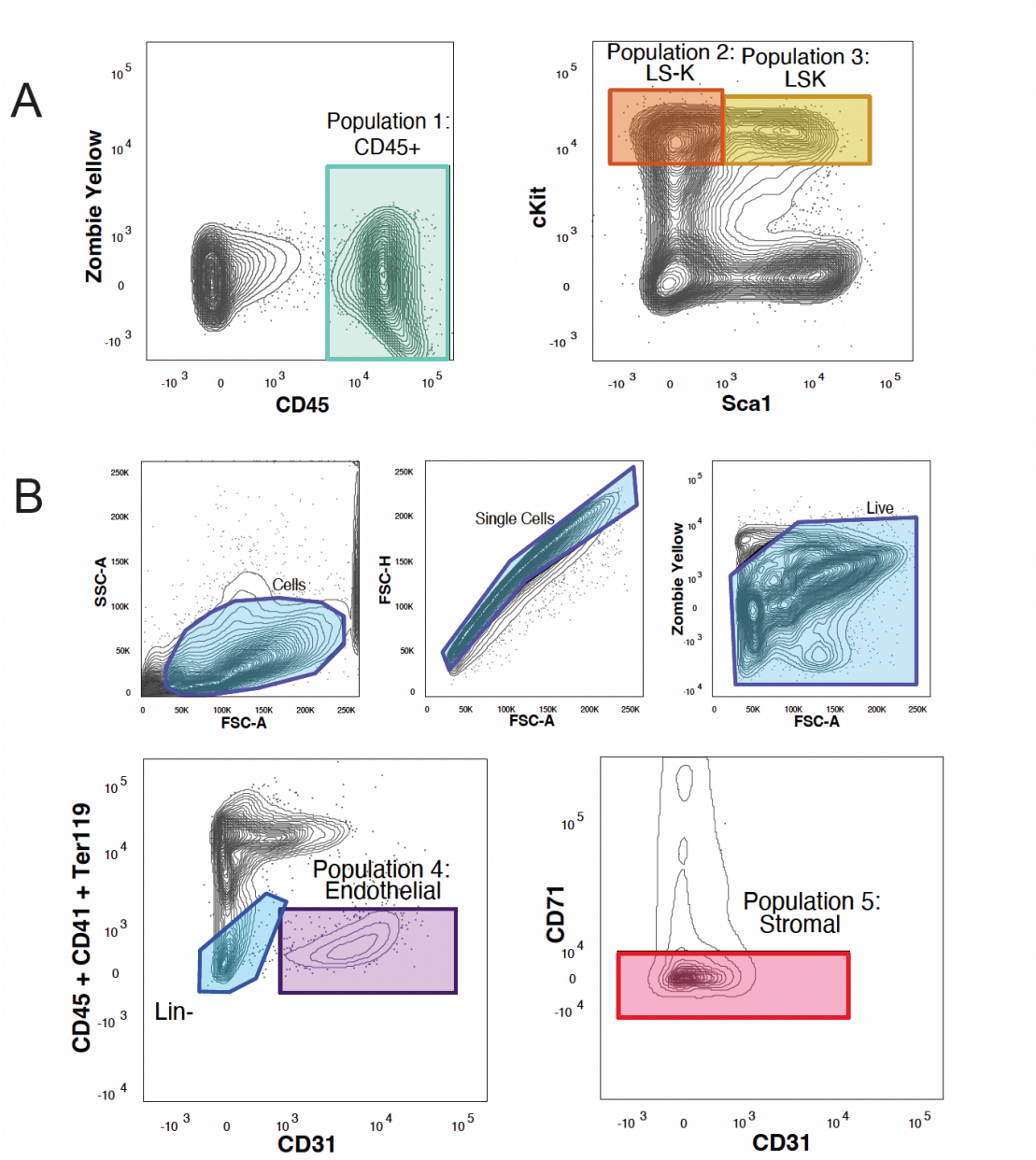

Figure 8.4. Populations sorted for the scRNA-seq. A) Hematopoietic populations. The samples are pregated for Cells-→ Single cells→ Live for the left panel, and Cells-→ Single cells→ Live→Lin- for the right panel. **B)** Sorting strategy for the niche cells. The gating flow is indicated by the blue gates.

8.9 Statistics and further data analysis

For visualization, statistics and data analysis, I used R v4.3.0 and R studio v2023.12.0+369 locally, as well as the Rstudio Workbench provided by the Omics IT and Data Management Core Facility. Statistical tests included unpaired Welch's t-test for 2-group comparisons and One-way ANOVA with Tukey's HSD test for multiple comparisons among 3 groups. I performed linear regression analysis using the `lm()` function. Differences in the variant annotation frequencies between the groups were assessed with chi-squared tests. Group variances were calculated with

the `nice_var()` function from *rempsyc*[208] (v1.0.7.4) package. Multiple linear correlation analysis was performed using *ggcorrplot* (v0.1.4.1) and the calculated p-values were corrected with the Benjamini-Hochberg method. For PCA, I used the packages *FactoMineR*[209] (v2.10.0) and *factoextra*[210] (v1.07), after missing values imputation with the `imputePCA()` function from the *missMDA*[211] (v1.19) package. Finally, for the survival analysis with Cox PH I used the *survival* package (v3.5-8)[212].

8.10 Code and file availability

Examples of scripts used for Project 1 are available on DKFZ Gitlab (internal): `https://git.dkfz.de/a012/hsc-mutagenesis.git` . Files necessary for these runs and summary tables with sample information can also be found there.

Contributions

This thesis has benefited from the contributions of the following colleagues:

Dr. Michael Milsom supervised this thesis.

Dr. Megan Druce, former PhD student in the Milsom lab, initiated Project 1, optimized the variant calling pipelines and acquired a significant body of colony WGS data used in this thesis (old, young, active and dormant groups).

Dr. Ruzhica Bogeska, former post-doc in the Milsom lab, conducted the experiments for the groups mentioned above.

Viktoria Flore, former MSc student under my supervision, updated the variant calling pipelines (SNVs and indels) and the normalization strategy. Moreover, she setup from scratch the *Delly* pipeline for somatic SV detection.

Dr. Charles Dussiau, current post-doc fellow in the Milsom & Zaugg labs, performed a thorough QC analysis of the scRNA-seq data, annotated the niche fraction, performed the gene signature analysis, and studied the intercellular interactions across the entire dataset.

Melanie Ball, former technician in the Milsom lab, provided extensive experimental support and animal management at almost every experiment required for this thesis.

Esther Rodriguez Correa, PhD student in the Milsom lab, performed the majority of the bone marrow transplantations. **Ian Ghezzi** and **Theo Aurich,** also colleagues from the lab**,** have contributed in the transplantations, too. Additionally, **Ian Ghezzi** has provided support with pI:pC treatments.

Dr. Susanne Lux, former post-doc in the Milsom lab, provided assistance with WGS and scRNA-seq library preps.

Franziska Pills, former technician in the Essers lab, assisted with some endpoints for Project 2 and performed all the bone digestions for the isolation of niche cells. Additionally, **Dr. Shubhankar Sood**, former PhD student in the Essers lab, performed the sorting for the niche populations.

The single-cell Open Lab, DKFZ generated scRNA-seq libraries for 2/3 batches used in this thesis.

In addition, apart from the aforementioned, other members of the Milsom lab that have consistently supported me with mouse dissections and occasionally sample processing for both projects are **Ana-Matea Mikecin, Marleen Büchler-Schäff, Julia Knoch, Dhyani Shah, Jeyan Jayarajan, Robin Berner, Lina Merg, Melanie Ball, Sena Alptekin, Lena Bognar, Sercan Öz,** and **Helene Foissner.**

Barriere D animal caretakers performed the irradiations of the recipient animals and provided daily monitoring.

The members of the **DKFZ flow cytometry core facility** ensured proper sorter set-up for each experiment.

Finally, this thesis was proofread in parts by **Esther Rodriguez Correa, Dr. Charles Dussiau** and **Lina Merg.**

Bibliography

1. eurostat. Ageing Europe-statistics on population developments. https://ec.europa.eu/eurostat/statistics-explained/index.php?title=Ageing_Europe_-_statistics_on_population_developments

2. World Health Organization. Ageing and health. https://www.who.int/news-room/fact-sheets/detail/ageing-and-health

3. Wu R, Sun F, Zhang W, Ren J, Liu GH. Targeting aging and age-related diseases with vaccines. *Nat Aging*. 2024;4(4):464-482. doi:10.1038/s43587-024-00597-0

4. Divo MJ, Martinez CH, Mannino DM. Ageing and the epidemiology of multimorbidity. *Eur Respir J*. 2014;44(4):1055-1068. doi:10.1183/09031936.00059814

5. López-Otín C, Blasco MA, Partridge L, Serrano M, Kroemer G. Hallmarks of aging: An expanding universe. *Cell*. 2023;186(2):243-278. doi:10.1016/j.cell.2022.11.001

6. Vijg J, Dong X. Pathogenic Mechanisms of Somatic Mutation and Genome Mosaicism in Aging. *Cell*. 2020;182(1):12-23. doi:10.1016/j.cell.2020.06.024

7. Singh PP, Demmitt BA, Nath RD, Brunet A. The Genetics of Aging: A Vertebrate Perspective. *Cell*. 2019;177(1):200-220. doi:10.1016/j.cell.2019.02.038

8. Rossiello F, Jurk D, Passos JF, d'Adda Di Fagagna F. Telomere dysfunction in ageing and age-related diseases. *Nat Cell Biol*. 2022;24(2):135-147. doi:10.1038/s41556-022-00842-x

9. Jayarajan J, Milsom MD. The role of the stem cell epigenome in normal aging and rejuvenative therapy. *Hum Mol Genet*. 2020;29(R2):R236-R247. doi:10.1093/hmg/ddaa167

10. Zhang L, Pitcher LE, Yousefzadeh MJ, Niedernhofer LJ, Robbins PD, Zhu Y. Cellular senescence: a key therapeutic target in aging and diseases. *J Clin Invest*. 2022;132(15):e158450. doi:10.1172/JCI158450

11. Ferrucci L, Fabbri E. Inflammageing: chronic inflammation in ageing, cardiovascular disease, and frailty. *Nat Rev Cardiol*. 2018;15(9):505-522. doi:10.1038/s41569-018-0064-2

12. Sharpless NE, DePinho RA. How stem cells age and why this makes us grow old. *Nat Rev Mol Cell Biol*. 2007;8(9):703-713. doi:10.1038/nrm2241

13. Fafián-Labora JA, O'Loghlen A. Classical and Nonclassical Intercellular Communication in Senescence and Ageing. *Trends Cell Biol*. 2020;30(8):628-639. doi:10.1016/j.tcb.2020.05.003

14. Beerman I, Maloney WJ, Weissmann IL, Rossi DJ. Stem cells and the aging hematopoietic system. *Curr Opin Immunol*. 2010;22(4):500-506. doi:10.1016/j.coi.2010.06.007

15. Warren LA, Rossi DJ. Stem cells and aging in the hematopoietic system. *Mech Ageing Dev*. 2009;130(1-2):46-53. doi:10.1016/j.mad.2008.03.010

16. De Haan G, Lazare SS. Aging of hematopoietic stem cells. *Blood*. 2018;131(5):479-487. doi:10.1182/blood-2017-06-746412

17. Rossi DJ, Seita J, Czechowicz A, Bhattacharya D, Bryder D, Weissman IL. Hematopoietic Stem Cell Quiescence Attenuates DNA Damage Response and Permits DNA Damage Accumulation During Aging. *Cell Cycle*. 2007;6(19):2371-2376. doi:10.4161/cc.6.19.4759

18. Ottersbach K, Dzierzak E. The Murine Placenta Contains Hematopoietic Stem Cells within the Vascular Labyrinth Region. *Dev Cell*. 2005;8(3):377-387. doi:10.1016/j.devcel.2005.02.001

19. Laurenti E, Göttgens B. From haematopoietic stem cells to complex differentiation landscapes. *Nature*. 2018;553(7689):418-426. doi:10.1038/nature25022

20. Rieger MA, Schroeder T. Hematopoiesis. *Cold Spring Harb Perspect Biol*. 2012;4(12):a008250-a008250. doi:10.1101/cshperspect.a008250

21. Wilson A, Laurenti E, Oser G, et al. Hematopoietic Stem Cells Reversibly Switch from Dormancy to Self-Renewal during Homeostasis and Repair. *Cell*. 2008;135(6):1118-1129. doi:10.1016/j.cell.2008.10.048

22. Morganti C, Cabezas-Wallscheid N, Ito K. Metabolic Regulation of Hematopoietic Stem Cells. *HemaSphere*. 2022;6(7):e740. doi:10.1097/HS9.0000000000000740

23. Ito K, Turcotte R, Cui J, Zimmerman SE. Self-renewal of a purified Tie2+ hematopoietic stem cell population relies on mitochondrial clearance. 2016;354(6316):1156-1160.

24. Ho TT, Warr MR, Adelman ER, et al. Autophagy maintains the metabolism and function of young and old stem cells. *Nature*. 2017;543(7644):205-210. doi:10.1038/nature21388

25. Dong S, Wang Q, Kao YR, et al. Chaperone-mediated autophagy sustains haematopoietic stem-cell function. *Nature*. 2021;591(7848):117-123. doi:10.1038/s41586-020-03129-z

26. Essers MAG, Offner S, Blanco-Bose WE, et al. IFNα activates dormant haematopoietic stem cells in vivo. *Nature*. 2009;458(7240):904-908. doi:10.1038/nature07815

27. Walter D, Lier A, Geiselhart A, et al. Exit from dormancy provokes DNA-damage-induced attrition in haematopoietic stem cells. *Nature*. 2015;520(7548):549-552. doi:10.1038/nature14131

28. Challen GA, Boles N, Lin KK, Goodell MA. Mouse hematopoietic stem cell identification and analysis. *Cytometry A*. 2009;75A(1):14-24. doi:10.1002/cyto.a.20674

29. Harrison DE, Astle CM, Stone M. Numbers and functions of transplantable primitive immunohematopoietic stem cells. Effects of age. *J Immunol Baltim Md 1950*. 1989;142(11):3833-3840.

30. Amoah A, Keller A, Emini R, et al. Aging of human hematopoietic stem cells is linked to changes in Cdc42 activity. *Haematologica*. 2021;107(2):393-402. doi:10.3324/haematol.2020.269670

31. Dykstra B, Olthof S, Schreuder J, Ritsema M, De Haan G. Clonal analysis reveals multiple functional defects of aged murine hematopoietic stem cells. *J Exp Med*. 2011;208(13):2691-2703. doi:10.1084/jem.20111490

32. Sudo K, Ema H, Morita Y, Nakauchi H. Age-Associated Characteristics of Murine Hematopoietic Stem Cells. *J Exp Med*. 2000;192(9):1273-1280. doi:10.1084/jem.192.9.1273

33. Yamamoto R, Wilkinson AC, Ooehara J, et al. Large-Scale Clonal Analysis Resolves Aging of the Mouse Hematopoietic Stem Cell Compartment. *Cell Stem Cell*. 2018;22(4):600-607.e4. doi:10.1016/j.stem.2018.03.013

34. Haas S, Trumpp A, Milsom MD. Causes and Consequences of Hematopoietic Stem Cell Heterogeneity. *Cell Stem Cell*. 2018;22(5):627-638. doi:10.1016/j.stem.2018.04.003

35. van Galen P, Kreso A, Wienholds E, et al. Reduced Lymphoid Lineage Priming Promotes Human Hematopoietic Stem Cell Expansion. *Cell Stem Cell*. 2014;14(1):94-106. doi:10.1016/j.stem.2013.11.021

36. Konturek-Ciesla A, Dhapola P, Zhang Q, et al. Temporal multimodal single-cell profiling of native hematopoiesis illuminates altered differentiation trajectories with age. *Cell Rep*. 2023;42(4):112304. doi:10.1016/j.celrep.2023.112304

37. Ross JB, Myers LM, Noh JJ, et al. Depleting myeloid-biased haematopoietic stem cells rejuvenates aged immunity. *Nature*. 2024;628(8006):162-170. doi:10.1038/s41586-024-07238-x

38. Cunha LL, Perazzio SF, Azzi J, Cravedi P, Riella LV. Remodeling of the Immune Response With Aging: Immunosenescence and Its Potential Impact on COVID-19 Immune Response. *Front Immunol*. 2020;11:1748. doi:10.3389/fimmu.2020.01748

39. Kovtonyuk LV, Fritsch K, Feng X, Manz MG, Takizawa H. Inflamm-Aging of Hematopoiesis, Hematopoietic Stem Cells, and the Bone Marrow Microenvironment. *Front Immunol*. 2016;7. doi:10.3389/fimmu.2016.00502

40. Stubbins RJ, Platzbecker U, Karsan A. Inflammation and myeloid malignancy: quenching the flame. *Blood*. 2022;140(10):1067-1074. doi:10.1182/blood.2021015162

41. Gowanlock Z, Sriram S, Martin A, Xenocostas A, Lazo-Langner A. Erythropoiesis-stimulating agents in elderly patients with anemia: response and cardiovascular outcomes. *Blood Adv*. 2017;1(19):1538-1545. doi:10.1182/bloodadvances.2017007559

42. Le Blanc J, Lordkipanidzé M. Platelet Function in Aging. *Front Cardiovasc Med*. 2019;6:109. doi:10.3389/fcvm.2019.00109

43. Bakker ST, Passegué E. Resilient and resourceful: Genome maintenance strategies in hematopoietic stem cells. *Exp Hematol*. 2013;41(11):915-923. doi:10.1016/j.exphem.2013.09.007

44. Blasco MA. Mice with bad ends: mouse models for the study of telomeres and telomerase in cancer and aging. *EMBO J*. 2005;24(6):1095-1103. doi:10.1038/sj.emboj.7600598

45. Rossi DJ, Bryder D, Seita J, Nussenzweig A, Hoeijmakers J, Weissman IL. Deficiencies in DNA damage repair limit the function of haematopoietic stem cells with age. *Nature*. 2007;447(7145):725-729. doi:10.1038/nature05862

46. Beerman I, Seita J, Inlay MA, Weissman IL, Rossi DJ. Quiescent Hematopoietic Stem Cells Accumulate DNA Damage during Aging that Is Repaired upon Entry into Cell Cycle. *Cell Stem Cell*. 2014;15(1):37-50. doi:10.1016/j.stem.2014.04.016

47. Flach J, Bakker ST, Mohrin M, et al. Replication stress is a potent driver of functional decline in ageing haematopoietic stem cells. *Nature*. 2014;512(7513):198-202. doi:10.1038/nature13619

48. Yahata T, Takanashi T, Muguruma Y, et al. Accumulation of oxidative DNA damage restricts the self-renewal capacity of human hematopoietic stem cells. *Blood*. 2011;118(11):2941-2950. doi:10.1182/blood-2011-01-330050

49. Garaycoechea JI, Crossan GP, Langevin F, et al. Alcohol and endogenous aldehydes damage chromosomes and mutate stem cells. *Nature*. 2018;553(7687):171-177. doi:10.1038/nature25154

50. Wang M, Brandt LTL, Wang X, et al. Genotoxic aldehyde stress prematurely ages hematopoietic stem cells in a p53-driven manner. *Mol Cell*. 2023;83(14):2417-2433.e7. doi:10.1016/j.molcel.2023.05.035

51. Zeman MK, Cimprich KA. Causes and consequences of replication stress. *Nat Cell Biol*. 2014;16(1):2-9. doi:10.1038/ncb2897

52. Moehrle BM, Nattamai K, Brown A, et al. Stem Cell-Specific Mechanisms Ensure Genomic Fidelity within HSCs and upon Aging of HSCs. *Cell Rep*. 2015;13(11):2412-2424. doi:10.1016/j.celrep.2015.11.030

53. Chatterjee N, Walker GC. Mechanisms of DNA damage, repair, and mutagenesis. *Environ Mol Mutagen*. 2017;58(5):235-263. doi:10.1002/em.22087

54. Biechonski S, Yassin M, Milyavsky M. DNA-damage response in hematopoietic stem cells: an evolutionary trade-off between blood regeneration and leukemia suppression. *Carcinogenesis*. 2017;38(4):367-377. doi:10.1093/carcin/bgx002

55. Dertinger SD, Avlasevich SL, Torous DK, et al. Persistence of Cisplatin-Induced Mutagenicity in Hematopoietic Stem Cells: Implications for Secondary Cancer Risk Following Chemotherapy. *Toxicol Sci*. 2014;140(2):307-314. doi:10.1093/toxsci/kfu078

56. Vitale I, Manic G, De Maria R, Kroemer G, Galluzzi L. DNA Damage in Stem Cells. *Mol Cell*. 2017;66(3):306-319. doi:10.1016/j.molcel.2017.04.006

57. Weterings E, Chen DJ. The endless tale of non-homologous end-joining. *Cell Res*. 2008;18(1):114-124. doi:10.1038/cr.2008.3

58. Saxena S, Zou L. Hallmarks of DNA replication stress. *Mol Cell*. 2022;82(12):2298-2314. doi:10.1016/j.molcel.2022.05.004

59. Desai A, Qing Y, Gerson SL. Exonuclease 1 is a Critical Mediator of Survival During DNA Double Strand Break Repair in Nonquiescent Hematopoietic Stem and Progenitor Cells. *Stem Cells*. 2014;32(2):582-593. doi:10.1002/stem.1596

60. Park W, Wei S, Kim BS, et al. Diversity and complexity of cell death: a historical review. *Exp Mol Med*. 2023;55(8):1573-1594. doi:10.1038/s12276-023-01078-x

61. Kapadia CD, Goodell MA. Tissue mosaicism following stem cell aging: blood as an exemplar. *Nat Aging*. Published online March 4, 2024. doi:10.1038/s43587-024-00589-0

62. Hardwick JM, Soane L. Multiple Functions of BCL-2 Family Proteins. *Cold Spring Harb Perspect Biol*. 2013;5(2):a008722-a008722. doi:10.1101/cshperspect.a008722

63. Domen J, Cheshier SH, Weissman IL. The Role of Apoptosis in the Regulation of Hematopoietic Stem Cells. *J Exp Med*. 2000;191(2):253-264. doi:10.1084/jem.191.2.253

64. Van Galen P, Kreso A, Mbong N, et al. The unfolded protein response governs integrity of the haematopoietic stem-cell pool during stress. *Nature*. 2014;510(7504):268-272. doi:10.1038/nature13228

65. Yu H, Shen H, Yuan Y, et al. Deletion of Puma protects hematopoietic stem cells and confers long-term survival in response to high-dose γ-irradiation. *Blood*. 2010;115(17):3472-3480. doi:10.1182/blood-2009-10-248278

66. Alioto TS, Buchhalter I, Derdak S, et al. A comprehensive assessment of somatic mutation detection in cancer using whole-genome sequencing. *Nat Commun*. 2015;6(1):10001. doi:10.1038/ncomms10001

67. Jager M, Blokzijl F, Sasselli V, et al. Measuring mutation accumulation in single human adult stem cells by whole-genome sequencing of organoid cultures. *Nat Protoc*. 2018;13(1):59-78. doi:10.1038/nprot.2017.111

68. Osorio FG, Rosendahl Huber A, Oka R, et al. Somatic Mutations Reveal Lineage Relationships and Age-Related Mutagenesis in Human Hematopoiesis. *Cell Rep*. 2018;25(9):2308-2316.e4. doi:10.1016/j.celrep.2018.11.014

69. Mitchell E, Spencer Chapman M, Williams N, et al. Clonal dynamics of haematopoiesis across the human lifespan. *Nature*. 2022;606(7913):343-350. doi:10.1038/s41586-022-04786-y

70. Blokzijl F, De Ligt J, Jager M, et al. Tissue-specific mutation accumulation in human adult stem cells during life. *Nature*. 2016;538(7624):260-264. doi:10.1038/nature19768

71. Ellis P, Moore L, Sanders MA, et al. Reliable detection of somatic mutations in solid tissues by laser-capture microdissection and low-input DNA sequencing. *Nat Protoc*. 2021;16(2):841-871. doi:10.1038/s41596-020-00437-6

72. Cagan A, Baez-Ortega A, Brzozowska N, et al. Somatic mutation rates scale with lifespan across mammals. *Nature*. 2022;604(7906):517-524. doi:10.1038/s41586-022-04618-z

73. Salk JJ, Schmitt MW, Loeb LA. Enhancing the accuracy of next-generation sequencing for detecting rare and subclonal mutations. *Nat Rev Genet*. 2018;19(5):269-285. doi:10.1038/nrg.2017.117

74. Abascal F, Harvey LMR, Mitchell E, et al. Somatic mutation landscapes at single-molecule resolution. *Nature*. 2021;593(7859):405-410. doi:10.1038/s41586-021-03477-4

75. Biezuner T, Raz O, Amir S, et al. Comparison of seven single cell whole genome amplification commercial kits using targeted sequencing. *Sci Rep*. 2021;11(1):17171. doi:10.1038/s41598-021-96045-9

76. Gonzalez-Pena V, Natarajan S, Xia Y, et al. Accurate genomic variant detection in single cells with primary template-directed amplification. *Proc Natl Acad Sci*. 2021;118(24):e2024176118. doi:10.1073/pnas.2024176118

77. Kennedy SR, Schmitt MW, Fox EJ, et al. Detecting ultralow-frequency mutations by Duplex Sequencing. *Nat Protoc*. 2014;9(11):2586-2606. doi:10.1038/nprot.2014.170

78. Dickerson SK, Market E, Besmer E, Papavasiliou FN. AID Mediates Hypermutation by Deaminating Single Stranded DNA. *J Exp Med*. 2003;197(10):1291-1296. doi:10.1084/jem.20030481

79. Machado HE, Mitchell E, Øbro NF, et al. Diverse mutational landscapes in human lymphocytes. *Nature*. 2022;608(7924):724-732. doi:10.1038/s41586-022-05072-7

80. Alexandrov LB, Kim J, Haradhvala NJ, et al. The repertoire of mutational signatures in human cancer. *Nature*. 2020;578(7793):94-101. doi:10.1038/s41586-020-1943-3

81. Alexandrov LB, Nik-Zainal S, Wedge DC, Campbell PJ, Stratton MR. Deciphering Signatures of Mutational Processes Operative in Human Cancer. *Cell Rep*. 2013;3(1):246-259. doi:10.1016/j.celrep.2012.12.008

82. Australian Pancreatic Cancer Genome Initiative, ICGC Breast Cancer Consortium, ICGC MMML-Seq Consortium, et al. Signatures of mutational processes in human cancer. *Nature*. 2013;500(7463):415-421. doi:10.1038/nature12477

83. Koh G, Degasperi A, Zou X, Momen S, Nik-Zainal S. Mutational signatures: emerging concepts, caveats and clinical applications. *Nat Rev Cancer*. 2021;21(10):619-637. doi:10.1038/s41568-021-00377-7

84. Everall A, Tapinos A, Hawari A, et al. Comprehensive repertoire of the chromosomal alteration and mutational signatures across 16 cancer types from 10,983 cancer patients. Published online June 10, 2023. doi:10.1101/2023.06.07.23290970

85. Steele CD, Abbasi A, Islam SMA, et al. Signatures of copy number alterations in human cancer. *Nature*. 2022;606(7916):984-991. doi:10.1038/s41586-022-04738-6

86. Mutational Signatures (v3.4- October 2023), Cosmic Catalogue of Somatic Mutations in Cancer. https://cancer.sanger.ac.uk/signatures/sbs/

87. Spisak N, De Manuel M, Milligan W, Sella G, Przeworski M. *Disentangling Sources of Clock-like Mutations in Germline and Soma*. Genetics; 2023. doi:10.1101/2023.09.07.556720

88. Maura F, Degasperi A, Nadeu F, et al. A practical guide for mutational signature analysis in hematological malignancies. *Nat Commun*. 2019;10(1):2969. doi:10.1038/s41467-019-11037-8

89. Fabre MA, De Almeida JG, Fiorillo E, et al. The longitudinal dynamics and natural history of clonal haematopoiesis. *Nature*. 2022;606(7913):335-342. doi:10.1038/s41586-022-04785-z

90. Genovese G, Kähler AK, Handsaker RE, et al. Clonal Hematopoiesis and Blood-Cancer Risk Inferred from Blood DNA Sequence. *N Engl J Med*. 2014;371(26):2477-2487. doi:10.1056/NEJMoa1409405

91. Jaiswal S, Fontanillas P, Flannick J, et al. Age-Related Clonal Hematopoiesis Associated with Adverse Outcomes. *N Engl J Med*. 2014;371(26):2488-2498. doi:10.1056/NEJMoa1408617

92. Robertson NA, Latorre-Crespo E, Terradas-Terradas M, et al. Longitudinal dynamics of clonal hematopoiesis identifies gene-specific fitness effects. *Nat Med*. 2022;28(7):1439-1446. doi:10.1038/s41591-022-01883-3

93. Steensma DP, Bejar R, Jaiswal S, et al. Clonal hematopoiesis of indeterminate potential and its distinction from myelodysplastic syndromes. *Blood*. 2015;126(1):9-16. doi:10.1182/blood-2015-03-631747

94. Issa JP. The Two-Hit Hypothesis Meets Epigenetics. *Cancer Res*. 2022;82(7):1167-1169. doi:10.1158/0008-5472.CAN-22-0405

95. Dolgalev I, Tikhonova AN. Connecting the Dots: Resolving the Bone Marrow Niche Heterogeneity. *Front Cell Dev Biol*. 2021;9:622519. doi:10.3389/fcell.2021.622519

96. Galán-Díez M, Kousteni S. The Osteoblastic Niche in Hematopoiesis and Hematological Myeloid Malignancies. *Curr Mol Biol Rep*. 2017;3(2):53-62. doi:10.1007/s40610-017-0055-9

97. Pinho S, Frenette PS. Haematopoietic stem cell activity and interactions with the niche. *Nat Rev Mol Cell Biol*. 2019;20(5):303-320. doi:10.1038/s41580-019-0103-9

98. Wu Q, Zhang J, Kumar S, et al. Resilient anatomy and local plasticity of naive and stress haematopoiesis. *Nature*. 2024;627(8005):839-846. doi:10.1038/s41586-024-07186-6

99. Zhang J, Wu Q, Johnson CB, et al. In situ mapping identifies distinct vascular niches for myelopoiesis. *Nature*. 2021;590(7846):457-462. doi:10.1038/s41586-021-03201-2

100. Baccin C, Al-Sabah J, Velten L, et al. Combined single-cell and spatial transcriptomics reveal the molecular, cellular and spatial bone marrow niche organization. *Nat Cell Biol*. 2020;22(1):38-48. doi:10.1038/s41556-019-0439-6

101. Mercier FE, Ragu C, Scadden DT. The bone marrow at the crossroads of blood and immunity. *Nat Rev Immunol*. 2012;12(1):49-60. doi:10.1038/nri3132

102. Tratwal J, Rojas-Sutterlin S, Bataclan C, Blum S, Naveiras O. Bone marrow adiposity and the hematopoietic niche: A historical perspective of reciprocity, heterogeneity, and lineage commitment. *Best Pract Res Clin Endocrinol Metab*. 2021;35(4):101564. doi:10.1016/j.beem.2021.101564

103. Saçma M, Pospiech J, Bogeska R, et al. Haematopoietic stem cells in perisinusoidal niches are protected from ageing. *Nat Cell Biol*. 2019;21(11):1309-1320. doi:10.1038/s41556-019-0418-y

104. Mitchell CA, Verovskaya EV, Calero-Nieto FJ, et al. Stromal niche inflammation mediated by IL-1 signalling is a targetable driver of haematopoietic ageing. *Nat Cell Biol*. 2023;25(1):30-41. doi:10.1038/s41556-022-01053-0

105. Bousounis P, Bergo V, Trompouki E. Inflammation, Aging and Hematopoiesis: A Complex Relationship. *Cells*. 2021;10(6):1386. doi:10.3390/cells10061386

106. Druce, Megan C. *The Impact of Ageing, Replication and Stress on Genome Stability in Hematopoietic Stem Cells*. University of Heidelberg; 2021. https://archiv.ub.uni-heidelberg.de/volltextserver/29501/1/MeganDruce_PhDthesis.pdf

107. Jones D, Raine KM, Davies H, et al. cgpCaVEManWrapper: Simple Execution of CaVEMan in Order to Detect Somatic Single Nucleotide Variants in NGS Data. *Curr Protoc Bioinforma*. 2016;56(1). doi:10.1002/cpbi.20

108. Ye K, Schulz MH, Long Q, Apweiler R, Ning Z. Pindel: a pattern growth approach to detect break points of large deletions and medium sized insertions from paired-end short reads. *Bioinformatics*. 2009;25(21):2865-2871. doi:https://doi.org/10.1093/bioinformatics/btp394

109. Raine KM, Hinton J, Butler AP, et al. cgpPindel: Identifying Somatically Acquired Insertion and Deletion Events from Paired End Sequencing. *Curr Protoc Bioinforma*. 2015;52(1). doi:10.1002/0471250953.bi1507s52

110. Rausch T, Zichner T, Schlattl A, Stütz AM, Benes V, Korbel JO. DELLY: structural variant discovery by integrated paired-end and split-read analysis. *Bioinformatics*. 2012;28(18):i333-i339. doi:10.1093/bioinformatics/bts378

111. Blokzijl F, Janssen R, Van Boxtel R, Cuppen E. MutationalPatterns: comprehensive genome-wide analysis of mutational processes. *Genome Med*. 2018;10(1):33. doi:10.1186/s13073-018-0539-0

112. Manders F, Brandsma AM, De Kanter J, et al. MutationalPatterns: the one stop shop for the analysis of mutational processes. *BMC Genomics*. 2022;23(1):134. doi:10.1186/s12864-022-08357-3

113. Nik-Zainal S, Alexandrov LB, Wedge DC, et al. Mutational Processes Molding the Genomes of 21 Breast Cancers. *Cell*. 2012;149(5):979-993. doi:10.1016/j.cell.2012.04.024

114. Brandsma AM, Bertrums EJM, Van Roosmalen MJ, et al. Mutation Signatures of Pediatric Acute Myeloid Leukemia and Normal Blood Progenitors Associated with Differential Patient Outcomes. *Blood Cancer Discov*. 2021;2(5):484-499. doi:10.1158/2643-3230.BCD-21-0010

115. Tümpel S, Rudolph KL. Quiescence: Good and Bad of Stem Cell Aging. *Trends Cell Biol*. 2019;29(8):672-685. doi:10.1016/j.tcb.2019.05.002

116. Kao YR, Chen J, Kumari R, et al. An iron rheostat controls hematopoietic stem cell fate. *Cell Stem Cell*. 2024;31(3):378-397.e12. doi:10.1016/j.stem.2024.01.011

117. Takeuchi O, Fisher J, Suh H, Harada H, Malynn BA, Korsmeyer SJ. Essential role of BAX,BAK in B cell homeostasis and prevention of autoimmune disease. *Proc Natl Acad Sci*. 2005;102(32):11272-11277. doi:10.1073/pnas.0504783102

118. Whitfield J, Littlewood T, Evan GI, Soucek L. The Estrogen Receptor Fusion System in Mouse Models: A Reversible Switch. *Cold Spring Harb Protoc*. 2015;2015(3):pdb.top069815. doi:10.1101/pdb.top069815

119. Robinson JT, Thorvaldsdóttir H, Winckler W, et al. Integrative genomics viewer. *Nat Biotechnol*. 2011;29(1):24-26. doi:10.1038/nbt.1754

120. Mohrin M, Bourke E, Alexander D, et al. Hematopoietic Stem Cell Quiescence Promotes Error-Prone DNA Repair and Mutagenesis. *Cell Stem Cell*. 2010;7(2):174-185. doi:10.1016/j.stem.2010.06.014

121. Bernitz JM, Kim HS, MacArthur B, Sieburg H, Moore K. Hematopoietic Stem Cells Count and Remember Self-Renewal Divisions. *Cell*. 2016;167(5):1296-1309.e10. doi:10.1016/j.cell.2016.10.022

122. Thapa R, Elfassy E, Olender L, Sharabi O, Gazit R. Rapid activation of hematopoietic stem cells. *Stem Cell Res Ther*. 2023;14(1):152. doi:10.1186/s13287-023-03377-6

123. Bogeska R, Mikecin AM, Kaschutnig P, et al. Inflammatory exposure drives long-lived impairment of hematopoietic stem cell self-renewal activity and accelerated aging. *Cell Stem Cell*. 2022;29(8):1273-1284.e8. doi:10.1016/j.stem.2022.06.012

124. Fortier ME, Kent S, Ashdown H, Poole S, Boksa P, Luheshi GN. The viral mimic, polyinosinic:polycytidylic acid, induces fever in rats via an interleukin-1-dependent

mechanism. *Am J Physiol-Regul Integr Comp Physiol.* 2004;287(4):R759-R766. doi:10.1152/ajpregu.00293.2004

125. Avagyan S, Zon LI. Clonal hematopoiesis and inflammation – the perpetual cycle. *Trends Cell Biol.* 2023;33(8):695-707. doi:10.1016/j.tcb.2022.12.001

126. Vijg J, Schumacher B, Abakir A, et al. Mitigating age-related somatic mutation burden. *Trends Mol Med.* 2023;29(7):530-540. doi:10.1016/j.molmed.2023.04.002

127. Brazhnik K, Sun S, Alani O, et al. Single-cell analysis reveals different age-related somatic mutation profiles between stem and differentiated cells in human liver. *Sci Adv.* 2020;6(5):eaax2659. doi:10.1126/sciadv.aax2659

128. Manders F, Van Boxtel R, Middelkamp S. The Dynamics of Somatic Mutagenesis During Life in Humans. *Front Aging.* 2021;2:802407. doi:10.3389/fragi.2021.802407

129. Martincorena I, Roshan A, Gerstung M, et al. High burden and pervasive positive selection of somatic mutations in normal human skin. *Science.* 2015;348(6237):880-886. doi:10.1126/science.aaa6806

130. Martincorena I, Fowler JC, Wabik A, et al. Somatic mutant clones colonize the human esophagus with age. *Science.* 2018;362(6417):911-917. doi:10.1126/science.aau3879

131. Yizhak K, Aguet F, Kim J, et al. RNA sequence analysis reveals macroscopic somatic clonal expansion across normal tissues. *Science.* 2019;364(6444):eaaw0726. doi:10.1126/science.aaw0726

132. Gao T, Kastriti ME, Ljungström V, et al. A pan-tissue survey of mosaic chromosomal alterations in 948 individuals. *Nat Genet.* 2023;55(11):1901-1911. doi:10.1038/s41588-023-01537-1

133. Moore L, Leongamornlert D, Coorens THH, et al. The mutational landscape of normal human endometrial epithelium. *Nature.* 2020;580(7805):640-646. doi:10.1038/s41586-020-2214-z

134. Chin DWL, Yoshizato T, Virding Culleton S, et al. Aged healthy mice acquire clonal hematopoiesis mutations. *Blood.* 2022;139(4):629-634. doi:10.1182/blood.2021014235

135. Morrison SJ, Wandycz AM, Akashi K, Globerson A, Weissman IL. The aging of hematopoietic stem cells. *Nat Med.* 1996;2(9):1011-1016.

136. Lodato MA, Rodin RE, Bohrson CL, et al. Aging and neurodegeneration are associated with increased mutations in single human neurons. *Science.* 2018;359(6375):555-559. doi:10.1126/science.aao4426

137. Kucab JE, Zou X, Morganella S, et al. A Compendium of Mutational Signatures of Environmental Agents. *Cell.* 2019;177(4):821-836.e16. doi:10.1016/j.cell.2019.03.001

138. Al-Aamri HM, Irving HR, Bradley C, Meehan-Andrews T. Intrinsic and extrinsic apoptosis responses in leukaemia cells following daunorubicin treatment. *BMC Cancer*. 2021;21(1):438. doi:10.1186/s12885-021-08167-y

139. Gutierrez-Martinez P, Hogdal L, Nagai M, et al. Diminished apoptotic priming and ATM signalling confer a survival advantage onto aged haematopoietic stem cells in response to DNA damage. *Nat Cell Biol*. 2018;20(4):413-421. doi:10.1038/s41556-018-0054-y

140. Lin T, Chao C, Saito S, et al. p53 induces differentiation of mouse embryonic stem cells by suppressing Nanog expression. *Nat Cell Biol*. 2005;7(2):165-171. doi:10.1038/ncb1211

141. Inomata K, Aoto T, Binh NT, et al. Genotoxic Stress Abrogates Renewal of Melanocyte Stem Cells by Triggering Their Differentiation. *Cell*. 2009;137(6):1088-1099. doi:10.1016/j.cell.2009.03.037

142. Wang J, Sun Q, Morita Y, et al. A Differentiation Checkpoint Limits Hematopoietic Stem Cell Self-Renewal in Response to DNA Damage. *Cell*. 2012;148(5):1001-1014. doi:10.1016/j.cell.2012.01.040

143. Behm M, Baeza Centurión P, Penso-Dolfin L, et al. An interactive cellular ecosystem blocks epithelial transformation in naked mole-rat. Published online October 12, 2023. doi:10.1101/2023.10.10.561212

144. Kaufmann KB, Zeng AGX, Coyaud E, et al. A latent subset of human hematopoietic stem cells resists regenerative stress to preserve stemness. *Nat Immunol*. 2021;22(6):723-734. doi:10.1038/s41590-021-00925-1

145. Zhang YW, Mess J, Aizarani N, et al. Hyaluronic acid–GPRC5C signalling promotes dormancy in haematopoietic stem cells. *Nat Cell Biol*. 2022;24(7):1038-1048. doi:10.1038/s41556-022-00931-x

146. Skinder N, Sanz Fernández I, Dethmers-Ausema A, Weersing E, De Haan G. CD61 identifies a superior population of aged murine HSCs and is required to preserve quiescence and self-renewal. *Blood Adv*. 2024;8(1):99-111. doi:10.1182/bloodadvances.2023011585

147. Rodriguez-Meira A, Norfo R, Wen S, et al. Single-cell multi-omics identifies chronic inflammation as a driver of TP53-mutant leukemic evolution. *Nat Genet*. 2023;55(9):1531-1541. doi:10.1038/s41588-023-01480-1

148. Bondar T, Medzhitov R. p53-Mediated Hematopoietic Stem and Progenitor Cell Competition. *Cell Stem Cell*. 2010;6(4):309-322. doi:10.1016/j.stem.2010.03.002

149. Valent P, Büsche G, Theurl I, et al. Normal and pathological erythropoiesis in adults: from gene regulation to targeted treatment concepts. *Haematologica*. 2018;103(10):1593-1603. doi:10.3324/haematol.2018.192518

150. Gekas C, Graf T. CD41 expression marks myeloid-biased adult hematopoietic stem cells and increases with age. *Blood*. 2013;121(22):4463-4472. doi:10.1182/blood-2012-09-457929

151. Ferrucci L, Kuchel GA. Heterogeneity of Aging: Individual Risk Factors, Mechanisms, Patient Priorities, and Outcomes. *J Am Geriatr Soc*. 2021;69(3):610-612. doi:10.1111/jgs.17011

152. Nguyen QD, Moodie EM, Forget M, Desmarais P, Keezer MR, Wolfson C. Health Heterogeneity in Older Adults: Exploration in the Canadian Longitudinal Study on Aging. *J Am Geriatr Soc*. 2021;69(3):678-687. doi:10.1111/jgs.16919

153. Ferrucci L, Guralnik JM, Studenski S, et al. Designing Randomized, Controlled Trials Aimed at Preventing or Delaying Functional Decline and Disability in Frail, Older Persons: A Consensus Report. *J Am Geriatr Soc*. 2004;52(4):625-634. doi:10.1111/j.1532-5415.2004.52174.x

154. McBride JA, Striker R. Imbalance in the game of T cells: What can the CD4/CD8 T-cell ratio tell us about HIV and health? Coyne CB, ed. *PLOS Pathog*. 2017;13(11):e1006624. doi:10.1371/journal.ppat.1006624

155. Swirski FK, Nahrendorf M, Etzrodt M, et al. Identification of Splenic Reservoir Monocytes and Their Deployment to Inflammatory Sites. *Science*. 2009;325(5940):612-616. doi:10.1126/science.1175202

156. Morita Y, Iseki A, Okamura S, Suzuki S, Nakauchi H, Ema H. Functional characterization of hematopoietic stem cells in the spleen. *Exp Hematol*. 2011;39(3):351-359.e3. doi:10.1016/j.exphem.2010.12.008

157. Tupin E, Kinjo Y, Kronenberg M. The unique role of natural killer T cells in the response to microorganisms. *Nat Rev Microbiol*. 2007;5(6):405-417. doi:10.1038/nrmicro1657

158. Plackett TP, Boehmer ED, Faunce DE, Kovacs EJ. Aging and innate immune cells. *J Leukoc Biol*. 2004;76(2):291-299. doi:10.1189/jlb.1103592

159. Faunce DE, Palmer JL, Paskowicz KK, Witte PL, Kovacs EJ. CD1d-Restricted NKT Cells Contribute to the Age-Associated Decline of T Cell Immunity. *J Immunol*. 2005;175(5):3102-3109. doi:10.4049/jimmunol.175.5.3102

160. Gunin G, Kornilova NK, Petrov VV, Vasilyeva OV. Age changes in the number and proliferation of fibroblasts in the human skin. *Adv Gerontol*. 2011;1(4):299-303. doi:10.1134/S2079057011040059

161. Badia-i-Mompel P, Vélez Santiago J, Braunger J, et al. decoupleR: ensemble of computational methods to infer biological activities from omics data. Kuijjer ML, ed. *Bioinforma Adv*. 2022;2(1):vbac016. doi:10.1093/bioadv/vbac016

162. Schubert M, Klinger B, Klünemann M, et al. Perturbation-response genes reveal signaling footprints in cancer gene expression. *Nat Commun*. 2018;9(1):20. doi:10.1038/s41467-017-02391-6

163. Pulit-Penaloza JA, Scherbik SV, Brinton MA. Activation of Oas1a gene expression by type I IFN requires both STAT1 and STAT2 while only STAT2 is required for Oas1b activation. *Virology*. 2012;425(2):71-81. doi:10.1016/j.virol.2011.11.025

164. Banday AR, Stanifer ML, Florez-Vargas O, et al. Genetic regulation of OAS1 nonsense-mediated decay underlies association with COVID-19 hospitalization in patients of European and African ancestries. *Nat Genet*. 2022;54(8):1103-1116. doi:10.1038/s41588-022-01113-z

165. Matsumiya T, Stafforini DM. Function and Regulation of Retinoic Acid-Inducible Gene-I. *Crit Rev Immunol*. 2010;30(6):489-513. doi:10.1615/CritRevImmunol.v30.i6.10

166. Jang JS, Lee JH, Jung NC, et al. Rsad2 is necessary for mouse dendritic cell maturation via the IRF7-mediated signaling pathway. *Cell Death Dis*. 2018;9(8):823. doi:10.1038/s41419-018-0889-y

167. Hu X, Li J, Fu M, Zhao X, Wang W. The JAK/STAT signaling pathway: from bench to clinic. *Signal Transduct Target Ther*. 2021;6(1):402. doi:10.1038/s41392-021-00791-1

168. Ergen AV, Boles NC, Goodell MA. Rantes/Ccl5 influences hematopoietic stem cell subtypes and causes myeloid skewing. *Blood*. 2012;119(11):2500-2509. doi:10.1182/blood-2011-11-391730

169. Calaminus SDJ, Guitart A, Sinclair A, et al. Lineage Tracing of Pf4-Cre Marks Hematopoietic Stem Cells and Their Progeny. Freson K, ed. *PLoS ONE*. 2012;7(12):e51361. doi:10.1371/journal.pone.0051361

170. Zhao Y, Xiong J, Chen HX, et al. A Spontaneous H2-Aa Point Mutation Impairs MHC II Synthesis and CD4+ T-Cell Development in Mice. *Front Immunol*. 2022;13:810824. doi:10.3389/fimmu.2022.810824

171. Stables MJ, Shah S, Camon EB, et al. Transcriptomic analyses of murine resolution-phase macrophages. *Blood*. 2011;118(26):e192-e208. doi:10.1182/blood-2011-04-345330

172. Krawczyk M, Seguín-Estévez Q, Leimgruber E, et al. Identification of CIITA Regulated Genetic Module Dedicated for Antigen Presentation. Roopenian DC, ed. *PLoS Genet*. 2008;4(4):e1000058. doi:10.1371/journal.pgen.1000058

173. Browaeys R, Gilis J, Sang-Aram C, et al. *MultiNicheNet: A Flexible Framework for Differential Cell-Cell Communication Analysis from Multi-Sample Multi-Condition Single-Cell Transcriptomics Data*. Bioinformatics; 2023. doi:10.1101/2023.06.13.544751

174. Ulyanova T, Scott LM, Priestley GV, et al. VCAM-1 expression in adult hematopoietic and nonhematopoietic cells is controlled by tissue-inductive signals and reflects their developmental origin. *Blood*. 2005;106(1):86-94. doi:10.1182/blood-2004-09-3417

175. Kobberø SD, Gajhede M, Mirza OA, et al. Structure of the proteolytic enzyme PAPP-A with the endogenous inhibitor stanniocalcin-2 reveals its inhibitory mechanism. *Nat Commun*. 2022;13(1):6084. doi:10.1038/s41467-022-33698-8

176. Matsuoka S, Facchini R, Luis TC, et al. Loss of endothelial membrane KIT ligand affects systemic KIT ligand levels but not bone marrow hematopoietic stem cells. *Blood*. 2023;142(19):1622-1632. doi:10.1182/blood.2022019018

177. Zhou BO, Ding L, Morrison SJ. Hematopoietic stem and progenitor cells regulate the regeneration of their niche by secreting Angiopoietin-1. *eLife*. 2015;4:e05521. doi:10.7554/eLife.05521

178. Young K, Eudy E, Bell R, et al. Decline in IGF1 in the bone marrow microenvironment initiates hematopoietic stem cell aging. *Cell Stem Cell*. 2021;28(8):1473-1482.e7. doi:10.1016/j.stem.2021.03.017

179. Young KA, Telpoukhovskaia MA, Hofmann J, Mistry JJ, Kokkaliaris K, Trowbridge JJ. Variation in Mesenchymal KITL/SCF and IGF1 Expression at Middle Age Underlies Steady-State Hematopoietic Stem Cell Aging. *Blood J*. Published online April 10, 2024:blood.2024024275. doi:10.1182/blood.2024024275

180. Guo D, Dunbar JD, Yang CH, Pfeffer LM, Donner DB. Induction of Jak/STAT Signaling by Activation of the Type 1 TNF Receptor. *J Immunol*. 1998;160(6):2742-2750. doi:10.4049/jimmunol.160.6.2742

181. Kovtonyuk LV, Caiado F, Garcia-Martin S, et al. IL-1 mediates microbiome-induced inflammaging of hematopoietic stem cells in mice. *Blood*. 2022;139(1):44-58. doi:10.1182/blood.2021011570

182. Caiado F, Pietras EM, Manz MG. Inflammation as a regulator of hematopoietic stem cell function in disease, aging, and clonal selection. *J Exp Med*. 2021;218(7):e20201541. doi:10.1084/jem.20201541

183. Hernandez G, Mills TS, Rabe JL, et al. Pro-inflammatory cytokine blockade attenuates myeloid expansion in a murine model of rheumatoid arthritis. *Haematologica*. 2020;105(3):585-597. doi:10.3324/haematol.2018.197210

184. Medawar PB. *An Unresolved Problem of Biology: An Inaugural Lecture Delivered at the University College, London, 6 December, 1951*. H.K. Lewis and Company; 1952.

185. Enge M, Arda HE, Mignardi M, et al. Single-Cell Analysis of Human Pancreas Reveals Transcriptional Signatures of Aging and Somatic Mutation Patterns. *Cell*. 2017;171(2):321-330.e14. doi:10.1016/j.cell.2017.09.004

186. Dussiau C, Boussaroque A, Gaillard M, et al. Hematopoietic differentiation is characterized by a transient peak of entropy at a single-cell level. *BMC Biol*. 2022;20(1):60. doi:10.1186/s12915-022-01264-9

187. Rosales-Alvarez RE, Rettkowski J, Herman JS, Dumbović G, Cabezas-Wallscheid N, Grün D. VarID2 quantifies gene expression noise dynamics and unveils functional heterogeneity of ageing hematopoietic stem cells. *Genome Biol*. 2023;24(1):148. doi:10.1186/s13059-023-02974-1

188. Cawthorn WP, Scheller EL, Learman BS, et al. Bone Marrow Adipose Tissue Is an Endocrine Organ that Contributes to Increased Circulating Adiponectin during Caloric Restriction. *Cell Metab*. 2014;20(2):368-375. doi:10.1016/j.cmet.2014.06.003

189. Uccelli A, Moretta L, Pistoia V. Mesenchymal stem cells in health and disease. *Nat Rev Immunol*. 2008;8(9):726-736. doi:10.1038/nri2395

190. Raz Y, Cohen N, Shani O, et al. Bone marrow–derived fibroblasts are a functionally distinct stromal cell population in breast cancer. *J Exp Med*. 2018;215(12):3075-3093. doi:10.1084/jem.20180818

191. De Jong MME, Kellermayer Z, Papazian N, et al. The multiple myeloma microenvironment is defined by an inflammatory stromal cell landscape. *Nat Immunol*. 2021;22(6):769-780. doi:10.1038/s41590-021-00931-3

192. Bandyopadhyay S, Duffy M, Ahn KJ, et al. Mapping the Cellular Biogeography of Human Bone Marrow Niches Using Single-Cell Transcriptomics and Proteomic Imaging. Published online March 16, 2024. doi:10.1101/2024.03.14.585083

193. Roche PA, Furuta K. The ins and outs of MHC class II-mediated antigen processing and presentation. *Nat Rev Immunol*. 2015;15(4):203-216. doi:10.1038/nri3818

194. Tikhonova AN, Dolgalev I, Hu H, et al. The bone marrow microenvironment at single-cell resolution. *Nature*. 2019;569(7755):222-228. doi:10.1038/s41586-019-1104-8

195. Yamashita M, Passegué E. TNF-α Coordinates Hematopoietic Stem Cell Survival and Myeloid Regeneration. *Cell Stem Cell*. 2019;25(3):357-372.e7. doi:10.1016/j.stem.2019.05.019

196. Pietras EM, Mirantes-Barbeito C, Fong S, et al. Chronic interleukin-1 exposure drives haematopoietic stem cells towards precocious myeloid differentiation at the expense of self-renewal. *Nat Cell Biol*. 2016;18(6):607-618. doi:10.1038/ncb3346

197. Pioli PD, Casero D, Montecino-Rodriguez E, Morrison SL, Dorshkind K. Plasma Cells Are Obligate Effectors of Enhanced Myelopoiesis in Aging Bone Marrow. *Immunity*. 2019;51(2):351-366.e6. doi:10.1016/j.immuni.2019.06.006

198. Caiado F, Kovtonyuk LV, Gonullu NG, Fullin J, Boettcher S, Manz MG. Aging drives *Tet2* +/− clonal hematopoiesis via IL-1 signaling. *Blood*. 2023;141(8):886-903. doi:10.1182/blood.2022016835

199. Pedersen BS, Quinlan AR. Mosdepth: quick coverage calculation for genomes and exomes. Hancock J, ed. *Bioinformatics*. 2018;34(5):867-868. doi:10.1093/bioinformatics/btx699

200. Quinlan AR, Hall IM. BEDTools: a flexible suite of utilities for comparing genomic features. *Bioinformatics*. 2010;26(6):841-842. doi:10.1093/bioinformatics/btq033

201. McLaren W, Gil L, Hunt SE, et al. The Ensembl Variant Effect Predictor. *Genome Biol*. 2016;17(1):122. doi:10.1186/s13059-016-0974-4

202. Monaco G, Chen H, Poidinger M, Chen J, De Magalhães JP, Larbi A. flowAI: automatic and interactive anomaly discerning tools for flow cytometry data. *Bioinformatics*. 2016;32(16):2473-2480. doi:10.1093/bioinformatics/btw191

203. Zheng GXY, Terry JM, Belgrader P, et al. Massively parallel digital transcriptional profiling of single cells. *Nat Commun*. 2017;8(1):14049. doi:10.1038/ncomms14049

204. Young MD, Behjati S. SoupX removes ambient RNA contamination from droplet-based single-cell RNA sequencing data. *GigaScience*. 2020;9(12):giaa151. doi:10.1093/gigascience/giaa151

205. Germain PL, Lun A, Garcia Meixide C, Macnair W, Robinson MD. Doublet identification in single-cell sequencing data using scDblFinder. *F1000Research*. 2022;10:979. doi:10.12688/f1000research.73600.2

206. Butler A, Hoffman P, Smibert P, Papalexi E, Satija R. Integrating single-cell transcriptomic data across different conditions, technologies, and species. *Nat Biotechnol*. 2018;36(5):411-420. doi:10.1038/nbt.4096

207. Phipson B, Sim CB, Porrello ER, Hewitt AW, Powell J, Oshlack A. *propeller:* testing for differences in cell type proportions in single cell data. Mathelier A, ed. *Bioinformatics*. 2022;38(20):4720-4726. doi:10.1093/bioinformatics/btac582

208. Thériault R. rempsyc: Convenience functions for psychology. *J Open Source Softw*. 2023;8(87):5466. doi:10.21105/joss.05466

209. Lê S, Josse J, Husson F. FactoMineR : An *R* Package for Multivariate Analysis. *J Stat Softw*. 2008;25(1). doi:10.18637/jss.v025.i01

210. Kassambara A. factoextra. https://github.com/kassambara/factoextra

211. Josse J, Husson F. missMDA : A Package for Handling Missing Values in Multivariate Data Analysis. *J Stat Softw*. 2016;70(1). doi:10.18637/jss.v070.i01

212. Therneau T. A package for survival analysis in R. Published online April 22, 2024. https://cran.r-project.org/web/packages/survival/vignettes/survival.pdf

Supplementary

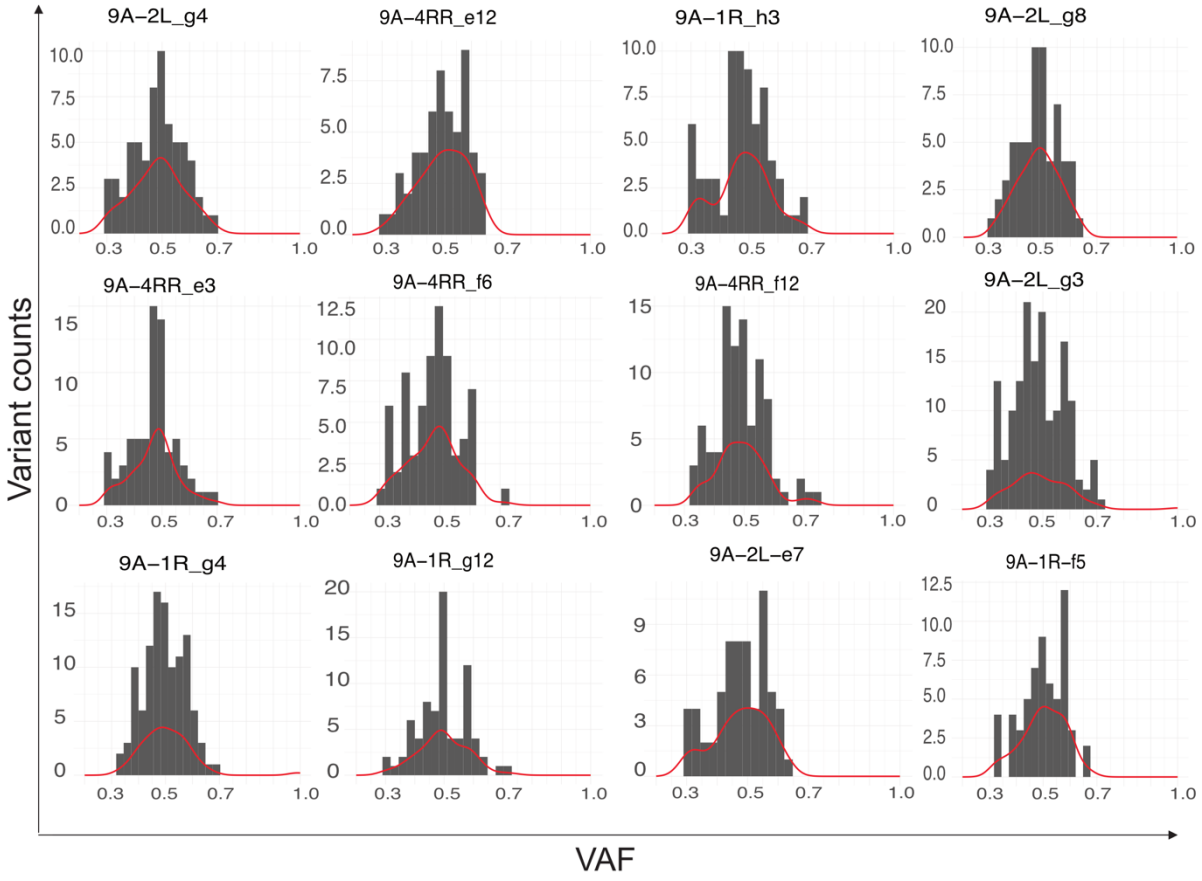

Figure S1. VAF distribution of SNVs per young sample. The clonal nature of the samples is represented by the characteristic distribution of the variants around VAF=0.5. Each histogram represents one cell.

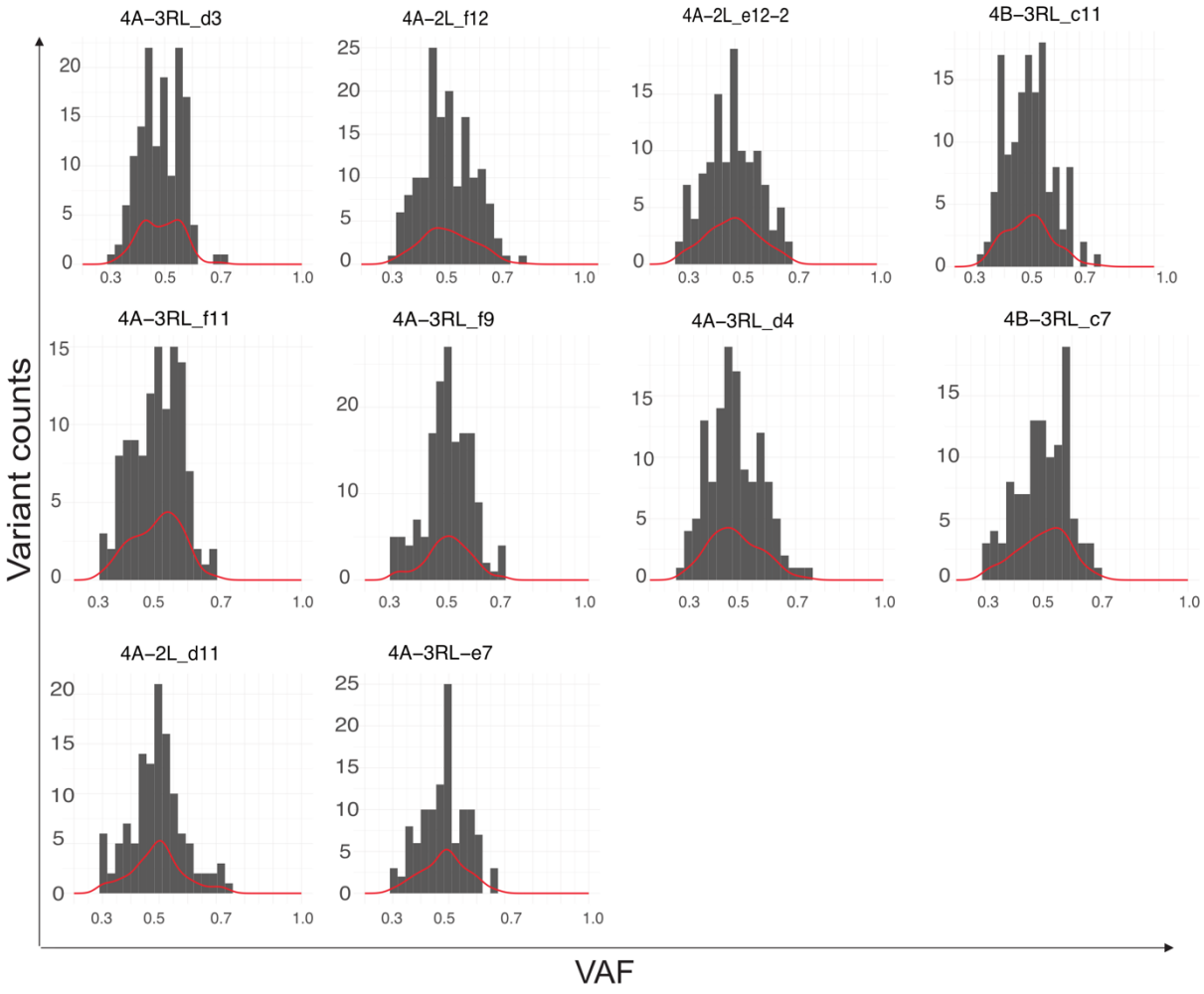

Figure S2. VAF distribution of SNVs per old sample. The clonal nature of the samples is represented by the characteristic distribution of the variants around VAF=0.5. Each histogram represents one cell.

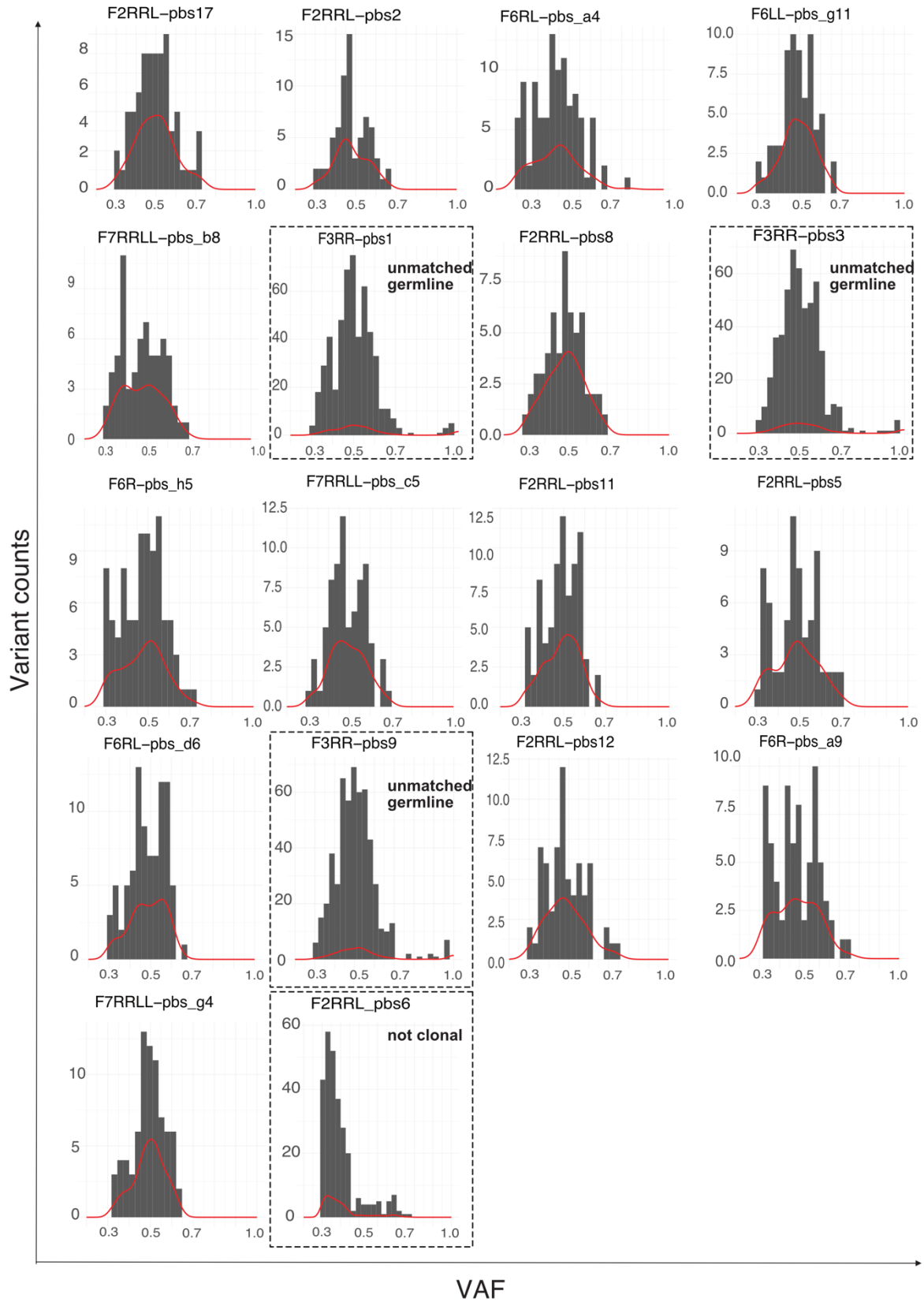

Figure S3. VAF distribution of SNVs per Bak$^{-/-}$ Bax $^{\delta/\delta}$ sample. The clonal nature of the samples is represented by the characteristic distribution of the variants around VAF=0.5. In contrast, the F2RRL-pbs6 sample did not display clonal distribution and was excluded from the analysis. Each histogram represents one cell.

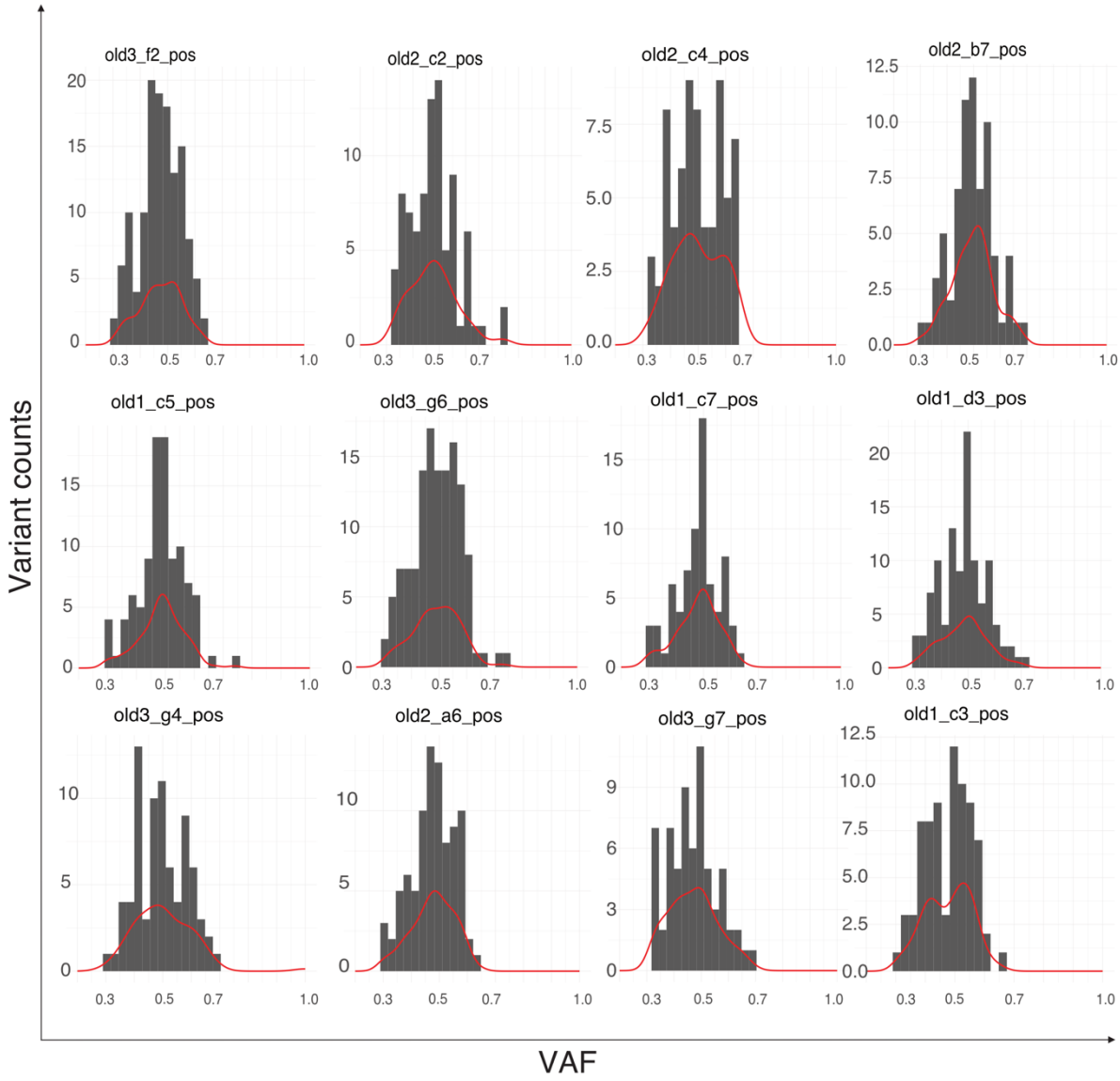

Figure S4. VAF distribution of SNVs per dormant sample. The clonal nature of the samples is represented by the characteristic distribution of the variants around VAF=0.5. Each histogram represents one cell.

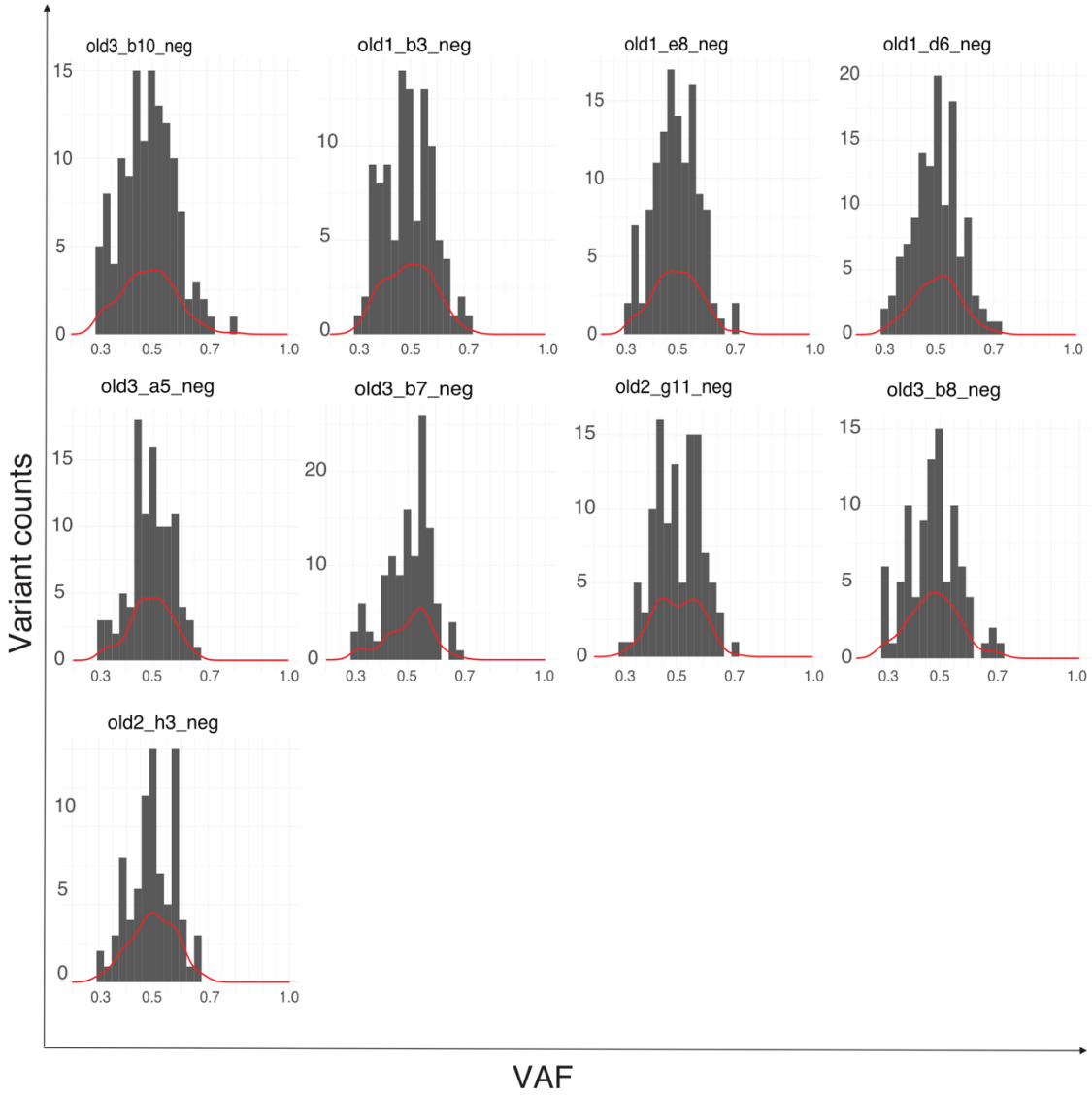

Figure S5. VAF distribution of SNVs per active (cycling) sample. The clonal nature of the samples is represented by the characteristic distribution of the variants around VAF=0.5. Each histogram represents one cell.

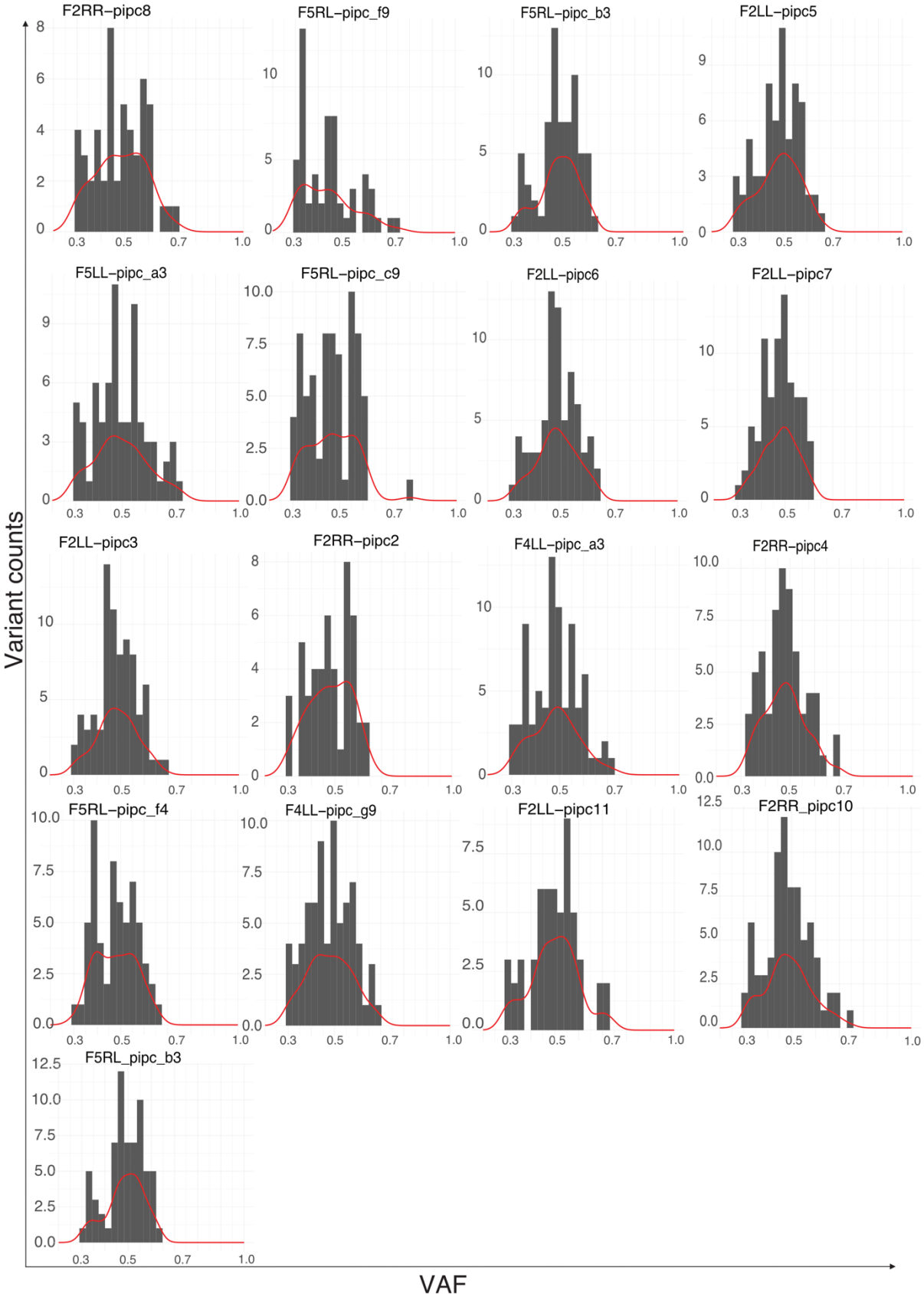

Figure S6. VAF distribution of SNVs per Bak$^{-/-}$ Bax $^{\delta/\delta}$ sample treated with pI:pC. The clonal nature of the samples is represented by the characteristic distribution of the variants around VAF=0.5. Each histogram represents one cell.

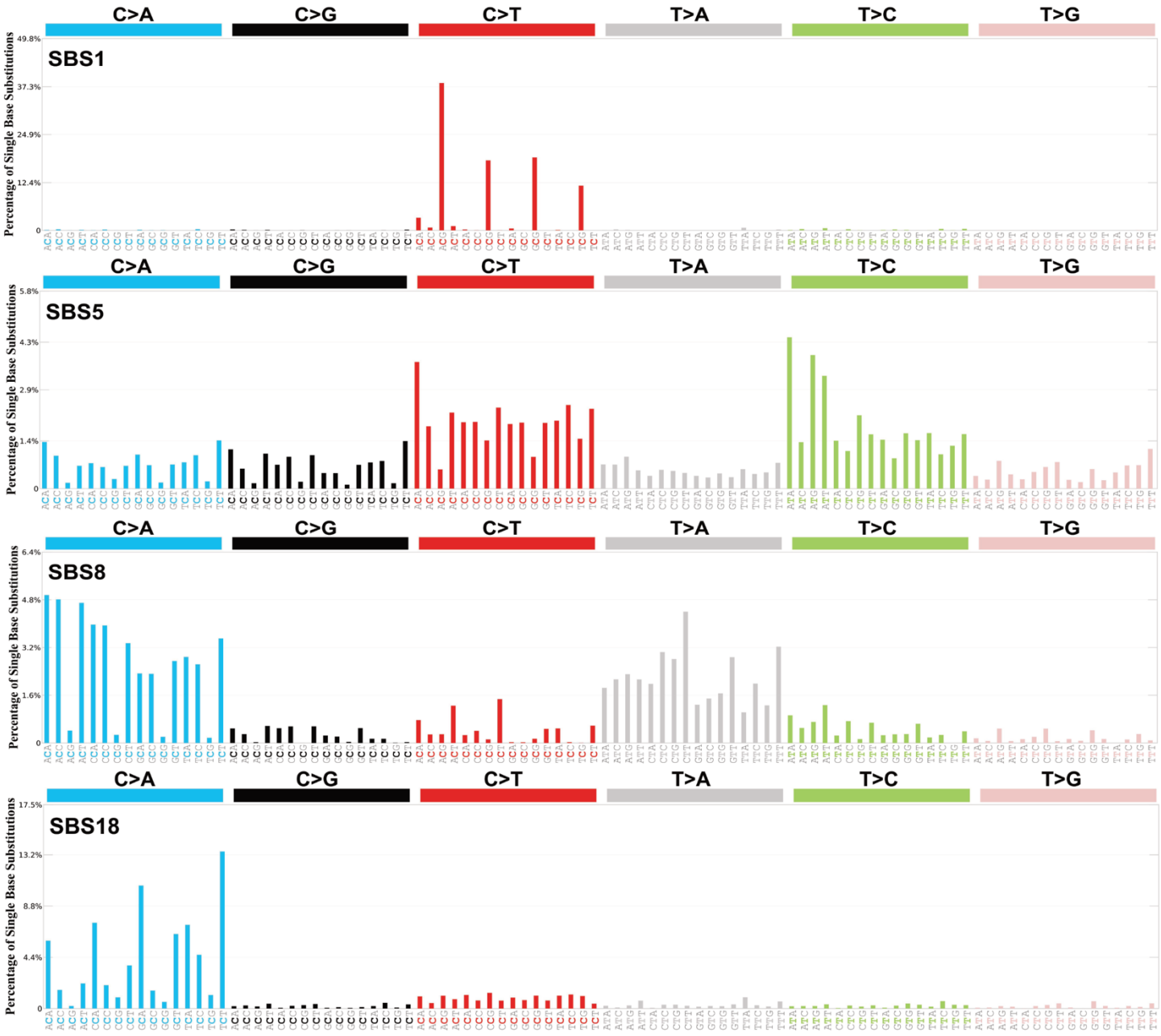

Figure S7. Patterns of the COSMIC signatures SBS1, SBS5, SBS8 and SBS18, as reported for the mm10 reference genome. Taken from the COSMIC database: https://cancer.sanger.ac.uk/signatures/sbs/

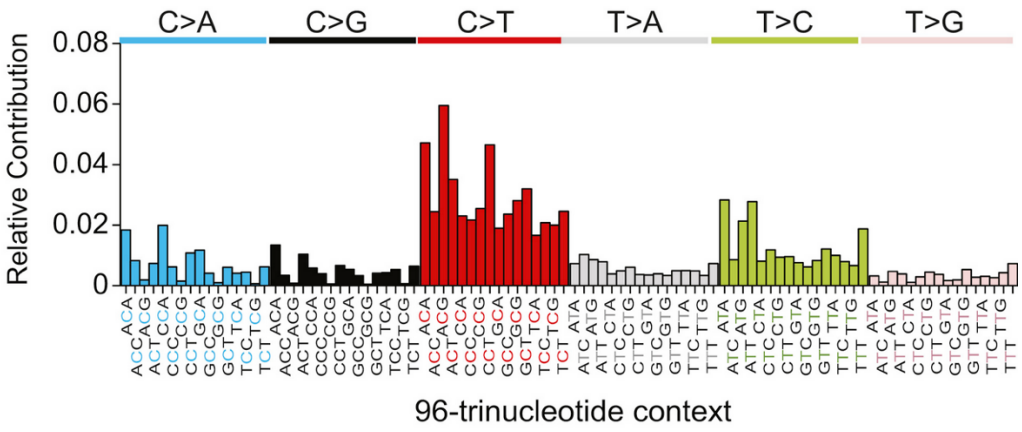

Figure S8. The HSPC signature. Taken from Osorio et al. Cell Rep (2018) and reprinted under a Creative Commons license Attribution-NonCommercial-NoDerivs (BY-NC-ND) 4.0 International: https://creativecommons.org/licenses/by-nc-nd/4.0/

Blood (donor)	Bone marrow (donor)	Spleen (donor)	Blood (recipient, 12 weeks pTx)	Blood (recipient, 24 weeks pTx)	Bone marrow (recipient, 24 weeks pTx)
WBC	Femur cellularity	Spleen weight	WBC	WBC	Femur cellularity
RBC	% HSC/MPP2/MPP3-4/MPP5 (in LSK)	WBC	RBC	RBC	% Donor chimerism in bone marrow
Hemoglobin	% LT-HSC/ST-HSC (in LSK)	% LSK (in Lin- gate)	Hemoglobin	Hemoglobin	% HSC/MPP2/MPP3-4/MPP5 (in donor-derived LSK)
Hematocrit	% LT-HSC/ST-HSC (of total HSC)	% CMP/GMP/MEP (in LS-K)	Hematocrit	Hematocrit	% LT-HSC/ST-HSC (in donor-derived LSK)
MCV	% CD41+ LT-HSC (of total LT-HSC)	CMPs/GMPs/ MEPs per spleen	MCV	MCV	% LT-HSC/ST-HSC (in donor-derived HSCs)
MCH	HSCs/LT-HSCs/ST-HSCs/MPP2/MPP3-4/MPP5 per femur	% CD4+/CD8+ T cells (of total T cells)	MCH	MCH	% Donor chimerism in HSC/MPP2/MPP3-4/MPP5/LT-HSC/ST-HSC
MCHC	% CMP/GMP/MEP (in LS-K)	% Effector /Memory/Naïve CD4+ T cells (of total CD4+ T cells)	MCHC	MCHC	% HSC/MPP2/MPP3-4/MPP5 (in total LSK)
RDW	CMPs/GMPs/MEPs/ CLPs per femur	% Effector /Memory/Naïve CD8+ T cells (of total CD8+ T cells)	RDW	RDW	% LT-HSC/ST-HSC in LSK gate
Platelets	% CD4+/CD8+ T cells (of total T cells)	T /B /Myeloid cells per spleen	Platelets	Platelets	HSCs/LT-HSCs/ST-HSCs/MPP2/MPP3-4/MPP5 per femur
MPV	% Effector /Memory/Naïve CD4+ T cells (of total CD4+ T cells)	% Inflammatory monocytes/Patrolling monocytes/Granulocytes (of total myeloid cells)	MPV	MPV	% Donor chimerism in CMPs/GMPs/MEPs
% CD4+/CD8+ T cells (of total T cells)	% Effector /Memory/Naïve CD8+ T cells (of total CD8+ T cells)	% T/B/Myeloid cells in spleen	% Donor chimerism in blood	% Donor chimerism in blood	% CMP/GMP/MEP in LS-K
% Effector /Memory/Naïve CD4+ T cells (of total CD4+ T cells)	T /B /Myeloid cells per femur		% Donor chimerism in T/B/Myeloid cells	% Donor chimerism in T/B/Myeloid cells	CMPs/GMPs/ MEPs/CLPs per femur
% Effector /Memory/Naïve CD8+ T cells (of total CD8+ T cells)	CD4+ /CD8+ T cells per femur		T /B /Myeloid cells per ml of blood	T /B /Myeloid cells per ml of blood	
T /B /Myeloid cells per ml of blood	Inflammatory and patrolling monocytes/Granulocytes per femur		% T/B/Myeloid cells in the donor-derived	% T/B/Myeloid cells in the donor-derived	

			fraction of blood	fraction of blood	
CD4+ /CD8+ T cells per ml of blood	% Inflammatory monocytes/Patrolling monocytes/Granulocytes (of total myeloid cells)		% CD4+/CD8+ T cells (of total T cells)	% CD4+/CD8+ T cells (of total T cells)	
Inflammatory and patrolling monocytes/Granulocytes per ml of blood	% T/B/Myeloid cells in total bone marrow				
% Inflammatory monocytes/Patrolling monocytes/Granulocytes (in total myeloid cells)					
% T/B/Myeloid cells in total blood					

Table S 1. Summary of the hematological metrics measured for Project 2 via flow cytometry. Abbreviations are explained in the abbreviation list.

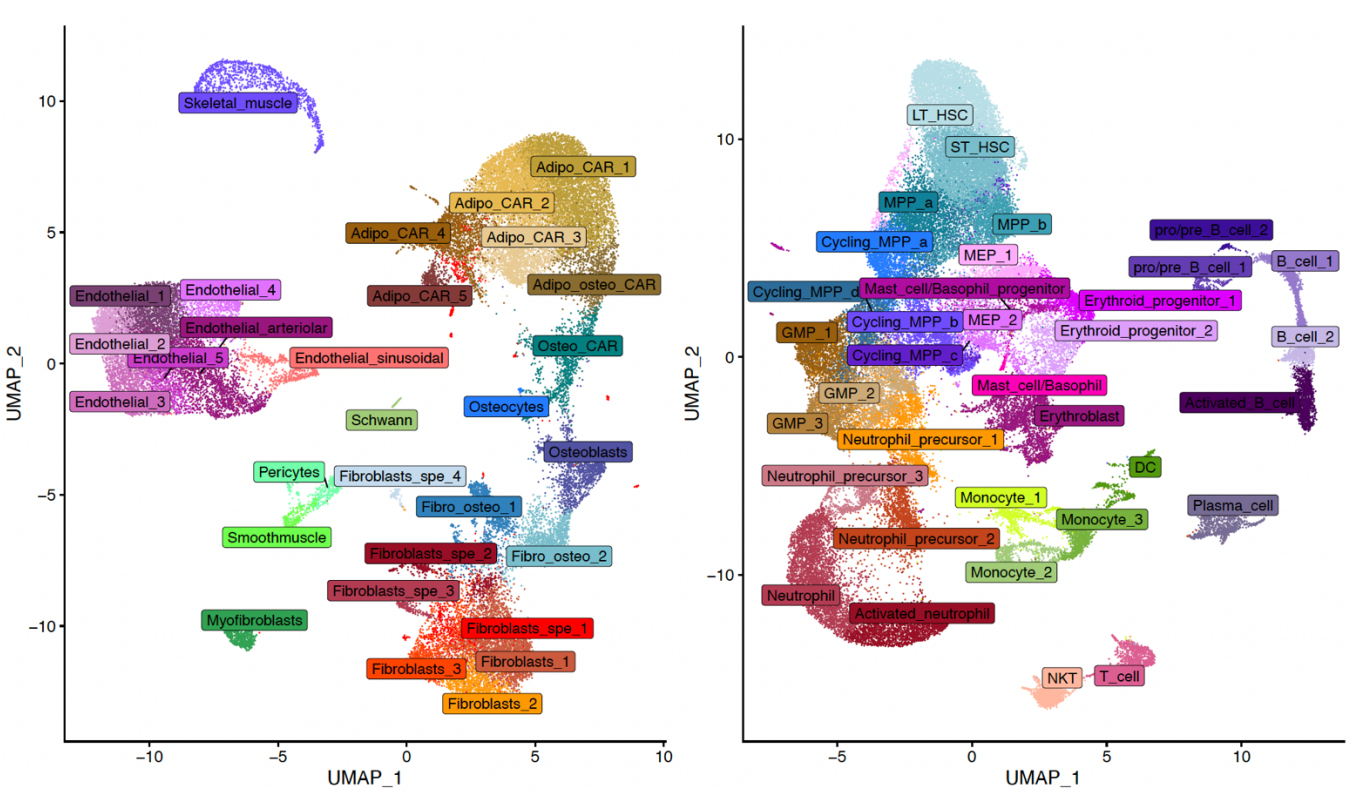

Figure S9. UMAP with detailed annotation of the clusters detected in the scRNA-seq dataset. Left: niche compartment, right: hematopoietic compartment. Clustering resolution is equal to 1.8.

List of abbreviations

A

ADIPOQ=adiponectin
AML=acute myeloid leukemia
ANGPT1=angiopoietin 1
ARCH=age-related clonal hematopoiesis

B

Bcl-2=B-cell lymphoma 2
BER=base excision repair
BND=breakend
BRCA= breast cancer genes

C

CAR=Cxcl-12-abundant reticular cell
Cas3/6/8/10= caspase 3/6/8/10
CHIP=clonal hematopoiesis of indeterminate potential
CMP=common myeloid progenitor
CNV=copy number variations

D

DDR=DNA damage response
DNA-PKcs= DNA-dependent protein kinase, catalytic subunit
Dox=doxycycline
DS=duplex-consensus sequencing
DSB=double-strand break

G

GMP=granulocyte-monocyte progenitor

H

HR=homologous recombination
HSC= hematopoietic stem cell
HSPC=hematopoietic stem and progenitor cell

I

Ifitm6=interferon-induced transmembrane protein 6
IGF1=insulin-like growth factor 1
IL-1/6/7=interleukin 1/6/7
IL-1R1=interleukin 1 receptor 1
Indel= insertion and deletion
i.p.=intraperitoneal
IR=ionizing radiation
Itga4=integrin a4
i.v.=intravenous

K

KO=knock-out

L

LepR=leptin receptor
LSK=Lin- Sca1+ cKit+, bone marrow fraction that represents the most primitive cells
LS-K=Lin- Sca1- cKit+, bone marrow fraction that represents the committed myeloid progenitors
LT-HSC=long-term hematopoietic stem cell

M

5-metC=5-methyl-cytosine
MCH=mean corpuscular hemoglobin
MCHC=mean corpuscular hemoglobin concentration
MCV=mean corpuscular volume
MDS=myelodysplastic syndrome
MEP=megakaryocytic-erythrocytic progenitor
MHC=major histocompatibility complex
MMR=mismatch repair
MPP=multipotent progenitor
MPV=mean platelet volume
MSC=mesenchymal stromal cell

N

NER=nucleotide excision repair
NHEJ=non-homologous end joining
NKT=natural killer T cells
NMF=non-negative matrix factorization

O

OPN=osteopontin
Osm=oncostatin M
Osmr=oncostatin M receptor
OxPhos=oxidative phosphorylation

P

PB=peripheral blood
PCA=principal component analysis
PDGFRα=platelet-derived growth factor receptor α
PE=paired-end
pI:pC=polyinosinic:polycytidylic acid
pTx=post-transplantation

R

RBC=red blood cells
RDW=red blood cell distribution width
ROS=reactive oxygen species

S

SASP=senescence-associated secretory phenotype
SBS=single-base signature
SCF=stem cell factor
scRNA-seq=single-cell RNA sequencing
SFEM=serum-free expansion medium
SHM=somatic hypermutation

SNS=sympathetic nervous system
SNV= single nucleotide variant
SSB=single-strand break
ST-HSC=short-term hematopoietic stem cell
SV=structural variant

T

TCR=T cell receptor
TLS=translesion synthesis
TLR3=toll-like receptor 3
TNFα=tumor necrosis factor α
TNFRI/II= tumor necrosis factor receptor I/II
TP53= tumor protein 53
t-SNE=t-distributed stochastic neighbor embedding

U

UMAP=uniform manifold approximation and projection
UMI=unique molecular identifier
UV=ultraviolet

V

VAF=variant allele frequency
VCAM1=vascular cell adhesion protein 1
VCF=variant call format
VEGFA=vascular endothelial growth factor A

W

WBC=white blood cells
WBM=whole bone marrow
WES=whole exome sequencing
WGA=whole genome amplification
WGS= whole genome sequencing
WT=wild type

Selected Presentations & Publications

Poster Presentations

- *"During ageing, the hematopoietic stem cell genome is protected by dormancy, not apoptosis."*
  The ageing genome: from mechanisms to disease, EMBL Symposium
  04-07.06.2023, Heidelberg, Germany

Oral Presentations

- *"During ageing, the hematopoietic stem cell genome is protected by dormancy, not apoptosis."*
  Annual Scientific Meeting of International Society of Experimental Hematology (ISEH)
  17-20.08.2023, New York, USA

- *"During ageing, the hematopoietic stem cell genome is protected by dormancy, not apoptosis."*
  Annual Meeting of the German Association for Aging Research (DGfA)
  29-30.06.2023, Jena, Germany

Publications

- **Fotopoulou., F**. et al., Dissection of the mechanisms that maintain genomic stability in HSCs during ageing in single-genome resolution. In preparation.

- Rommel, M. G., Walz, L., **Fotopoulou, F.**, Kohlscheen, S., et al. (2022). Influenza A virus infection instructs hematopoiesis to megakaryocyte-lineage output. *Cell Reports*, *41*(1), 111447. https://doi.org/10.1016/j.celrep.2022.111447